

Center for Tropical Marine Ecology
Zentrum für Marine Tropenökologie (ZMT)

Spatial Pattern Analysis Applied to Plant Ecology

João Marcelo Brazão Protázio

Thesis submitted in partial fulfillment of the
requirements for the degree of
Doctor of Natural Sciences.

Faculty 2 (Biology/Chemistry)
University of Bremen

March 2007



Erste Gutachter: Prof. Dr. rer. nat. Ulrich Saint-Paul, ZMT an der Universität Bremen

Zweite Gutachter: Dr. habil. Thorsten Wiegand, UFZ Centre for Environmental Research, Leipzig-Halle

Erste Prüfer: PD. Dr. Uta Berger, ZMT an der Universität Bremen

Zweite Prüfer: Prof. Dr. rer. nat. Juliane Filser, UFT an der Universität Bremen

Erste Mitglieder: Paula Cilene Alves de Oliveira, Cand.rer.nat., ZMT and der Universität Bremen

Zweite Mitglieder: Jürgen Alves Bischof, Student der Biologie and der Universität Bremen

Abstract

The spatial structure of a forest stand is an important signature of forest dynamics. The local environment determines competition among the trees, growth, death and regeneration. Therefore, the spatial configuration of the individual trees in a forest stand can provide information about the underlying ecological processes at the site.

This thesis focuses on the determination and analysis of the local constellation of individual trees (characterized by species, age, size etc.) in a forest stand. A large number of spatial statistical methods can be applied to this spatial pattern analysis. Besides using some classical statistical methods, I propose two new methods for spatial analysis.

In Chapter 1, I review some classical spatial statistical methods currently applied to plant ecology. These methods are suitable for the analysis of spatial configurations of individuals, such as plants or trees. Additionally, I present some explicit formulas for an area based edge effect correction method and compare this method with the Ripley edge correction factor.

Chapter 2 shows an application of the methods presented in Chapter 1 to a data set obtained from two real mangrove forests located in the North of Brazil. The idea behind is to infer about the underlying ecological processes occurring in those sites from the spatial configuration of individual trees.

In Chapter 3, I develop a new method for the spatial analysis of objects. The method approximates each individual tree as a circle, instead of a point, thus minimizing the bias of the classical methods.

In Chapter 4, I finally propose a new method to obtain spatial scale information about the point processes occurring within a study site. This approach combines Multiresolution Decomposition Analysis through Wavelet Transform with the Kernel Density Estimation method. This methodology provides information not only about the type of spatial distributions but also about their particular locations. By this, this approach goes beyond classical point-pattern methods and is innovative.

List of Abbreviations

CSR	Complete Spatial Random
QC	Quadrat Count
NN	Nearest Neighbor
FT	Fourier Transform
WT	Wavelet Transform
CWT	Continuous Wavelet Transform
DWT	Discrete Wavelet Transform
KDE	Kernel Density Estimation
MDA	Multiresolution Decomposition Analysis

Table of contents

Table of contents	1
List of figures	5
List of tables	13
1 Introduction	15
2 Spatial Pattern Analysis	19
2.1 Introduction	19
2.2 Methods	20
2.2.1 Quadrat counts analysis	21
2.2.1.1 Quadrat count indices	22
2.2.1.2 Quadrat counts method applied to study site Lagoa A	23
2.2.2 First-order analysis	23
2.2.2.1 Nearest neighbor methods	24
2.2.2.2 Nearest neighbor methods applied to study site Lagoa A	24
2.2.3 Second-order analysis	25
2.2.3.1 Ripley's K-function	25
2.2.3.2 Simulations interval	27
2.2.4 Edge effects	31
2.2.4.1 Area based edge effect correction method	32
2.3 Results	34
2.3.1 Time processing	34
2.3.2 Simulation envelope width	35
2.3.3 A Guard Area	37
2.3.4 Real Dataset	40
2.4 Discussion	42
3 Spatial Pattern Analysis - an Application	45
3.1 Introduction	45
3.1.1 Mangrove Forest	48
3.1.1.1 <i>Avicennia germinans</i>	49
3.1.1.2 <i>Rhizophora mangle</i>	50
3.1.1.3 <i>Laguncularia racemosa</i>	51

3.1.2 Mangrove forest evolution	52
3.2 Results	54
3.2.1 Lagoa A	54
3.2.2 Lagoa B	65
3.3 Discussion	76
4 Object Pattern Analysis	81
4.1 Introduction	81
4.2 Method	83
4.2.1 Univariate Analysis	83
4.2.2 Bivariate Analysis	87
4.2.3 Simulations Envelope	88
4.3 Results	89
4.3.1 Lagoa A	89
4.3.2 Lagoa B	95
4.4 Discussion	101
5 Wavelet Transform applied to Ecology	103
5.1 Introduction	103
5.2 Methods	106
5.2.1 Kernel Density Estimation Method	106
5.2.2 Variogram Analysis	107
5.2.3 Wavelet Transform	108
5.2.3.1 Continuous Wavelet Transform	109
5.2.3.2 Discrete Wavelet Transform	112
5.2.4 Inhomogeneous Poisson Process	115
5.2.5 Density Map Generation	116
5.3 Results	117
5.3.1 Heterogeneity detection	117
5.3.1.1 <i>Laguncularia racemosa</i> - Lagoa A	117
5.3.1.2 <i>Laguncularia racemosa</i> - Lagoa B	120
5.3.1.3 Dead Trees - Lagoa B	122
5.3.2 Spatial-Scale Resolution	124
5.3.2.1 Spatial relationship between <i>Laguncularia racemosa</i> and <i>Avicennia germi-</i> <i>nans</i> - Lagoa A	124
5.3.2.2 Spatial relationship between <i>Laguncularia racemosa</i> and <i>Avicennia germi-</i> <i>nans</i> - Lagoa B	126
5.3.3 Simulating an Inhomogeneous Poisson Process	129
5.3.3.1 <i>Laguncularia racemosa</i> - Lagoa B	129
5.3.3.2 Dead trees - Lagoa B	130
5.4 Discussion	131

6 Conclusion	133
7 Acknowledgements	137
8 References	139
9 Appendix	145

List of figures

Figure 1.1 Interaction between stand spatial structure, tree local environment and natural processes. Adapted from (Goreaud <i>et al.</i> 1998)	16
Figure 1.2 Thesis structure.	18
Figure 2.1 Three point patterns with 100 points representing a (a) CSR pattern, (b) regular pattern and (c) cluster pattern.	19
Figure 2.2 Study area Lagoa A with 560 trees. (black dot) <i>Avicennia germinans</i> and (blue dot) <i>Laguncularia racemosa</i> . The axis x and y are given in m.	21
Figure 2.3 (a) Regular pattern with 50 points, (b) cluster pattern with 50 points and (c) CSR pattern with 50 points and (d), (e) and (f) are their respective L-function (black) and 99% confidence interval (dashed red). The confidence interval was calculated via Monte Carlo method (Besag 1977) for the CSR hypothesis with 10000 simulations.	28
Figure 2.4 Study site Lagoa A. (a) <i>Avicennia</i> , (b) <i>Laguncularia</i> , (c) <i>Avicennia</i> (blue) and <i>Laguncularia</i> (red). (d) and (e) are the univariate L-function (black) and 99% simulation envelope for CSR hypothesis (dashed red) for the point pattern in (a) and (b) respectively. The univariate simulation envelope was calculated via Monte Carlo method (Besag 1977) with 1000 simulations. (f) Bivariate K-function (black) and its simulation envelope for independence hypothesis (dashed red) calculated for the point pattern contained in (c). The bivariate simulation envelope was calculated via random shifting method (Lotwick & Silverman, Diggle 1983) with 1000 simulations.	30
Figure 2.5 Study area Ω with dimensions $[0, a] \times [0, b]$ and a search circle $c_i(r)$ with radius r centered on a point p_i within this region. $A_i^-(r)$ and $A_i^+(r)$ are the area of the region of $c_i(r)$ outside and inside Ω respectively.	31
Figure 2.6 The four possibilities of intersection between the search circle $c_i(r)$ and the edges of the study region Ω	33
Figure 2.7 Time processing for the Area's method (dashed) and Ripley's method (filled).	34
Figure 2.8 Results obtained for a CSR pattern simulated within a study region $\Omega = [0, 1] \times [0, 1]$. 99% simulation envelope for the CSR model for $n = 50$ (a) and $n = 200$ (c) with 10000 simulations using the Area method (filled) and Ripley method (dashed) and (b) and (d) shows the respective simulation envelope width.	36
Figure 2.9 Confidence interval width of a regular model with parameters (a) $n = 50$ and $r = 0.01$, (b) $n = 50$ and $r = 0.03$, (c) $n = 50$ and $r = 0.05$, (d) $n = 200$ and $r = 0.01$, (e) $n = 200$ and $r = 0.03$, (f) $n = 200$ and $r = 0.05$ obtained by the Area method (filled) and Ripley method (dashed). The simulation envelope width was obtained via Monte Carlo method (Besag & Diggle 1977) with 10000 simulations.	36
Figure 2.10 Confidence interval width for a clumped model with parameters (a) $n = 50$ and $r = 0.05$, (b) $n = 50$ and $r = 0.08$, (c) $n = 50$ and $r = 0.1$, (d) $n = 200$ and $r = 0.05$, (e) $n = 200$ and $r = 0.08$ and (f) $n = 200$ and $r = 0.1$ obtained by the Area method (filled) and Ripley method (dashed). The simulation envelope width was obtained via Monte Carlo method (Besag & Diggle 1977) with 10000 simulations.	37
Figure 2.11 A whole study region $\Omega = [0, 2] \times [0, 2]$ divided as a guard area $\Omega_g = [0.5, 1.5] \times [0.5, 1.5]$ (gray region) and an buffer area Ω_b (hatched region) surrounding Ω_g	38
Figure 2.12 Study area Lagoa A with 560 trees: 118 trees inside the guard area Ω_g (points) and 442 trees inside the buffer area Ω_b (crosses).	41
Figure 3.1 Coastal zone of norther Brazil where the study sites Lagoa A and Lagoa B (black dots) are located.	47

Figure 3.2 Black mangrove or <i>Avicennia germinans</i>	50
Figure 3.3 Red mangrove or <i>Rhizophora mangle</i>	50
Figure 3.4 White mangrove or <i>Laguncularia racemosa</i>	51
Figure 3.5 All trees at stand site Lagoa A. (black cross) dead tree, (blue dot) <i>Laguncularia racemosa</i> and (red dot) <i>Avicennia germinans</i> . The size of dot is proportional to the dbh of <i>Avicennia</i> and <i>Laguncularia</i> (there's no information about the dbh of the dead trees). (scale in meters)	54
Figure 3.6 Lagoa A - Histograms showing the size class distribution of the mean stem diameter in breast height (dbh) in cm obtained for (a) all trees (excluding dead trees), (b) <i>Avicennia germinans</i> and (c) <i>Laguncularia racemosa</i> . (scale in cm)	55
Figure 3.7 (left) Spatial point pattern relative to all trees of the stand Lagoa A and its (right) respective L-function (black) and 99% simulation envelope (dashed red). The simulation envelope was calculated via Monte Carlo method (Besag 1977) for the CSR hypothesis with 10000 simulations.	56
Figure 3.8 (left) Spatial point pattern relative to the species <i>Avicennia germinans</i> within stand Lagoa A. Its (right) respective L-function (black) and 99% simulation envelope (dashed red). The simulation envelope was calculated via Monte Carlo method (Besag 1977) for the CSR hypothesis with 10000 simulations.	56
Figure 3.9 (left) Spatial point pattern relative to the species <i>Laguncularia racemosa</i> within stand Lagoa A. Its (right) respective L-function (black) and 99% simulation envelope (dashed red). The simulation envelope was calculated via Monte Carlo method (Besag 1977) for the CSR hypothesis with 10000 simulations.	57
Figure 3.10 (left) Spatial point pattern relative to dead trees within stand Lagoa A. Its (right) respective L-function (black) and 99% simulation envelope (dashed red). The simulation envelope was calculated via Monte Carlo method (Besag 1977) for the CSR hypothesis with 10000 simulations.	57
Figure 3.11 The point patterns (a) and (c) represents respectively the big trees (n=232) and small trees (n=328). (b) and (d) represents their L-function (black) and 99% simulation envelope for CSR hypothesis (dashed red) respectively. The point pattern (e) represent the large trees (blue) and small trees (red). (f) represents its bivariate L-function (black) and 99% simulation envelope for spatial independence hypothesis (dashed red). The simulation envelopes were calculated via Monte Carlo method (Besag 1977) with 10000 simulations.	58
Figure 3.12 The point patterns (a) and (c) represents respectively the large <i>Avicennia</i> (n=100) and small <i>Avicennia</i> (n=209). (b) and (d) represent their L-function (black) and 99% simulation envelope for CSR hypothesis (dashed red) respectively. The point pattern (e) represents the big <i>Avicennia</i> (blue) and small <i>Avicennia</i> (red). (f) represents its bivariate L-function (black) and 99% simulation envelope for spatial independence hypothesis (dashed red). The simulation envelopes were calculated via Monte Carlo method (Besag 1977) with 10000 simulations.	59
Figure 3.13 The point patterns (a) and (c) represents respectively the large <i>Laguncularia</i> (n=132) and small <i>Laguncularia</i> (n=132). (b) and (d) represents their L-function (black) and 99% simulation envelope for CSR hypothesis (dashed red) respectively. The point pattern (e) represents the big <i>Laguncularia</i> (blue) and small <i>Laguncularia</i> (red). (f) represents its bivariate L-function (black) and 99% simulation envelope for spatial independence hypothesis (dashed red). The simulation envelopes were calculated via Monte Carlo method (Besag 1977) with 10000 simulations.	60
Figure 3.14 The point patterns (a) and (c) represents respectively the dead trees (n=252) and living trees (n=560). (b) and (c) represents their L-function (black) and 99% simulation envelope for CSR hypothesis (dashed red) respectively. The point pattern (e) represents the dead trees (blue) and living trees (red). (f) represents its $K_1(r) - K_2(r)$ (black) and 99% simulation envelope for random labeling hypothesis (dashed red). The simulation envelopes were calculated via Monte Carlo method (Besag 1977) with 10000 simulations.	61
Figure 3.15 The point patterns (a) and (c) represents respectively the species <i>Avicennia</i> (n=309) and <i>Laguncularia</i> (n=251). (b) and (c) represents their L-function (black) and 99% simulation envelope for CSR hypothesis (dashed red) respectively. The point pattern (e) represents the species <i>Avicennia</i> (blue) and <i>Laguncularia</i> (red). (f) represents its bivariate L-function (black) and 99% simulation envelope for spatial	

independence hypothesis (dashed red). The simulation envelopes were calculated via Monte Carlo method (Besag 1977) with 10000 simulations.	62
Figure 3.16 All trees of the stand Lagoa B. (black cross) dead tree, (blue dot) <i>Laguncularia racemosa</i> and (red dot) <i>Avicennia germinans</i> and (green dot) <i>Rhizophora mangle</i> . The size of dot is proportional to the dbh of Avicennia and Laguncularia (there's no information about the dbh of the dead trees).	65
Figure 3.17 Lagoa B - Histograms showing the size class distribution of mean stem diameter in breast height (dbh) in cm obtained for (a) all trees (excluding dead trees), (b) <i>Avicennia germinans</i> and (c) <i>Laguncularia racemosa</i>	66
Figure 3.18 (left) Spatial point pattern relative to all trees of the stand Lagoa B and its (right) respective L-function (black) and 99% simulation envelope (dashed red). The simulation envelope was calculated via Monte Carlo method (Besag 1977) for the CSR hypothesis with 10000 simulations.	67
Figure 3.19 (left) Spatial point pattern relative to the species <i>Avicennia germinans</i> within stand Lagoa B. Its (right) respective L-function (black) and 99% simulation envelope (dashed red). The simulation envelope was calculated via Monte Carlo method (Besag 1977) for the CSR hypothesis with 10000 simulations.	67
Figure 3.20 (left) Spatial point pattern relative to species <i>Laguncularia racemosa</i> within stand Lagoa B. Its (right) respective L-function (black) and 99% simulation envelope (dashed red). The simulation envelope was calculated via Monte Carlo method (Besag 1977) for the CSR hypothesis with 10000 simulations.	68
Figure 3.21 (left) Spatial point pattern relative to dead trees within stand Lagoa A. Its (right) respective L-function (black) and 99% simulation envelope (dashed red). The simulation envelope was calculated via Monte Carlo method (Besag 1977) for the CSR hypothesis with 10000 simulations.	68
Figure 3.22 The point patterns (a) and (c) represents respectively the large trees (n=179) and small trees (n=255). (b) and (d) represents their L-function (black) and 99% simulation envelope for CSR hypothesis (dashed red) respectively. The point pattern (e) represents the big trees (blue) and small trees (red). (f) represents its bivariate L-function (black) and 99% simulation envelope for spatial independence hypothesis (dashed red). The simulation envelopes were calculated via Monte Carlo method (Besag 1977) with 10000 simulations.	69
Figure 3.23 The point patterns (a) and (c) represents respectively the large <i>Avicennia</i> (n=46) and small <i>Avicennia</i> (n=210). (b) and (d) represents their L-function (black) and 99% simulation envelope for CSR hypothesis (dashed red) respectively. The point pattern (e) represents the big <i>Avicennia</i> (blue) and small <i>Avicennia</i> (red). (f) represents its bivariate L-function (black) and 99% simulation envelope for spatial independence hypothesis (dashed red). The simulation envelopes were calculated via Monte Carlo method (Besag 1977) with 10000 simulations.	70
Figure 3.24 The point patterns (a) and (c) represents respectively the large <i>Laguncularia</i> (n=129) and small <i>Laguncularia</i> (n=42). (b) and (d) represents their L-function (black) and 99% simulation envelope for CSR hypothesis (dashed red) respectively. The point pattern (e) represents the big <i>Laguncularia</i> (blue) and small <i>Laguncularia</i> (red). (f) represents its bivariate L-function (black) and 99% simulation envelope for spatial independence hypothesis (dashed red). The simulation envelopes were calculated via Monte Carlo method (Besag 1977) with 10000 simulations.	71
Figure 3.25 The point patterns (a) and (c) represents respectively the dead trees (n=116) and living trees (n=434). (b) and (d) represents their L-function (black) and 99% simulation envelope for CSR hypothesis (dashed red) respectively. The point pattern (e) represents the dead trees (blue) and living trees (red). (f) represents its $K_1(r) - K_2(r)$ (black) and 99% simulation envelope for random labeling hypothesis (dashed red). The simulation envelopes were calculated via Monte Carlo method (Besag 1977) with 10000 simulations.	72
Figure 3.26 The point patterns (a) and (c) represents respectively the species <i>Avicennia</i> (n=256) and <i>Laguncularia</i> (n=171). (b) and (d) represents their L-function (black) and 99% simulation envelope for CSR hypothesis (dashed red) respectively. The point pattern (e) represents the species <i>Avicennia</i> (blue) and <i>Laguncularia</i> (red). (f) represents its bivariate L-function (black) and 99% simulation envelope for spatial independence hypothesis (dashed red). The simulation envelopes were calculated via Monte Carlo method	

(Besag 1977) with 10000 simulations.	73
Figure 3.27 The point patterns (a) and (c) represents respectively the species <i>Laguncularia</i> (n=171) and dead trees (n=171). (b) and (d) represents their L-function (black) and 99% simulation envelope for CSR hypothesis (dashed red) respectively. The point pattern (e) represents the species <i>Laguncularia</i> (blue) and dead trees (red). (f) represents its bivariate L-function (black) and 99% simulation envelope for spatial independence hypothesis (dashed red). The simulation envelopes were calculated via Monte Carlo method (Besag 1977) with 10000 simulations.	74
Figure 4.1 Steps of a transformation of a tridimensional object (tree) tree into a point. (left) Real trees, (middle) bidimensional abstraction of a real tree with crown (green) and stem (brown) and (right) point pattern representing the bidimensional abstraction.	81
Figure 4.2 The circle-to-point transformation T_2 indicates regularity at lower scales, instead of small-scale aggregation.	82
Figure 4.3 Two circular objects $c_i(r_i)$ and $c_j(r_j)$ and a search circle $c_i(r)$ inside a study region Ω	83
Figure 4.4 Estimating the expected specific area within a distance r of an arbitrary circular object of the study region Ω	84
Figure 4.5 Estimating the expected specific area inside a ring.	86
Figure 4.6 Histogram calculated for the R_{ZOI} distribution relative to (a) all trees, (b) small trees (dbh<5 cm), (c) large trees (dbh \geq 5 cm), (d) <i>Avicennia germinans</i> , (e) small <i>Avicennia</i> (dbh<5 cm), (f) large <i>Avicennia</i> (dbh \geq 5 cm), (g) <i>Laguncularia racemosa</i> , (h) small <i>Laguncularia</i> (dbh<5 cm) and (i) large <i>Laguncularia</i> (dbh \geq 5 cm).	90
Figure 4.7 (a) Object pattern relative to all trees within study site Lagoa A. (b) Object ring analysis (blue) and respective 90% simulation envelope (red) obtained via Monte Carlo Method (Besag 1977) for the Model I hypothesis with 200 simulations.	91
Figure 4.8 (a) Object pattern relative to <i>Avicennia germinans</i> within study site Lagoa A. (b) Object ring analysis (blue) and respective 90% simulation envelope (red) obtained via Monte Carlo Method (Besag 1977) for the Model I hypothesis with 200 simulations.	91
Figure 4.9 (a) Object pattern relative to <i>Laguncularia racemosa</i> within study site Lagoa A. (b) Object ring analysis (blue) and respective 90% simulation envelope (red) obtained via Monte Carlo Method (Besag 1977) for the Model I hypothesis with 200 simulations.	92
Figure 4.10 (a) Object pattern relative to small (dbh<5 cm) (red) and large (dbh \geq 5 cm) (blue) trees within study site Lagoa A. (b) Bivariate object ring analysis (blue) and respective 90% simulation envelope (red) obtained via Monte Carlo Method (Besag 1977) for the Model II hypothesis with 200 simulations.	92
Figure 4.11 (a) Object pattern relative to <i>Avicennia germinans</i> (red) and <i>Laguncularia racemosa</i> (blue) trees within study site Lagoa A. (b) Bivariate object ring analysis (blue) and respective 90% simulation envelope (red) obtained via Monte Carlo Method (Besag 1977) for the Model II hypothesis with 200 simulations.	93
Figure 4.12 Object pattern relative to small (dbh<5 cm) (red) and large (dbh \geq 5 cm) (blue) <i>Avicennia</i> trees within study site Lagoa A. (b) Bivariate object ring analysis (blue) and respective 90% simulation envelope (red) obtained via Monte Carlo Method (Besag 1977) for the Model II hypothesis with 200 simulations.	93
Figure 4.13 Object pattern relative to small (dbh<5 cm) (red) and large (dbh \geq 5 cm) (blue) <i>Laguncularia</i> trees within study site Lagoa A. (b) Bivariate object ring analysis (blue) and respective 90% simulation envelope (red) obtained via Monte Carlo Method (Besag 1977) for the Model II hypothesis with 200 simulations.	94
Figure 4.14 Histogram calculated for the R_{ZOI} distribution relative to (a) all trees, (b) small trees (dbh<5 cm), (c) large trees (dbh \geq 5 cm), (d) <i>Avicennia germinans</i> , (e) small <i>Avicennia</i> (dbh<5 cm), (f) large <i>Avicennia</i> (dbh \geq 5 cm), (g) <i>Laguncularia racemosa</i> , (h) small <i>Laguncularia</i> (dbh<5 cm) and (i) large <i>Laguncularia</i> (dbh \geq 5 cm).	96
Figure 4.15 (a) Object pattern relative to all trees within study site Lagoa B. (b) Object ring analysis (blue) and respective 90% simulation envelope (red) obtained via Monte Carlo Method (Besag 1977) for the	

Model I hypothesis with 200 simulations. 97

Figure 4.16 (a) Object pattern relative to *Avicennia germinans* within study site Lagoa B. **(b)** Object ring analysis (blue) and respective 90% simulation envelope (red) obtained via Monte Carlo Method (Besag 1977) for the Model I hypothesis with 200 simulations. 97

Figure 4.17 (a) Object pattern relative to *Laguncularia racemosa* within study site Lagoa B. **(b)** Object ring analysis (blue) and respective 90% simulation envelope (red) obtained via Monte Carlo Method (Besag 1977) for the Model I hypothesis with 200 simulations. 98

Figure 4.18 (a) Object pattern relative to small ($dbh < 5$ cm) (red) and large ($dbh \geq 5$ cm) (blue) trees within study site Lagoa A. **(b)** Bivariate object ring analysis (blue) and respective 90% simulation envelope (red) obtained via Monte Carlo Method (Besag 1977) for the Model II hypothesis with 200 simulations. 98

Figure 4.19 (a) Object pattern relative to *Avicennia germinans* (red) and *Laguncularia racemosa* (blue) trees within study site Lagoa A. **(b)** Bivariate object ring analysis (blue) and respective 90% simulation envelope (red) obtained via Monte Carlo Method (Besag 1977) for the Model II hypothesis with 200 simulations. 99

Figure 4.20 Object pattern relative to small ($dbh < 5$ cm) (red) and large ($dbh \geq 5$ cm) (blue) *Avicennia* trees within study site Lagoa A. **(b)** Bivariate object ring analysis (blue) and respective 90% simulation envelope (red) obtained via Monte Carlo Method (Besag 1977) for the Model II hypothesis with 200 simulations. 99

Figure 4.21 Object pattern relative to small ($dbh < 5$ cm) (red) and large ($dbh \geq 5$ cm) (blue) *Laguncularia* trees within study site Lagoa A. **(b)** Bivariate object ring analysis (blue) and respective 90% simulation envelope (red) obtained via Monte Carlo Method (Besag 1977) for the Model II hypothesis with 200 simulations. 100

Figure 5.1 Representation of the steps of our methodology. (left) Point Pattern \Rightarrow (middle) Density Map \Rightarrow (right) Multiresolution Analysis. 105

Figure 5.2 The Kernel Density Estimation method transforms a spatial point pattern (left) into a density map (right). The scale of the study site is provided in m and of the unity of the density map is points/ m^2 107

Figure 5.3 Characteristics of a Variogram. 108

Figure 5.4 The Multiresolution Decomposition Analysis performed to decompose a density map (left) in different scales (right). The unit of the study site is provided in m and of the density map is points/ m^2 108

Figure 5.5 The graphic **(a)** represents a time serie that contains a superposition of a low frequency signal ($\sin 10t$) and a high frequency signal ($\sin 20t$). The graphic **(b)** represents a time serie that contains a low frequency signal ($\sin 10t$) in the first half and a signal with high frequency signal ($\sin 20t$) in the second half. The graphics **(c)** and **(d)** represent the response of the **FT** to the time series represented at the graphics **(a)** and **(b)** respectively. The graphics **(e)** and **(f)** are represent the response of the **WT** to the time series represented at graphics **(a)** and **(b)** respectively. 109

Figure 5.6 The graphics **(a)**, **(b)** and **(c)** represent the same *mother wavelet* with parameter $\lambda = 1$, $\lambda = 0.5$ and $\lambda = 0.25$ respectively. 111

Figure 5.7 The graphics **(a)** and **(b)** represent the same *mother wavelet* with parameter $t = 0$ and $t = -0.25$ respectively. 111

Figure 5.8 MDA applied to a signal $f(t)$. A_1 is the approximation at level 1 and D_1 is the detail at level 1. 113

Figure 5.9 MDA applied to A_1 . A_2 is the approximation at level 2 and D_2 is the detail at level 2. 114

Figure 5.10 MDA at level n applied to a signal $f(t) = A_0$ 114

Figure 5.11 MDA applied to an image (density map). The original image (a density map) was decomposed at its higher, intermediate and lower scale components. 115

Figure 5.12 (a) Density map obtained from spatial point pattern relative to *Laguncularia racemosa* within stand Lagoa A. **(b)** and **(c)** are respectively the Histogram and the Variogram obtained from this density map in **(a)**. 117

Figure 5.13 (a) Approximation A1 relative to the density map at the Figure 5.13 . (b) and (c) are respectively the Histogram and the Variogram obtained from this density map in (a)	118
Figure 5.14 (a) Approximation A2 relative to the density map at the Figure 5.13a . (b) and (c) are respectively the Histogram and the Variogram obtained from this density map in (a)	118
Figure 5.15 (a) Approximation A3 relative to the density map at the Figure 5.13 . (b) and (c) are respectively the Histogram and the Variogram obtained from this density map in (a)	119
Figure 5.16 (a) Approximation A4 relative to the density map at the Figure 5.13a . (b) and (c) are respectively the Histogram and the Variogram obtained from this density map in (a)	119
Figure 5.17 (a) Point pattern relative to <i>Laguncularia racemosa</i> whit-in stand Lagoa A, now divided at two regions (red and yellow). (b) and (c) represents the the L-function (black) and 99% simulations interval (dashed red) calculated for the point pattern inside the red and yellow respectively. The simulations interval was calculated via Monte Carlo method (Besag 1977) for the CSR hypothesis with 10000 simulations.	120
Figure 5.18 (a) Density map obtained from spatial point pattern relative to <i>Laguncularia racemosa</i> within stand Lagoa B. (b) and (c) are respectively the Histogram and the Variogram obtained from this density map in (a)	121
Figure 5.19 (a) Approximation A4 relative to the density map at the Figure 5.18 . (b) and (c) are respectively the Histogram and the Variogram obtained from this density map in (a)	121
Figure 5.20 (a) Point pattern relative to <i>Laguncularia racemosa</i> whit-in stand Lagoa B, now divided at two regions (red and yellow). (b) and (c) represents the the L-function (black) and 99% simulations interval (dashed red) calculated for the point pattern inside the red and yellow respectively. The simulations interval was calculated via Monte Carlo method (Besag 1977) for the CSR hypothesis with 10000 simulations.	122
Figure 5.21 (a) Density map obtained from spatial point pattern relative to dead trees within stand Lagoa A. (b) and (c) are respectively the Histogram and the Variogram obtained from this density map in (a)	122
Figure 5.22 (a) Approximation A4 relative to the density map at the Figure 5.25a . (b) and (c) are respectively the Histogram and the Variogram obtained from this density map in (a)	123
Figure 5.23 (a) Point pattern relative to dead trees whit-in stand Lagoa B, now divided at two regions (red and yellow). (b) and (c) represents the the L-function (black) and 99% simulations interval (dashed red) calculated for the point pattern inside the red and yellow respectively. The simulations interval was calculated via Monte Carlo method (Besag 1977) for the CSR hypothesis with 10000 simulations.	123
Figure 5.24 (a) Density map obtained from spatial point pattern relative to <i>Avicennia germinans</i> within stand Lagoa A. (b) and (c) are respectively the Histogram and the Variogram obtained from this density map in (a)	124
Figure 5.25 (a) Density map obtained from spatial point pattern relative to <i>Laguncularia racemosa</i> within stand Lagoa A. (b) and (c) are respectively the Histogram and the Variogram obtained from this density map in (a)	125
Figure 5.26 <i>Avicennia germinans</i> (a) Approximation A4 relative to the density map at the Figure 5.24 . (b) and (c) are respectively the Histogram and the Variogram obtained from this density map in (a)	125
Figure 5.27 <i>Laguncularia racemosa</i> (a) Approximation A4 relative to the density map at the Figure 5.25 . (b) and (c) are respectively the Histogram and the Variogram obtained from this density map in (a)	126
Figure 5.28 (a) Approximation A4 relative to the density map obtained for the <i>Avicennia germinans</i> and (b) Approximation A4 relative to the density map obtained for the <i>Laguncularia racemosa</i> within Lagoa A.	126
Figure 5.29 (a) Density map obtained from spatial point pattern relative to <i>Avicennia germinans</i> within stand Lagoa B. (b) and (c) are respectively the Histogram and the Variogram obtained from this density map in (a)	127
Figure 5.30 (a) Density map obtained from spatial point pattern relative to <i>Laguncularia racemosa</i> within stand Lagoa B. (b) and (c) are respectively the Histogram and the Variogram obtained from this density map in (a)	127

Figure 5.31 *Avicennia germinans* (a) Approximation **A4** relative to the density map at the **Figure 5.29**. (b) and (c) are respectively the Histogram and the Variogram obtained from this density map in (a). 128

Figure 5.32 *Laguncularia racemosa* (a) Approximation **A4** relative to the density map at the **Figure 5.30**. (b) and (c) are respectively the Histogram and the Variogram obtained from this density map in (a). 128

Figure 5.33 (a) Approximation **A4** relative to the density map obtained for the *Avicennia germinans* and (b) Approximation **A4** relative to the density map obtained for the *Laguncularia racemosa* within Lagoa B. 129

Figure 5.34 Inhomogeneous L-function (black) and 90% simulations interval (dashed red) calculated for the *Laguncularia* trees inside Lagoa B. The simulations interval was calculated via Monte Carlo method (Besag 1977) for the inhomogeneous Poisson process hypothesis with 1000 simulations. 129

Figure 5.35 Inhomogeneous L-function (black) and 90% simulations interval (dashed red) calculated for the dead trees inside Lagoa B. The simulations interval was calculated via Monte Carlo method (Besag 1977) for the inhomogeneous Poisson process hypothesis with 1000 simulations. 130

List of tables

Table 1.1	Description of methods for analysis of spatial data. Adapted from Perry <i>et al.</i> (2002).	17
Table 2.1	Summary analysis using quadrat count methods applied to Lagoa A.	23
Table 2.2	Summary analysis using nearest neighbor methods applied to Lagoa A.	24
Table 2.3	Main characteristics of the null hypothesis of spatial independence and random labeling.	29
Table 2.4	Summary of K-function analysis applied to study site Lagoa A. The scale is meter.	30
Table 2.5	Edge correction factor $w_i(r)$ for the 4 possibilities presented in Figure 2.6 .	33
Table 2.6	Relationship between the time processing for the <i>Ripley's method</i> (t_1) and for the <i>Area's method</i> (t_2). The time is given in seconds.	34
Table 2.7	CSR model with 200 points representing a low density scenario and 800 points representing a high density scenario. Summary of the statistical results for the deviance factors D_R and D_A obtained from 10000 simulations.	39
Table 2.8	Summary of the statistical results of the deviance factor D_R and D_A calculated for the region Ω_g obtained from 10000 simulations. A regular model with 200 points and parameter $r = 0.01, 0.03$ and 0.05 representing a low density scenario and a regular model with 800 points and parameters $r = 0.01, 0.03$ and 0.05 representing a high density scenario.	40
Table 2.9	Summary of the statistical results of the deviance factor D_R and D_A calculated for the region Ω_g obtained with 10000 simulations. A clumped model with 200 points and parameter $c = 0.05, 0.08$ and 0.01 representing a low density scenario and a regular model with 800 points and parameters $r = 0.01, 0.03$ and 0.05 representing a high density scenario.	40
Table 2.10	Deviance factor D_R and D_A obtained for the study site Lagoa A.	41
Table 3.1	Summary of underlying process and an possible associated spatial point pattern. (+) Positive and (-) negative interaction.	48
Table 3.2	Characteristics of propagules of three mangrove species (adapted from Rabinowitz 1978). (S) Salt water conditions and (F) Fresh water conditions.	51
Table 3.3	Ecological Characteristics of various mangrove species. "Salinity" in ($^0/_{00}$). MS = Maximum pore water salinity measured in the fields at sites where the species was growing, OG = Salinity for optimum growth based on culture studies. Adapted from Smith III (1991).	52
Table 3.4	A preliminary model of stand development in mangroves. The forest collapses with "senescence" when the cycle resumes with re-colonization. Adapted from Duke (2001), Silvertown & Doust (1993) and Menezes <i>et al.</i> (2004).	52
Table 3.5	Short statistical summary of the mean stem diameter in breast height (dbh) for Lagoa A site. (-) There's no information about the dead trees's dbh. (*) Excluding the dead trees. (dbh in cm).	55
Table 3.6	Summary of the univariate L-function analysis obtained for the site Lagoa A. (*) tendency and (**) in particular. LS (Lower Scales), IS (Intermediate Scales) and HS (Higher Scales).	63
Table 3.7	Summary of the univariate and bivariate L-function analysis obtained for the site Lagoa A. small = (dbh ≤ 5 cm) and large = (dbh > 5 cm). (*) tendency and (**) in particular. LS (Lower Scales), IS (Intermediate Scales) and HS (Higher Scales).	64
Table 3.8	Short statistical summary of the mean stem diameter in breast height (dbh) for Lagoa B site. (-) There's no information about the dead trees's dbh. (*) Excluding the dead trees. (dbh in cm).	66
Table 3.9	Summary of the univariate L-function analysis obtained for the site Lagoa B. (*) tendency and (**) in particular. LS (Lower Scales), IS (Intermediate Scales) and HS (Higher Scales).	76

Table 3.10 Summary of the univariate and bivariate L-function analysis obtained for the site Lagoa B. small = (dbh \leq 5 cm) and large = (dbh > 5 cm). (*) tendency and (**) in particular. LS (Lower Scales), IS (Intermediate Scales) and HS (Higher Scales).	76
Table 4.1 Interpretation of the $K_c(r)$ function.	85
Table 4.2 Interpretation of the $L_c(r)$ function.	85
Table 4.3 Interpretation of the function $R_\varepsilon(r)$	86
Table 4.4 Interpretation of the function $\bar{R}_\varepsilon(r)$	86
Table 4.5 Interpretation of the function $\bar{R}_\varepsilon^B(r)$	88
Table 4.6 Basic statistics for Lagoa A. \bar{R}_{ZO1} , $\min(\bar{R}_{ZO1})$ and $\max(\bar{R}_{ZO1})$ in m and $\text{var}(\bar{R}_{ZO1})$ in m^2	89
Table 4.7 Basic statistics for Lagoa B. \bar{R}_{ZO1} , $\min(\bar{R}_{ZO1})$ and $\max(\bar{R}_{ZO1})$ in m and $\text{var}(\bar{R}_{ZO1})$ in m^2	95

Chapter 1

Introduction

The spatial structure of a forest stand is of fundamental importance for forest dynamics, because the local environment determines competition among the trees, growth, death and regeneration (see **Figure 1.1**). Furthermore, the spatial configuration of individual trees in a forest stand may provide an indirect indication of the underlying ecological processes that are occurring at the site (Malkinson et al. 2003). Analysis of the spatial configuration of the trees in a stand is of prime importance, for example, for the development of individual tree growth models (Goreaud et al. 1996) and to gain an understanding of ecological systems and the dynamics of plant communities (Greig-Smith 1964, Young et al. 1999). In summary, the spatial configuration of individuals could be a result of the natural processes occurring in the stand.

In the literature, a large number of spatial statistical methods have been described that could be applied to spatial pattern analysis. The principal aim of this study is to apply, modify and improve these methods in order to determine and to analyze the spatial structure of tree individuals in a forest stand.

In **Chapter 2**, I present some classical spatial statistical methods currently applied to plant ecology, such as: quadrat count methods, first order methods and second order methods (in particular, the well-known Ripley K-function). They are suitable for the analysis of spatial configurations and distribution patterns of individuals, such as plants or trees.

Additionally, I present some explicit formulas for an area-based edge effect correction method (hereinafter Area method). There are some references to this method in the literature, but the explicit formulas are absent or incompletely described. The edge effect correction factor is an essential part of those spatial statistical methods that require the counting of neighbors within a given distance (Goreaud & Pelissier 1999). An appropriate edge correction can improve the stability of the results obtained from spatial statistical methods and increase the sensitivity of the spatial statistical tests (Yamada & Rogerson 2003). A number of edge corrections methods are discussed in literature; I compare the Area method which is the principal focus of this study with another widely used method, the so called Ripley edge correction method (hereinafter Ripley method).

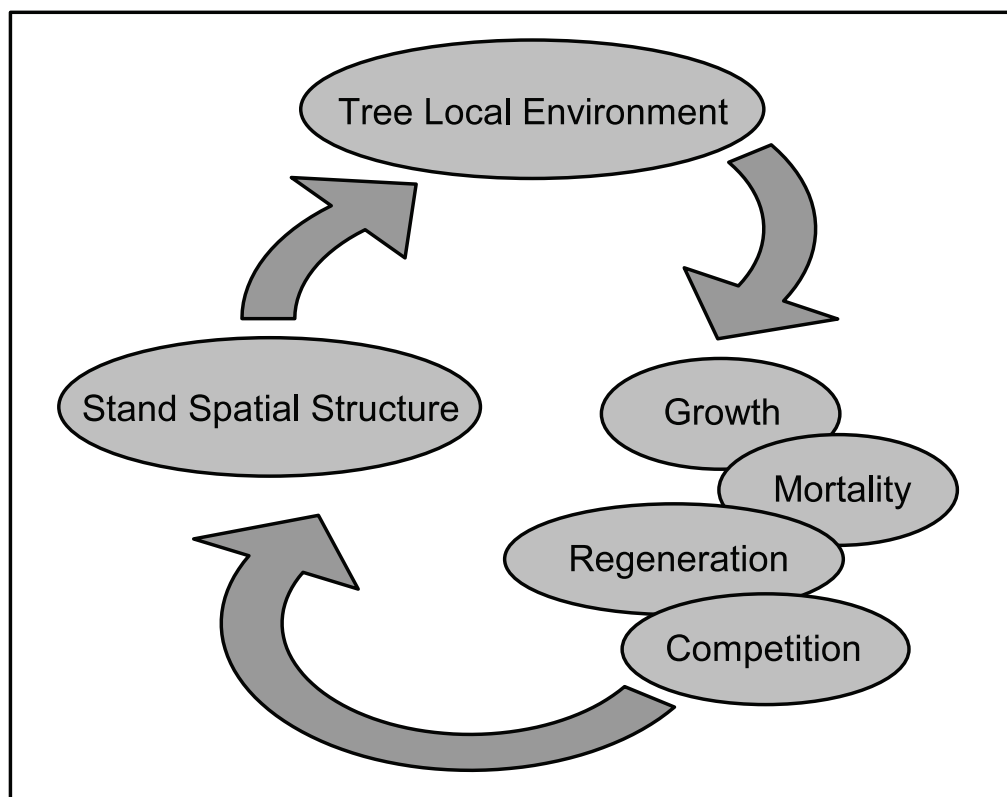


Figure 1.1. Interaction between stand spatial structure, tree local environment and natural processes. Adapted from (Goreaud *et al.* 1998)

The aim is to find out which edge correction method produces the better results and is easier to implement. The aim is to find out which edge correction method produces the best results and is easiest to implement.

The **Chapter 3** is a direct application of the methods presented in **Chapter 2**. I apply the Ripley K-function in combination with the Area method in order to analyze the spatial configuration of the trees at two study sites located in Northwestern Brazil. This dataset is used through the study. It is hoped by this means to obtain indirect information about the underlying ecological processes which might be giving rise to the spatial pattern of the trees observed in these sites.

It is important to list at least two limitations of the methods presented in **Chapter 2** and **Chapter 3**. First of all, they require the homogeneity of the spatial point pattern being analyzed. The hypothesis of homogeneity means that the point pattern is stationary (invariant under translation) and isotropic (invariant under rotation). However, it is well-known that heterogeneity is generally common in the nature. In summary, the second-order features of the point pattern depends only on the distance between the points, but not on direction or location (Goreaud *et al.* 1996, Wiegand & Moloney 2004). Additionally, the classical methods consider a three dimensional tree as a point. This abstraction is also

a limitation, because it can lead to misinterpretation of the ecological processes that are occurring in the stands.

To overcome this limitation, I develop a new method for the spatial analysis of objects in **Chapter 4**, which approximates each individual tree as a circle, instead as a point. The idea of this method is to minimize the bias of the classical methods presented in **Chapter 2**, which consider a real tree as a point. I then test this method by applying it to the same dataset analyzed in **Chapter 3**.

It is important to note that all methods presented in **Chapter 2** and also in **Chapter 4** have a common limitation. They neglect information about the spatial configuration of the individuals. These methods (under the hypothesis of homogeneity) are able to distinguish whether a point pattern or a pattern of objects tends towards complete spatial randomness, or towards a clumped or regular distribution and at which scale these characteristics occur, but they are not able to provide information about the spatial location of these features.

Finally in **Chapter 5**, I propose a new methodology that provides spatial-scale information (subject to certain restrictions) about the spatial processes occurring in a forest stand. The main idea is to adapt the Wavelet Transformation method (hereinafter **WT**) so that this can be used for the spatial analysis of point patterns and apply this methodology to plant ecology. In summary, the methodology consists in transforming a point pattern into a density map using a Kernel density estimation method (hereinafter **KDE**) and decompose this map at different scales using Multiresolution Decomposition Analysis (hereinafter **MDA**) obtained via **WT** method. Finally, I compare these results with the results obtained in **Chapter 3** and **Chapter 4** in order to demonstrate the power of for studying vegetation patterns. In **Table 1.1** I present a short summary of the principal characteristics of the statistical methods applied in this study. Additionally, in **Figure 1.2** I present a general description of the structure of the thesis.

Method	Data Type	Original Use	Scale Resolution	Spatial Resolution	Hypothesis Test
Quadrat Counts	(x, y)	Plant Ecology	no	no	no
Nearest Neighbor	z	Plant Ecology	no	no	yes
Ripley K-function	(x, y)	Plant Ecology	yes	no	yes
Variogram	(x, y, z)	Earth Sciences	yes	no	no
Wavelet Transform	(x, y, z)	Mathematics	yes	yes	possible

Table 1.1. Description of methods for analysis of spatial data. Adapted from Perry *et al.* (2002).

All graphic figures presented in this work were created using the software R, a language and environment for statistical computing and graphics. It is a GNU Project which is similar to the S language and environment which was developed at Bell Laboratories (formerly AT&T, now Lucent Technologies) by John Chambers and colleagues. The algorithms were implemented using the applications R, Scilab (a scientific software package for numerical computation providing a powerful open computing environment for engineering and scientific applications) and Intel Fortran Compiler 9.1 for Linux.

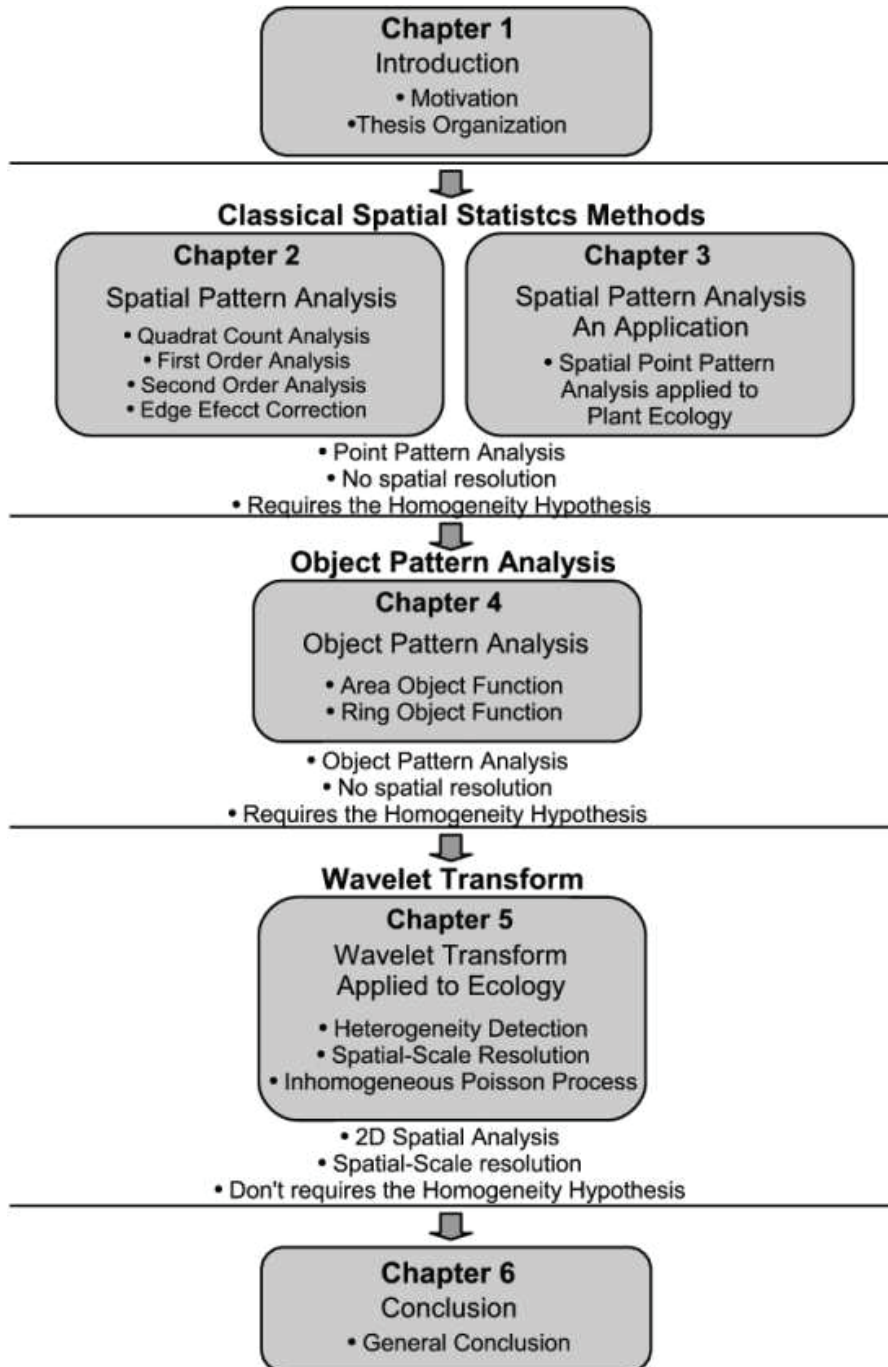


Figure 1.2. Thesis structure.

Chapter 2

Spatial Pattern Analysis

2.1 Introduction

Spatial point pattern analysis is a set of tools used to study the distribution of discrete points. It is a statistical method applied to obtain and to analyze information about the spatial structure of individuals dispersed within a study area. The idea is to distinguish between point patterns which tend toward complete spatial randomness (hereinafter CSR), clumping or regularity (see **Figure 2.1**) and at which scale these characteristics occur.

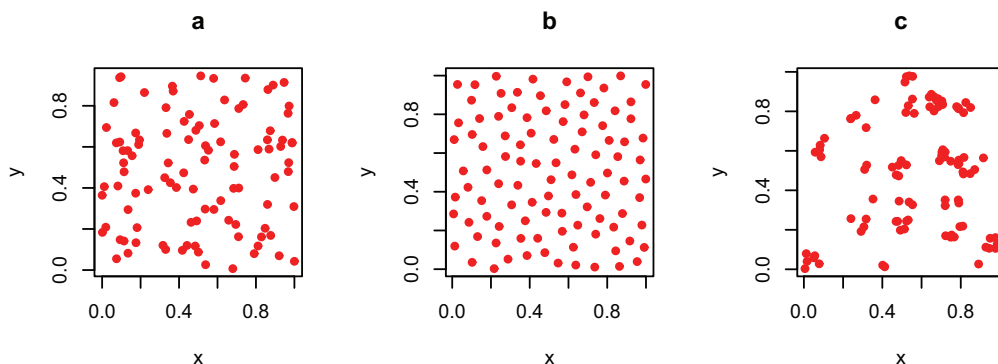


Figure 2.1. Three point patterns with 100 points representing a (a) CSR pattern, (b) regular pattern and (c) cluster pattern.

Stand spatial structure is a complicated concept that includes both horizontal and vertical use of space by trees. In order to simplify this approach, I consider only on the horizontal location of stems in the stand. Thus, the study area is represented by a part of the horizontal plane bounded by the stand borders, and each individual plants is mapped as a point in whose position is shown by the Cartesian coordinates (x, y) . This simplification or abstraction of the study area reduces it to a finite set of points, called point pattern. This “point process” representation of the stand permits us to describe and analyze point patterns, with the aim of determining global properties (laws) in the random locations of trees in the stand (Goreuad 1997).

A point process P is a random process, a mathematical object similar to random variable, whose realizations are point patterns. It generates random point patterns that share the same spatial structure, such as CSR, regular and clustered patterns. The properties of the process define constraints on its realizations (for example, in terms of density, distance between neighboring points, and structure). The main idea is to assume that there exists an underlying process P and to use the properties of that process to describe the structure of the pattern (Goreaud 1999).

2.2 Methods

Now I present some spatial statistical methods in order to analyze the spatial configuration of the trees within a study site named Lagoa A. It is located on the coast of the northeastern Brazilian State of Para, near the town of Bragança at a latitude and longitude of approximately (01 03' S, 46 45' W), (Mehlig 2001). This area is located on the Acarao Peninsula on the estuary of Caete River, 150 km south of the Amazon delta in northern Brazil (Berger et al. 1999). It forms part of the world's second largest continuous area of mangrove forest, estimated to cover a total area of 1.38 million ha along a coastline of ca. 6800 km (Kjerve et al. 1993).

Applying the “point process” representation to the study site Lagoa A, each tree individual is represented by its spatial position inside the stand (see **Figure 2.2**), species and radius at breast height in cm (exception for the dead trees). To avoid misunderstanding, it is important to explain the notation used in this chapter. “Location” means a position (x, y) inside the study area and “point” means an arbitrary point $p_i = (x_i, y_i)$ of the point pattern within the area.

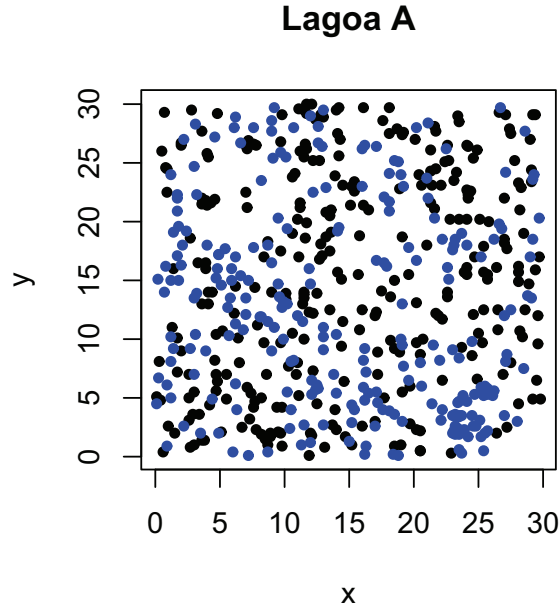


Figure 2.2. Study area Lagoa A with 560 trees. (black dot) *Avicennia germinans* and (blue dot) *Laguncularia racemosa*. The axis x and y are given in m.

2.2.1 Quadrat counts analysis

The quadrat count method is one of the early methods of spatial point pattern analysis. The basic procedure is to sample the study site using randomly located quadrates (e.g., a search circle of radius r centered inside the study area) and to count the number of points (representing each individual of the stand) that lies inside each one.

Under a hypothesis of CSR, the distribution of the number of points inside a quadrat with area a is given by a Poisson series with mean λa , where λ is the intensity of the point pattern inside the whole study area and it is estimated as

$$\lambda = \frac{n}{A}, \quad (2.1)$$

where A and n are respectively the area and the number of points of the study area.

The probability of encountering n points inside a quadrat with area a is given by

$$\Pr(N(a) = n) = e^{-\lambda a} \frac{(\lambda a)^n}{n!}. \quad (2.2)$$

To compare the observed values with the expected values, I need to perform a χ^2 test of significance. In this case, point clustering would be evidenced by counts that occurred more often than expected and regularity would be evidenced by counts that occurred less than expected.

2.2.1.1 Quadrat count indices

There are a number of indices described in the literature that could be used with the quadrat count method to detect a significant deviation from a CSR pattern (a Poisson distribution). The simplest and probably the oldest of these was developed by Fisher *et al.* (1922). It is defined as

$$I_1 = \frac{V}{\bar{X}}, \quad (2.3)$$

where V and \bar{X} are the sample variance and the sample mean of the quadrat counts respectively. The method is based on fact that the mean and the variance of a Poisson distribution are the same, thus the expected value of the indices under CSR hypothesis is $I_1 = 1.0$, $I_1 > 1.0$ if I have a clumped pattern and $I_1 < 1.0$ if I have a regular or a CSR pattern.

A further index was developed by Douglas (1975) and it is defined as

$$I_2 = \frac{\bar{X}^2}{V^2 - \bar{X}}, \quad (2.4)$$

where V and \bar{X} are defined as above. If I consider that the number of points inside a quadrat has a Poisson distribution with mean $\mu = \lambda a$ (where a is the area of the quadrat), then I_2 is equal to μ for large sample sizes.

A number of other indices have been described (David & Moore 1954, Lloyd 1967, Morisita 1959). For a review, see Cressie (1993).

2.2.1.2 Quadrat counts method applied to study site Lagoa A

I apply the quadrat count method to the study site Lagoa A to quadrats with dimensions 1 x 1 m (analysis at small scale), 3 x 3 m (analysis at intermediate scale) and 5 x 5 m (analysis at large scale) randomly dispersed inside this study area. The results of the analysis obtained for each scale are summarized in table below.

Quadrat Counts Analysis Lagoa A ($\lambda = 0.622$)						
Quadrat	Scale	a	I_1	I_2	$\mu = \lambda a$	Interpretation
1 x 1 m	small	1	1.175	0.798	0.622	clustering
3 x 3 m	intermediate	9	1.223	5.823	5.598	clustering
5 x 5 m	large	25	2.004	16.599	15.55	clustering

Table 2.1. Summary analysis using quadrat count methods applied to Lagoa A.

The results presented in **Table 2.1** shown that $I_1 > 1.0$ and $I_2 > \mu$ at all scales analyzed. It means that the point pattern shows clustering at different scales.

2.2.2 First-order analysis

Intensity λ (or density) is the simplest first order property of a point process. If I consider a homogeneous point pattern (if it is invariant under translation and rotation), λ is a constant and can be estimated by $\hat{\lambda} = n/A$, where n and A are respectively the number of points and the area of the study site.

To introduce the concept of local density, I define $c_{(x,y)}(r)$ as a circle with radius r centered on a location (x, y) inside of the study site. Then the local density in a neighborhood r of a location (x, y) of the study site can be estimated by

$$\hat{\lambda}_{x,y}(r) = \frac{N[c_{x,y}(r)]}{\pi r^2}, \quad (2.5)$$

where $N[c_{x,y}(r)]$ is the number of points inside $c_{x,y}(r)$.

2.2.2.1 Nearest neighbor methods

Nearest neighbor methods are based on the first-order property of a point process. They are based on the distance between a point and its nearest neighbor. The basic procedure of these methods is to estimate the mean point density $\hat{\lambda}$ (points per unit area) using information about the mean point-to-point distance. Then this estimated point density $\hat{\lambda}$ is compared with the expected point density λ to classify the point pattern as clumped, regular or CSR.

An advantage of these methods in comparison to quadrat count methods is that they make use of precise information about the locations of the points and do not depend on the size or shape of the quadrats (Cressie 1993).

The simplest index attributed to Fischer *et al* (1922) is defined as

$$I_3 = \frac{\text{Var}(d)}{\bar{d}}, \quad (2.6)$$

where d is the nearest neighbor distance over all points of the point pattern and \bar{d} is the mean nearest-neighbor distance defined as

$$\bar{d} = \frac{1}{n} \sum_{i=1}^n d_i, \quad (2.7)$$

where n is the number of points inside the study site and d_i is the nearest neighbor distance for point i inside the study site. The expected value of the index is 1 for a random pattern, $I_3 > 1$ indicates clustering and $I_3 < 1$ indicates regularity.

Another index was developed by Clark and Evans (1954) and it is defined as

$$I_4 = \frac{\bar{d}}{\frac{1}{2\sqrt{\lambda}}}, \quad (2.8)$$

where \bar{d} is as defined in equation (2.6), the denominator $\frac{1}{2\sqrt{\lambda}}$ is the expected mean nearest-neighbor distance under CSR assumption and λ is the density of the points inside the whole study site. Further indices can be founded in the literature, see Cressie (1993).

2.2.2.2 Nearest neighbor methods applied to study site Lagoa A

I now apply the nearest neighbor method to the study site Lagoa A. The results of the analysis obtained for each index are summarized in table below.

Nearest Neighbor Analysis Lagoa A ($\lambda = 0.622$)		
Indices	Result	Interpretation
I_3	3.565	clustering
I_4	1.124	clustering

Table 2.2. Summary analysis using nearest neighbor methods applied to Lagoa A.

The results presented in **Table 2.2** show that I_3 and $I_4 > 1.0$. This indicates that the point pattern presents clustering.

2.2.3 Second-order analysis

The second order property of a point pattern is related to the density of occurrence of two points within a given distance from each other (Ripley 1977, Diggle 1983). This property characterizes the number of points found in the neighborhood of an arbitrary point of the pattern and permits the spatial structure of these points to be described in terms of interaction processes: aggregation, repulsion, etc ... (Pelissier & Goreud 2001).

To calculate second order local neighbor density, I define $c_i(r)$ as a circle with radius r centered on a point p_i . Then the second order local neighbor density in a neighborhood r of an arbitrary point p_i of the pattern can be estimated by

$$\hat{\lambda}_i(r) = \frac{N[c_i(r)]}{\pi r^2}, \quad (2.9)$$

where $N[c_i(r)]$ corresponds to the number of points within $c_i(r)$.

2.2.3.1 Ripley's K-function

The Ripley K-function is a second order method based on distances between all pairs of points of the pattern. The advantage of this method in comparison to others (Quadrat Count Methods and First Order Analysis) is that it preserves information about distances between all points in the pattern. It can be used to analyze a point pattern at a range of scales and to determine at which scales these points tend to be regular, clumped or CSR. It can also be used to describe the relationship between one, two or more types of points contained inside the point pattern.

The general definition of the Ripley's K-function for a certain distance r is

$$K(r) = \lambda^{-1} \mathbf{E}[r], \quad (2.10)$$

where $\mathbf{E}[r]$ is the expected number of points within a distance r from an arbitrary point of the study region Ω and λ is the density of points inside this area estimated as

$$\hat{\lambda} = \frac{n}{A}, \quad (2.11)$$

where n and A are the number of points inside and the area of the study region Ω , respectively.

The K-function is defined so that $\lambda K(r)$ is the expected number of points contained at distance r from an arbitrary point of the pattern inside Ω . In practice, the univariate K-function (where only one type of point is being considered) is estimated as

$$\hat{K}(r) = \frac{A}{n^2} \sum_{i=1}^n \sum_{j \neq i}^n w_{ij}(r) \delta_{ij}(r), \quad (2.12)$$

where $w_{ij}(r)$ is an edge effect correction factor, $\delta_{ij}(r)$ is an indicator function which defines whether a point p_j is inside a neighborhood r of a point p_i or not and is defined as

$$\delta_{ij}(r) = \begin{cases} 1, & \text{if } d_{ij} \leq r \\ 0, & \text{otherwise} \end{cases}, \quad (2.13)$$

with

$$d_{ij} = \sqrt{(x_i - x_j)^2 + (y_i - y_j)^2}, \quad (2.14)$$

being the Euclidian distance between the points $p_i = (x_i, y_i)$ and $p_j = (x_j, y_j)$ within the study region Ω .

An advantage of the K-function is that calculated values are independent of the shape of the study region, providing that adequate adjustments are made for edge effects (Cressie 1991). Furthermore, an appropriate edge effect correction factor can improve the sensibility of the statistical results in the sampling data and can increase the power of the statistical tests (Yamada & Rogerson 2003).

Because of its hyperbolic behavior, the interpretation of K-function is not straightforward. For this reason, a modification called L-function has been proposed to normalize it (Besag 1977),

$$\hat{L}(r) = \sqrt{\frac{\hat{K}(r)}{\pi}} - r. \quad (2.15)$$

The expected value of the univariate L-function under CSR is 0 for all r , positive when the pattern tends to be clustered and negative when the patterns tends to be regular

The bivariate K-function is used to analyze the spatial relation between two or more different type of points. First, I have to define

$$\hat{K}_{12}(r) = \frac{A}{n_1 n_2} \sum_{i=1}^{n_1} \sum_{j \neq i}^{n_2} w_{ij}(r) \delta_{ij}(r), \quad (2.16)$$

where $w_{ij}(r)$ is an edge effect correction factor, $\delta_{ij}(r)$ is an indicator function which defines whether a point p_j of type 2 is inside a neighborhood r of a point p_i of type 1 or not and it is defined as

$$\delta_{ij}(r) = \begin{cases} 1, & \text{if } d_{ij} \leq r \\ 0, & \text{otherwise} \end{cases}, \quad (2.17)$$

with

$$d_{ij} = \sqrt{(x_i - x_j)^2 + (y_i - y_j)^2}, \quad (2.18)$$

being the Euclidian distance between the points $p_i^1 = (x_i, y_i)$ of type 1 and $p_j^2 = (x_j, y_j)$ of type 2 within the study region Ω . The associated L-function is defined as

$$\hat{L}_{12}(r) = \sqrt{\frac{\hat{K}_{12}(r)}{\pi}} - r. \quad (2.19)$$

The expected value of the bivariate L-function under spatial independence is 0 for all r , positive when the two point processes tends to be aggregated and negative when the two point processes tends to be repulsive.

Similarly, I define the function

$$\hat{K}_{21}(r) = \frac{A}{n_1 n_2} \sum_{i=1}^{n_2} \sum_{j \neq i}^{n_1} w_{ij}(r) \delta_{ij}(r), \quad (2.20)$$

where $w_{ij}(r)$ is an edge effect correction factor, $\delta_{ij}(r)$ is an indicator function which defines whether a point p_j of type 1 is inside a neighborhood r of a point p_i of type 2 or not and it is defined as

$$\delta_{ij}(r) = \begin{cases} 1, & \text{if } d_{ij} \leq r \\ 0, & \text{otherwise} \end{cases}, \quad (2.21)$$

with

$$d_{ij} = \sqrt{(x_i - x_j)^2 + (y_i - y_j)^2}, \quad (2.22)$$

being the Euclidian distance between the points $p_i^1 = (x_i, y_i)$ of type 1 and $p_j^2 = (x_j, y_j)$ of type 2 within the study region Ω , and the its associated L-function is defined as

$$\hat{L}_{21}(r) = \sqrt{\frac{\hat{K}_{21}(r)}{\pi}} - r. \quad (2.23)$$

Then the bivariate K-function is defined as

$$\hat{K}_B = \frac{n_1 \hat{K}_{21} + n_2 \hat{K}_{12}}{n_1 + n_2}, \quad (2.24)$$

and its linearization is defined as

$$\hat{L}_B = \sqrt{\frac{\hat{K}_B(r)}{\pi}} - r. \quad (2.25)$$

The bivariate K-function is defined so that $\lambda \hat{K}_B(r)$ is the expected number of points of type 2 contained at the distance r of an arbitrary point of type 1 of the point pattern.

2.2.3.2 Simulations interval

The estimators of the second order functions are random variables with certain variance and in order to test the null hypothesis of a CSR pattern using real data, I have to take this uncertainty into account. In our case, I used the Monte Carlo method to estimate these variations (Besag & Diggle 1977) and to generate the confidence interval.

The methods applied to calculate the confidence interval for the univariate K-function and the bivariate K-function are completely different and will be explained below.

Univariate K-function

In order to test the deviation from randomness (regularity or clustering) of the point pattern using the univariate K-function, I computed a 99% confidence interval of $L(r)$ using the Monte Carlo method (Besag & Diggle 1977) from 1000 simulated CSR patterns with the same number of points contained inside a region with the same geometry. If the L-function intercepts the lower bounds of confidence interval and/or the upper bounds of the confidence interval I have an indication of regularity and/or clustering respectively.

In **Figure 2.3** I show examples of the interpretation of the univariate K-function applied to three different point pattern models, each containing 50 points: a CSR pattern, a regular pattern and a clumped pattern.

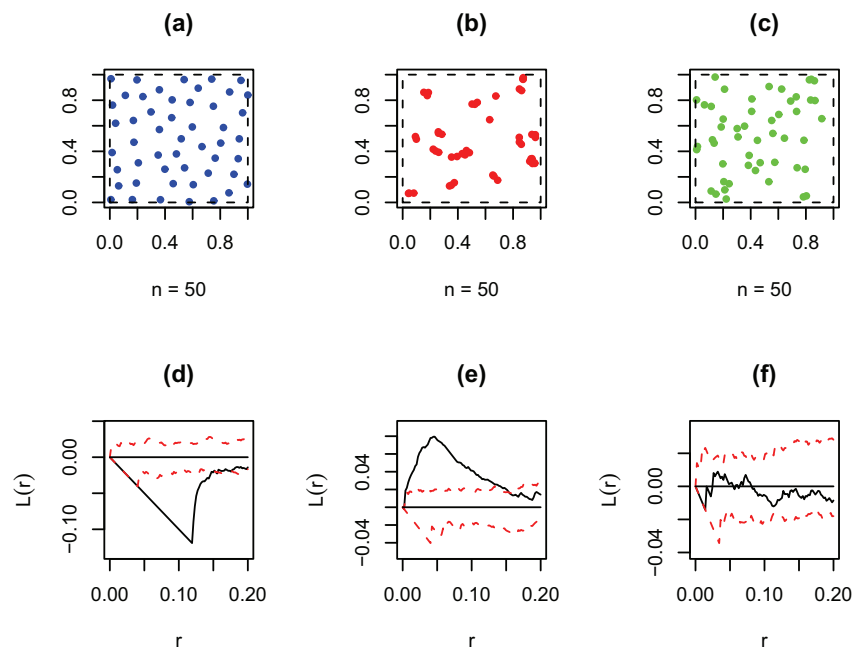


Figure 2.3. (a) Regular pattern with 50 points, (b) cluster pattern with 50 points and (c) CSR pattern with 50 points and (d), (e) and (f) are their respective L-function (black) and 99% confidence interval (dashed red). The confidence interval was calculated via Monte Carlo method (Besag 1977) for the CSR hypothesis with 10000 simulations.

Bivariate K-function

The generation of the simulation envelopes for the bivariate case is more complicated; for details of the methodology, see Goreaud & Pelissier (2003).

Basically, in order to generate the correct simulation envelope for the bivariate case, I have to choose one of two different null hypotheses: independence or random labeling.

The independence hypothesis must be chosen if the location of the points of type 1 and type 2 results from two *a priori* independent spatial point processes. In this case the location of the type 1 points is independent from the location of the type 2 points.

In order to generate the simulation envelope that corresponds to the hypothesis of spatial independence, I have to hold the point pattern of the points of type 1 and type 2 unchanged and randomize their relative position in each Monte Carlo simulation. For more details, see Lotwick & Silverman (1982), Diggle (1983) and Goreaud & Pelissier (2003).

The random labeling hypothesis must be chosen if the location of the points of type 1 and type 2 is result of events affecting *a posteriori* individuals of a single population. It means that the probability that one event occurs is the same for all points and does not depends on neighbor the identity of the neighboring point (Goreaud & Pelissier 2003).

In order to generate the simulation envelope that corresponds to the hypothesis of random labeling, I have to simulate point processes with the same observed spatial structure considering all points without type distinction. Then I hold the simulated pattern and simulate the point types in the same proportion as that observed in the study area. For more details, see Diggle (1983) and Goreaud & Pelissier (2003).

In **Table 2.3** I present a summary of the main characteristics of the null hypothesis applied to bivariate K-function.

General Framework		Independence	Random labeling
Null hypothesis		$L_B(r) = 0$	$L_B(r) = L(r)$
Aggregation		$L_B(r) > 0$	$L_B(r) > L(r)$
Repulsion		$L_B(r) < 0$	$L_B(r) < L(r)$
Simulation procedure	Random shifting of type 1 points		Random attributions of marks
Biological example	Between species or cohorts interaction		Disease attack or disturbances

Table 2.3. **Table 2.3** Main characteristics of the null hypothesis of spatial independence and random labeling.

Figure 2.4 show an example of the an application of the bivariate K-function applied to the stand Lagoa A. In **Table 2.5** I present a summary of the results presented in **Figure 2.4**.

K-function analysis		
Point Patter	Regularity	Clustering
Laguncularia	-	$1 < r < 9$
Avicennia	-	$r \simeq 1$
Laguncularia & Avicennia	$r < 4$	-

Table 2.4. Summary of K-function analysis applied to study site Lagoa A. The scale is meter.

The univariate analysis of the point pattern that represents *Laguncularia* trees shows clustering at different scales, $1 \text{ m} < r < 8 \text{ m}$. The univariate K-function analysis applied to *Avicennia* shows clumping at scale $r \simeq 1$ meter. But it is important to notice that a repulsion pattern exists between the *Laguncularia* and *Avicennia* trees at scale $r < 2 \text{ m}$. In summary, the trees of the same species tend to occupy the same area and the trees of different species tends to avoid each other.

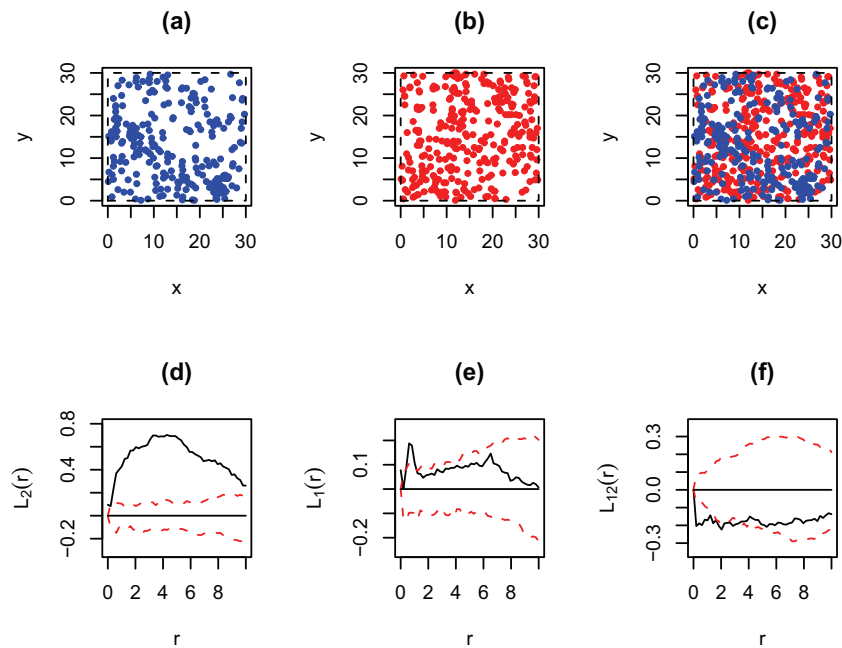


Figure 2.4. Study site Lagoa A. (a) *Avicennia*, (b) *Laguncularia*, (c) *Avicennia* (blue) and *Laguncularia* (red). (d) and (e) are the univariate L-function (black) and 99% simulation envelope for CSR hypothesis (dashed red) for the point pattern in (a) and (b) respectively. The univariate simulation envelope was calculated via Monte Carlo method (Besag 1977) with 1000 simulations. (f) Bivariate K-function (black) and its simulation envelope for independence hypothesis (dashed red) calculated for the point pattern contained in (c). The bivariate simulation envelope was calculated via random shifting method (Lotwick & Silverman, Diggle 1983) with 1000 simulations.

2.2.4 Edge effects

The edge effect problem usually occurs when it is necessary to count the number of points within a search circle $c_i(r)$ that intercepts the edges of the study area (see **Figure 2.5**). This search circle has a radius r and is centered at a point p_i located inside a study area Ω . It has two distinct parts $c_i^+(r)$ and $c_i^-(r)$, that respectively mark the regions of the search circle which belong or do not belong to Ω .

Usually, there is no information about the number of points within $c_i^-(r)$. However, if these points are not considered, $c_i(r)$ contains fewer points than expected. The purpose of edge effect correction factor is to minimize this effect. An alternative is to estimate the number of points within $c_i^-(r)$ using the information of the number of points within $c_i^+(r)$.

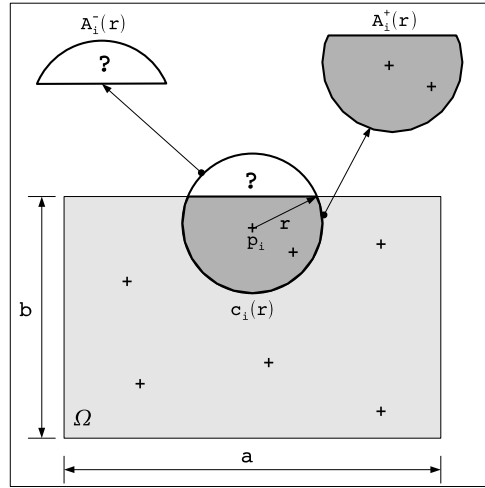


Figure 2.5. Study area Ω with dimensions $[0, a] \times [0, b]$ and a search circle $c_i(r)$ with radius r centered on a point p_i within this region. $A_i^-(r)$ and $A_i^+(r)$ are the area of the region of $c_i(r)$ outside and inside Ω respectively.

In what follows I present some explicit formulas for an area based edge effect correction method (hereinafter Area method). Some articles refer to this method (Getis & Franklin 1987, Besag 1977, Dale & Powell 2001), but details of the corresponding formulas are missing or incomplete.

Let define the total number of points within $c_i(r)$ as

$$N_i(r) = N_i^+(r) + N_i^-(r) \quad (2.26)$$

where $N_i^+(r)$ and $N_i^-(r)$ are the number of points within $c_i^+(r)$ and $c_i^-(r)$ respectively. By similarity, the total area of the circle $c_i(r)$ can be defined as

$$A_i(r) = A_i^+(r) + A_i^-(r) = \pi r^2 \quad (2.27)$$

where $A_i^+(r)$ and $A_i^-(r)$ are the areas of the regions $c_i^+(r)$ and $c_i^-(r)$ respectively (see **Figure 2.5**).

Furthermore, I suppose that the point density within $c_i^-(r)$ is equal to the point density within $c_i^+(r)$. Using this argument and the density definition, it follows that

$$\frac{N_i^-(r)}{A_i^-(r)} = \frac{N_i^+(r)}{A_i^+(r)} \Rightarrow N_i^-(r) = \frac{A_i^-(r)}{A_i^+(r)} N_i^+(r), \quad (2.28)$$

and combining the equations (1.26), (1.27) and (1.28), $N_i(r)$ can be estimated as

$$N_i(r) = \frac{A_i(r)}{A_i^+(r)} N_i^+(r) = w_i(r) N_i^+(r), \quad (2.29)$$

with $w_i(r)$ being an area based edge effect correction factor (hereinafter area correction factor).

The area correction factor depends on the relative position of the point p_i inside the study region Ω and on the radius of the search circle $c_i(r)$. This feature permits us to redefine the K-function in equation (2.3) as

$$K(r) = \frac{A}{n^2} \sum_{i=1}^n w_i(r) \sum_{j \neq i}^n \delta_{ij}(r). \quad (2.30)$$

This alteration significantly reduces the number of operations needed for the calculation of the K-function and consequently reduces the time needed to carry out the analysis, but without compromising its precision.

2.2.4.1 Area based edge effect correction method

The explicit formulae for the Area method are when the study region Ω is with rectangular and the radius of the search circle $c_i(r)$, used for the calculation of the K-function, is up to half the length of the shorter side of the study site Ω . Four different cases need to be distinguished and their $w_i(r)$ formulas are presented in **Table 2.5**.

- **Case 1.** The search circle $c_i(r)$ does not intercept the edges of the study region Ω (see **Figure 2.6** and **Table 2.5**).
- **Case 2.** The search circle $c_i(r)$ intercepts one edge of the study region Ω (see **Figure 2.6** and **Table 2.5**) and

$$\begin{aligned} \alpha &= \arccos(d/r) \\ e &= \sqrt{r^2 - d^2} \end{aligned} \quad (2.31)$$

where d is the distance between the center of the search circle $c_i(r)$ to the intercepted edge of the study area Ω .

- **Case 3.** The search circle $c_i(r)$ intercepts two edges of the study region Ω and $r^2 > d_1^2 + d_2^2$ (see **Figure 2.6** and **Table 2.5**)
- **Case 4.** The search circle $c_i(r)$ intercepts two edges of the study region Ω and $r^2 \leq d_1^2 + d_2^2$ (see **Figure 2.6** and **Table 2.5**).

In both cases 3 and 4 the following equation is valid

$$\begin{aligned} \alpha_i &= \arccos(d_i/r), i = 1, 2 \\ e_i &= \sqrt{r^2 - d_i^2}, i = 1, 2 \end{aligned} \quad (2.32)$$

where d_1 and d_2 are the distance from the center of the search circle $c_i(r)$ to the intercepted edges of the study area Ω .

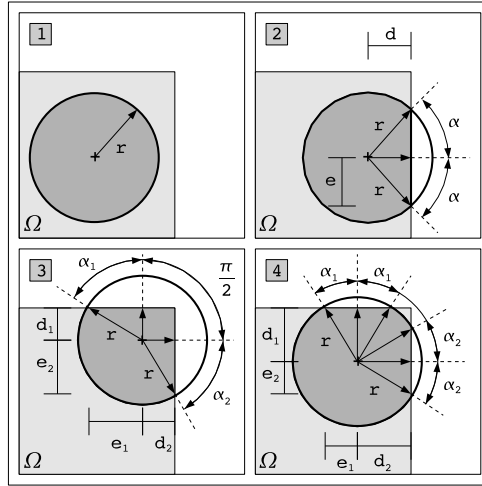


Figure 2.6. The four possibilities of intersection between the search circle $c_i(r)$ and the edges of the study region Ω .

Case	Condition	$w_i(r)$
1	no intersection	1
2	one intersection	$\pi r^2(ed + (\pi - \alpha)r^2)^{-1}$
3	two intersections with $r^2 > d_1^2 + d_2^2$	$\pi r^2(d_1d_2 + 0.5(e_1d_1 + e_2d_2) + (0.75\pi - 0.5\alpha_1 - 0.5\alpha_2)r^2)^{-1}$
4	two intersections with $r^2 \leq d_1^2 + d_2^2$	$\pi r^2(e_1d_1 + e_2d_2 + (\pi - \alpha_1 - \alpha_2)r^2)^{-1}$

Table 2.5. Table 2.5 Edge correction factor $w_i(r)$ for the 4 possibilities presented in **Figure 2.6**.

2.3 Results

2.3.1 Time processing

To compare the time required to calculate the Ripley K-function using the two methods presented above I simulated a CSR pattern varying the numbers of point inside a study area with square geometry $[0, 1] \times [0, 1]$. Then I obtained the time necessary to calculate the Ripley's K-function for these point patterns using Ripley method (t_1) and the Area method (t_2).

The graph in **Figure 2.7** shows that the Area method in relation to the Ripley method is at least 8.50 times faster (see also **Table 2.6**).

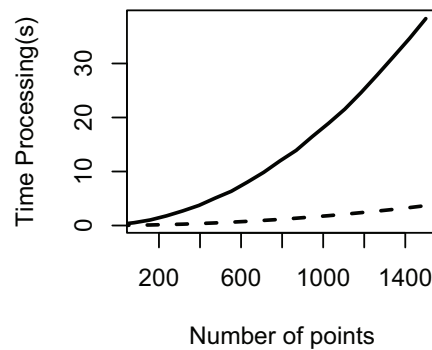


Figure 2.7. Time processing for the Area's method (dashed) and Ripley's method (filled).

n	100	500	1000	1500
t_1	0.17	3.72	11.96	24.59
t_2	0.02	0.36	1.13	2.38
t_1/t_2	8.50	10.33	10.58	10.33

Table 2.6. Relationship between the time processing for the *Ripley's method* (t_1) and for the *Area's method* (t_2). The time is given in seconds.

2.3.2 Simulation envelope width

The simulation envelope width is the difference between the upper and lower bounds of the simulation envelope obtained by the Monte Carlo method (Besag & Diggle 1977). Intuitively, an edge correction method with a wide simulation envelope width has lower statistical power to detect clumped and/or regular point patterns. An edge correction method with a narrower simulation envelope width is more stable under statistical fluctuations and has a higher statistical power (Yamada & Rogerson 2003).

In this work, a 99% simulation envelope was obtained for different point patterns inside a study area $\Omega = [0, 1] \times [0, 1]$ by performing 10.000 simulations. For each data set the simulation envelope width was calculated using either Ripley method other Area method.

The models used to generate the point pattern are listed below:

1. **Complete spatial randomness or CSR model.** I simulated a low density scenario with 50 points and a high density scenario with 200 points.
2. **Regular model.** This model was simulated using a sequential spatial inhibition process (Kaluzny *et al.* 1997) with parameter $c=0.01, 0.03$ and 0.05 (The parameter c specifies minimal distance between the points). For each parameter c , I simulated a low density scenario with 50 points and a high density scenario with 200 points.
3. **Clumped model.** This model was simulated using an algorithm presented by Yamada & Rogerson (2003) with parameter $c = 0.05, 0.08$ and 0.01 (the parameter c specifies the mean radius of the cluster). For each parameter c , I simulated a low density scenario with 50 points and a high density scenario with 200 points.

Figure 2.8 shows the simulation envelope and its respective width calculated for the CSR model. **Figure 2.9** and **Figure 2.10** show only simulation envelope widths obtained for the regular and clumped models respectively. For both cases, the simulation envelope width obtained by the Area method is more stable than those of Ripley method.

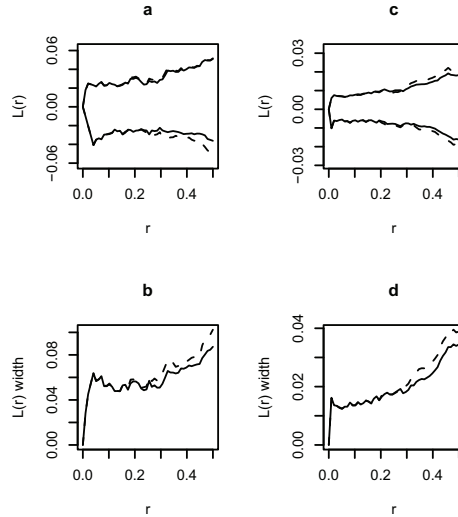


Figure 2.8. Results obtained for a CSR pattern simulated within a study region $\Omega = [0, 1] \times [0, 1]$. 99% simulation envelope for the CSR model for $n = 50$ (a) and $n = 200$ (c) with 10000 simulations using the Area method (filled) and Ripley method (dashed) and (b) and (d) shows the respective simulation envelope width.

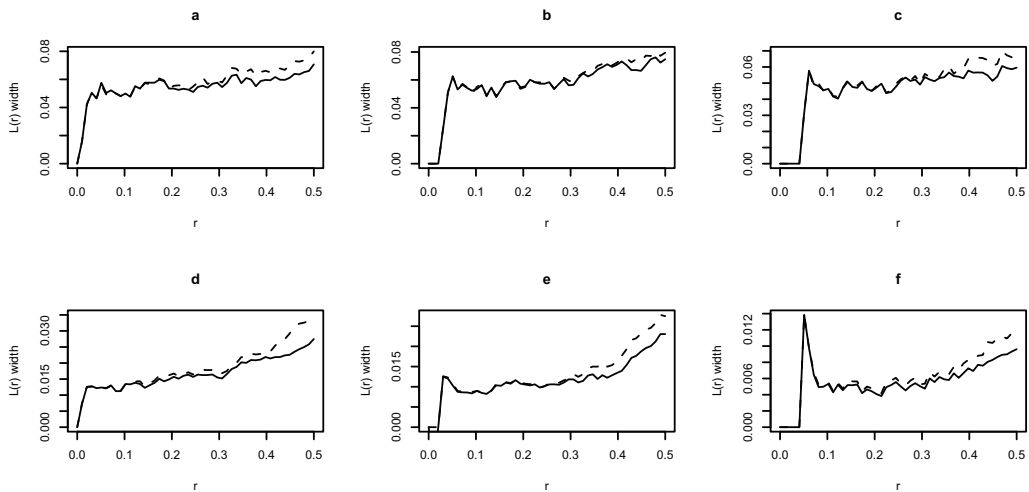


Figure 2.9. Confidence interval width of a regular model with parameters (a) $n = 50$ and $r = 0.01$, (b) $n = 50$ and $r = 0.03$, (c) $n = 50$ and $r = 0.05$, (d) $n = 200$ and $r = 0.01$, (e) $n = 200$ and $r = 0.03$, (f) $n = 200$ and $r = 0.05$ obtained by the Area method (filled) and Ripley method (dashed). The simulation envelope width was obtained via Monte Carlo method (Besag & Diggle 1977) with 10000 simulations.

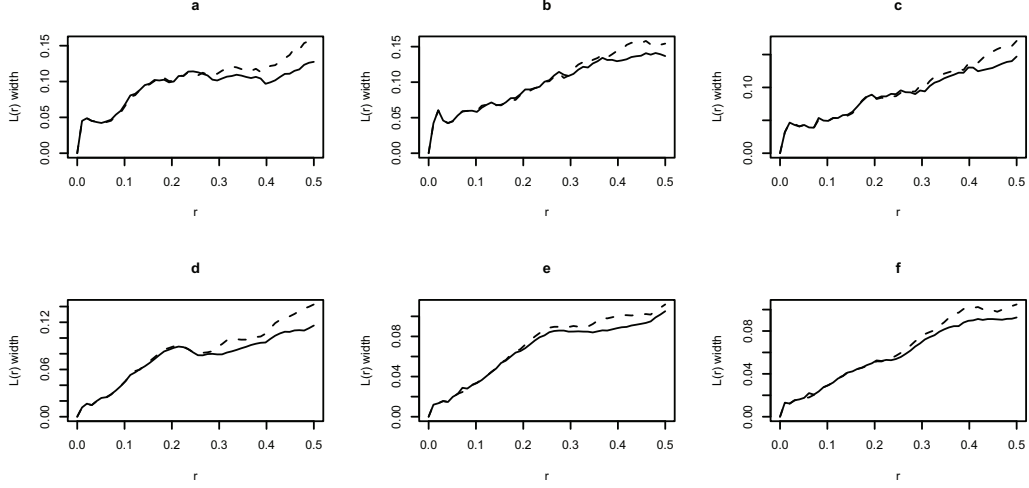


Figure 2.10. Confidence interval width for a clumped model with parameters **(a)** $n = 50$ and $r = 0.05$, **(b)** $n = 50$ and $r = 0.08$, **(c)** $n = 50$ and $r = 0.1$, **(d)** $n = 200$ and $r = 0.05$, **(e)** $n = 200$ and $r = 0.08$ and **(f)** $n = 200$ and $r = 0.1$ obtained by the Area method (filled) and Ripley method (dashed). The simulation envelope width was obtained via Monte Carlo method (Besag & Diggle 1977) with 10000 simulations.

2.3.3 A Guard Area

A virtual experiment can be carried out to evaluate the quality of the edge correction factors described above. The idea is to compare the estimated number of points outside the study region with the “real” number of points occurring in $A_i^-(r)$. For this, the study area Ω is now divided in two regions: a guard area Ω_g which contains the measurable points and a buffer area Ω_b that contains the points to be estimated (see **Figure 2.11**).

The K-function for the guard area Ω_g can be defined as

$$K_G(r) = \frac{A}{n_g^2} \sum_{i=1}^{n_g} \sum_{j \neq i}^n \delta_{ij}(r) \quad (2.33)$$

with the associated L-function

$$L_G(r) = \sqrt{\frac{K_G(r)}{\pi}} - r, \quad (2.34)$$

where n_g and n are the number of points inside the regions Ω_g and Ω respectively, whereas A is the area of Ω . Notice that $K_G(r)$ includes all points in the entire study region. It is, therefore, not necessary to use an edge correction factor in this case, because all necessary

information is already included. In order to evaluate the error associated with each edge correction factors, $K_G(r)$ is compared with the K-functions calculated for Ω_g without using the information inside Ω_b .

The K-function calculated for Ω_g using the Area method is

$$K_A(r) = \frac{A_g}{n_g^2} \sum_{i=1}^{n_g} w_i(r) \sum_{j \neq i}^{n_g} \delta_{ij}(r) \quad (2.35)$$

and its associated L-function is

$$L_A(r) = \sqrt{\frac{K_A(r)}{\pi}} - r. \quad (2.36)$$

The K-function calculated for Ω_g using the Ripley method is

$$K_R(r) = \frac{A_g}{n_g^2} \sum_{i=1}^{n_g} \sum_{j \neq i}^{n_g} w_{ij}(r) \delta_{ij}(r) \quad (2.37)$$

and its associated L-function is

$$L_R(r) = \sqrt{\frac{K_R(r)}{\pi}} - r, \quad (2.38)$$

where n_g and A_g are the number of points inside and the area of Ω_g respectively.

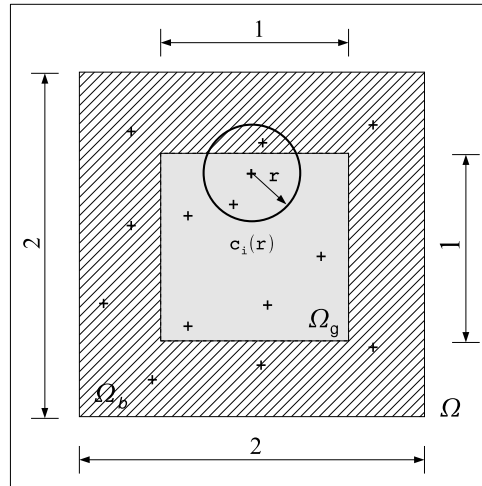


Figure 2.11. A whole study region $\Omega = [0, 2] \times [0, 2]$ divided as a guard area $\Omega_g = [0.5, 1.5] \times [0.5, 1.5]$ (gray region) and an buffer area Ω_b (hatched region) surrounding Ω_g .

To measure the deviation of the functions $L_A(r)$ and $L_R(r)$ from the reference function $L_G(r)$, deviance factors can be defined as

$$D_A = \int_0^{r_{\max}} [L_G(r) - L_A(r)]^2 dr \quad (2.39)$$

and

$$D_R = \int_0^{r_{\max}} [L_G(r) - L_R(r)]^2 dr, \quad (2.40)$$

where r_{\max} is the maximal scale of the analysis.

For this test, I simulated a point pattern within a study region $\Omega = [0, 2] \times [0, 2]$, separated into a guard area $\Omega_g = [0.5, 1.5] \times [0.5, 1.5]$ located in the center and a surrounding buffer area Ω_b . I performed 10.000 simulations for each point pattern model described above. In contrast to the analyses of the simulation envelope width, for each model two density scenarios were considered: a low density scenario with 200 points inside Ω and a high density scenario with 800 points inside Ω . These settings mean that an average of 50 and 200 points occur inside Ω_g , in the low and high density scenarios respectively.

Table 2.7 and **Table 2.9** show the mean deviance factor (D_A and D_R) and the corresponding variances for all CSR and clumped scenarios. The mean of the deviance factor obtained shows that the performance of the Area method is better than or equivalent to the Ripley method. A Student T-test calculated for the results presented for the regular scenarios in **Table 2.8** (LD^{2.1} and HD^{2.2}) shows that D_A and D_R are equivalent.

LD scenario	mean	variance
D_R	0.0051	6.834×10^{-5}
D_A	0.0049	6.062×10^{-5}
HD scenario	mean	variance
D_R	0.001	2.361×10^{-6}
D_A	0.001	2.197×10^{-6}

Table 2.7. CSR model with 200 points representing a low density scenario and 800 points representing a high density scenario. Summary of the statistical results for the deviance factors D_R and D_A obtained from 10000 simulations.

2.1. $t=-0.016$, $df=10$, $p\text{-value}=0.987$ and 95% confidence interval = $(-3.49, 3.44)$.

2.2. $t=-0.031$, $df=10$, $p\text{-value}=0.976$ and 95% confidence interval = $(-2.95, 3.03)$.

LD Scenario	r=0.01		r=0.03		r=0.08	
Deviance	mean	variance	mean	variance	mean	variance
D_R	0.0051	5.567×10^{-5}	0.0047	5.246×10^{-5}	0.0035	3.410×10^{-5}
D_A	0.0050	5.337×10^{-5}	0.0046	5.397×10^{-5}	0.0035	3.639×10^{-5}
HD Scenario	r=0.01		r=0.03		r=0.08	
Deviance	mean	variance	mean	variance	mean	variance
D_R	0.009	1.567×10^{-6}	0.0006	5.184×10^{-7}	0.0002	4.14×10^{-8}
D_A	0.009	1.562×10^{-6}	0.0005	5.700×10^{-7}	0.0002	3.41×10^{-8}

Table 2.8. Summary of the statistical results of the deviance factor D_R and D_A calculated for the region Ω_g obtained from 10000 simulations. A regular model with 200 points and parameter $r = 0.01, 0.03$ and 0.05 representing a low density scenario and a regular model with 800 points and parameters $r = 0.01, 0.03$ and 0.05 representing a high density scenario.

LD scenario	c=0.05		c=0.08		c=0.1	
Deviance	mean	variance	mean	variance	mean	variance
D_R	0.136	0.080	0.442	1.172	0.188	0.923
D_A	0.081	0.018	0.303	0.608	0.123	0.399
HD scenario	c=0.05		c=0.08		c=0.1	
Deviance	mean	variance	mean	variance	mean	variance
D_R	0.149	0.202	0.256	2.722	0.094	0.076
D_A	0.095	0.045	0.162	1.042	0.059	0.020

Table 2.9. Summary of the statistical results of the deviance factor D_R and D_A calculated for the region Ω_g obtained with 10000 simulations. A clumped model with 200 points and parameter $c = 0.05, 0.08$ and 0.01 representing a low density scenario and a regular model with 800 points and parameters $r = 0.01, 0.03$ and 0.05 representing a high density scenario.

2.3.4 Real Dataset

The virtual experiment described above is a powerful tool frequently applied in ecology to evaluate the quality of ecological parameters (see e.g. Berger *et al.* 1999b or Perner & Scüler 2004). In this simulation experiment, the guard area methodology applied to a real data set obtained from a mangrove forest.

The method was applied to the data set obtained from the study site Lagoa A. The site has geometry: $\Omega = [0, 30] \times [0, 30]$. For the analysis, it was separated into two regions: a guard area $\Omega_g = [7.5, 22.5] \times [7.5, 22.5]$ and a buffer area Ω_b surrounding the area Ω_g (see **Figure 2.12**).

The study site Lagoa A contains 560 trees: 118 trees inside the region Ω_g and 442 trees inside the region Ω_b .

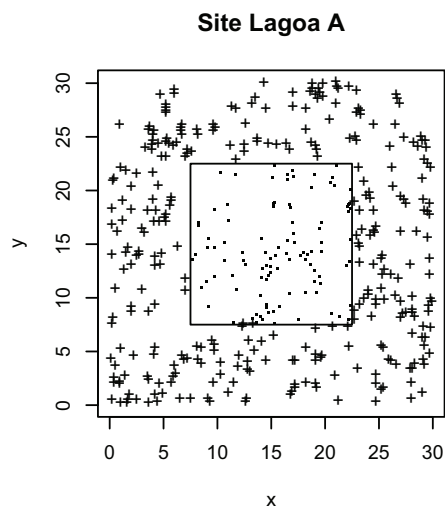


Figure 2.12. Study area Lagoa A with 560 trees: 118 trees inside the guard area Ω_g (points) and 442 trees inside the buffer area Ω_b (crosses).

A comparison of the deviance factors D_A and D_R shows that the performance of the Area method is better than to Ripley method (see **Table 2.10**).

Study area	D_R	D_A
Lagoa A	1.5032	1.2193

Table 2.10. Deviance factor D_R and D_A obtained for the study site Lagoa A.

2.4 Discussion

The results presented in this Chapter shown some characteristics of the QC and NN Methods, First Order Methods (Fischer *et al.* 1922, Douglas 1975, Clark & Evans 1954, Cressie 1993) based on the First Order Property (mean number of points per unit area at any arbitrary location in the study region).

The QC Method (Fischer *et al.* 1922, Douglas 1975) has at least two main limitations. This method reduces all spatial information of the point pattern into a single one-dimensional index. This characteristic implies that:

(1) The spatial pattern analysis can be performed only at a single scale. Because the method provides information about the intensity (number of events per unit area) of the spatial point pattern using only a single particular size quadrat. However, the choosing of the quadrat size can be quite complicated, because it depends generally on the scale of interest in the spatial pattern and/or the changing pattern at the changing scales.

(2) The analysis provides no information about the relative spatial position of the tree individuals inside the study site. In summary, the QC Method shows only the type of deviation from point randomness (i.e. regularity and/or clustering) and all other spatial information of the individuals is completely lost.

In the same way, the results show that the Nearest Neighbor Methods (hereinafter NN Method) (Fischer *et al.* 1922, Clark & Evans 1954, Cressie 1993) also have important limitations. All information about individual point-to-point distances is lost and summarized in a mean. These methods consider only on the closest points (i.e. distance to the nearest neighbor for each point in the pattern) and the spatial information of the individuals at larger scales is completely lost. Furthermore, while the indices can show the direction of deviation from randomness (i.e., toward clumping and/or regularity), the numerical behavior of many of these indices remains largely unexplored.

In summary, the QC and NN Methods show that the trees within the study site Lagoa A are clumped (see **Table 2.1** and **Table 2.2** respectively), but the methods do not provide the detection of the scale at which this pattern occurs. This is a common limitation of both QC and NN methods. All information about the spatial localization of the tree individuals is completely lost.

Recent studies in plant ecology reveal that positive and negative interactions between individual trees may occur together at different scales and determine simultaneously the horizontal and vertical structure of the plant community (Malkinson *et al.* 2003). Thus, to reduce all spatial information of all scales into one single index, is a critical limitation of the QC and NN methods. For this, the Ripley K-function (Ripley 1977), a second order method, was developed to overwhelm some of these limitations.

The main advantage of the Ripley K-Function in comparison the First Order Methods (Fischer *et al.* 1922, Douglas 1975, Clark & Evans 1954, Cressie 1993), such as QC and NN Methods is to preserve distance information and it permits to analyze a point pattern at a

range of scales and to determine at which scales these points tend to be regular, clumped or CSR. In this experiment, the analysis obtained by Ripley K-function confirm that the spatial configuration of trees in Lagoa A are clustered but show in addition that clustering occurs at lower and intermediate scales. This information was not possible to obtain using the QC and NN Methods.

In this chapter I also provide a complete description of an Area Based Edge Effect Correction Factor (hereinafter Area Method) (Getis & Franklin 1987, Besag 1977, Dale & Powell 2001) in order to improve the sensibility of the Ripley K-Function to detect deviation from randomness in spatial point patterns. Momentary, this method is only suitable to analyze the spatial configuration of a point pattern within a rectangular study area. Additionally, the maximal scale of the spatial analysis is restricted to a half of the shortest side of the study site (see **Table 2.6**).

However, the time processing simulation experiment shows that the Area Method is about eight times faster (see **Table 2.6**) than the Ripley Method for edge correction (Ripley 1977, Diggle 1983). The better time performance of the Area Method in comparison to the Ripley method can be explained by comparing equations (2.3) and (2.30). For a fixed scale r and n points, the calculation of the Ripley K-function using the Ripley edge correction method needs at n^2 operations. In contrast, the Area Method needs only n operations. This characteristic of the Area Method enables therefore more simulations to be performed in calculating the simulation envelope. It thus improves the statistical power and the sensibility of the Ripley K-function in order to detect clumping and regularity (Yamada & Rogerson 2003). This advantage is also particularly important for the analysis of large data sets, reducing the time processing of the analysis.

The comparison of the simulation envelope widths shows that the performance of both methods is similar until $r=0.25$ (considering $r_{max}=0.5$), but the Area Method performs better performance for $r>0.25$ (see **Figure 2.8**, **Figure 2.9** and **Figure 2.10**). This result provides additional evidence of the greater statistical power and sensibility of the Area Method in order to analyze spatial point patterns.

The results obtained with the guard area experiment show that spatial analysis performed with the Area Method is better or equivalent in comparison to the Ripley edge correction method (see **Figure 2.7**, **Figure 2.8**, **Figure 2.9** and **Figure 2.10**). Both virtual experiments (with computed and real field data) demonstrate, furthermore, the greater precision of the Area Method in relation to the Ripley Method.

Thus, I conclude that it is worthwhile applying this method when the study site is rectangular. Future studies will provide a complete set of equations also suitable for irregular study sites and no scale analysis constraints. Additionally, it is important to note that the Area Method can be applied in combination with any spatial statistical method that requires the use of an edge effect correction factor. In the next Chapter, I perform a more detailed analysis of the study sites Lagoa A and Lagoa B, using the Ripley K-function, with the intention to detect the underlying ecological process determining the spatial configuration of tree individuals here.

The algorithm for the calculation of the K-function and the Area Method utilized in this chapter was implemented in FORTRAN 95 and can be found in the Appendix.

Chapter 3

Spatial Pattern Analysis - an Application

3.1 Introduction

In this chapter, I perform a more complete analysis of two real data sets obtained from two mangrove forest stands Lagoa A and Lagoa B. They are located on the coast of the northeastern Brazilian State of Pará (for more details, see Chapter 2). The two forest study sites are located about 15 m apart near the lagoon in the central part of the peninsula (see **Figure 3.1**).

Site Lagoa A contains two species: *Laguncularia* and *Avicennia*. The forest at Lagoa B is formed by large sized *Laguncularia*, and a few *Rhizophora* and *Avicennia* trees.. Both areas are inundated once a month during very high tides under the influence of Caete River tidal regime. The inundation regime is not precisely known but the frequency of inundation is presumably lower at Lagoa A than at Lagoa B, due to its lower basin (Harum 2004).

The principal aim of this chapter is to analyze the spatial configurations of the trees in these stands. I interpret these to make inferences about the underlying ecological processes which are likely to be occurring within the study sites, such as competition or/and facilitation between the trees, seed dispersal (Sturner et al. 1986, Barot et al. 1999), nurse-plant effects (Tielbörger & Kadmon 2000), intraspecific competition (Kenkel 1998), interspecific competition (Barot et al. 1999), disturbance (Dale 1999), herbivore pressure (Jetsch et al. 1999), succession (Begon et al. 1976, Connell & Slatyer 1977) and zonation (Roels 2001). These ecological processes are important factors that determine the spatial structure and the organization of a community.

Under the assumption that the spatial heterogeneity of abiotic factors does not predetermine plant distribution, studies in plant ecology have shown that a tendency to regularity may be a result of competition for limited resources such as water, light and nutrients (King & Woodell 1973). By contrast, a tendency to clustering may be an indication of facilitation processes, such as ameliorative environmental conditions (Muller 1953, Haase et al. 1996), heterogeneous edaphic conditions (Couteron & Kokou 1997), local seed dispersal effects (Barot et al. 1999), stress gradients in the physical environment (Malkison et al. 2003) or environmental heterogeneity (Klaas et al. 2000).

Under the assumption that the spatial heterogeneity of abiotic factors does not predetermine plant distribution, studies in plant ecology have shown that a tendency to regularity may be a result of competition for limited resources such as water, light and nutrients (King & Woodell 1973). By contrast, a tendency to clustering may be an indication of facilitation processes, such as ameliorative environmental conditions (Muller 1953, Haase et al. 1996), heterogeneous edaphic conditions (Couteron & Kokou 1997), local seed dispersal effects (Barot et al. 1999), stress gradients in the physical environment (Malkison et al. 2003) or environmental heterogeneity (Klaas et al. 2000).

In summary, regular and clumped patterns can be associated with competition and facilitation processes respectively. Recent studies show that positive (facilitation) and negative (competition) interactions usually occur together simultaneously, exerting a combined affect on the structure of the plant community. The relative importance of these processes depends on the intensity of the environmental stress (Bertness & Callaway 1994).

It should be noted that the interpretation of the spatial point pattern depends on the scale of the observation in comparison to the scale of the study site. Here I assumed that variations at lower scales can be attributed to plant-plant interactions and that larger scale variations are due to environmental heterogeneity (Pelissier & Goreaud 2001) or provide evidence of an invasion process, by a species new to the location (Goreaud et al. 1996).

In **Table 3.1** I present a summary of some ecological processes and their possible associated spatial point patterns. In order to analyze the spatial configuration of individual trees in the sites Lagoa A and B, I applied the Ripley K-function in combination with the Area method introduced in **Chapter 2**.

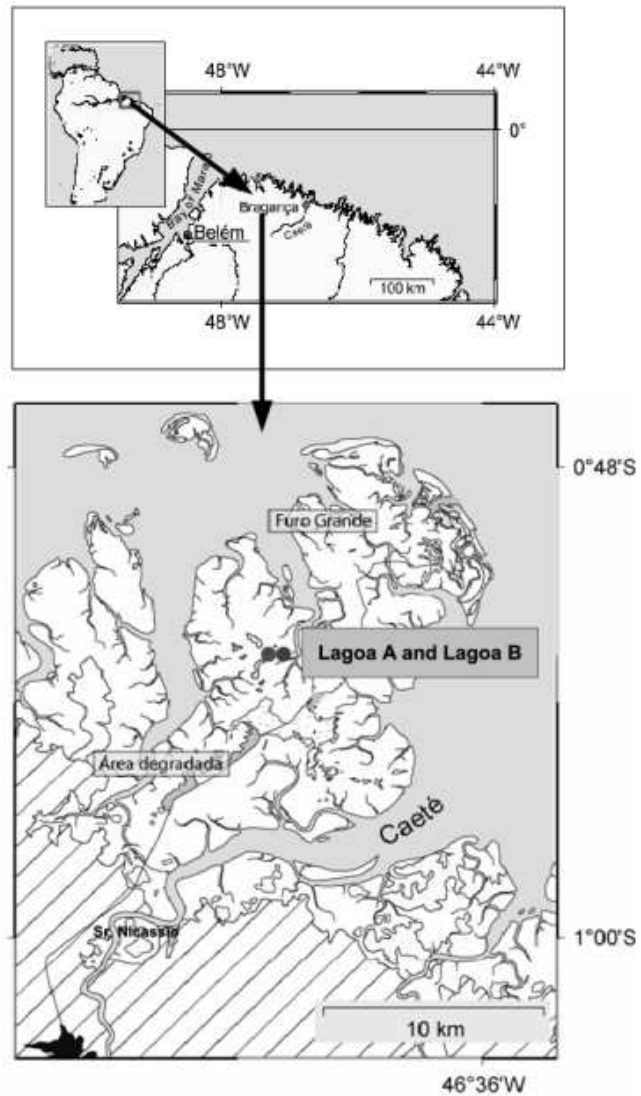


Figure 3.1. Coastal zone of northern Brazil where the study sites Lagoa A and Lagoa B (black dots) are located.

Spatial Pattern	Underlying Process
Clustering (+)	Seed-dispersion effect Nurse-plant effect Succession Zonation Environmental heterogeneity
Regularity (-)	Intraspecific competition Interspecific competition

Table 3.1. Summary of underlying process and an possible associated spatial point pattern. (+) Positive and (-) negative interaction.

3.1.1 Mangrove Forest

Mangrove forests are defined as associations of woody trees and bushes which prosper in mangal (mangrove habitat), an inhospitable habitat between land and sea. But they can also occur in other types of habitats (Hogarth 1999). They are relatively stable ecosystems dominated by only a few species (Tomlison 1986, Ricklefs & Latham 1993, Duke et al. 1998).

A wide variety of plant species can be found in mangrove habitat, but of the 110 recorded species only about 54 species, belonging to 20 genera in 16 families, are considered "true mangroves", that is, species that occur almost exclusively in mangrove habitats and rarely elsewhere (Hogarth 1999).

Mangrove habitats are constantly changing, growing, reestablishing and regenerating themselves. The main characteristics that permit mangrove forests to survive, occupy, dominate and stabilize tidal locations are their notable tolerance to saltwater tidal conditions and the fact that they are highly dispersive plants with floating propagules, which frequently display vivipary (Tomlison 1986, Duke 2001). They are complex ecosystems that can be considered at different spatial scales. At tree level scale, they are structurally and physiologically well adapted to respond to the conditions in the immediate environment, in particular to physical factors such as salinity. But at large scales, local variation in physical factors influences the overall structure of the mangrove forest (Hogarth 1999).

Mangroves have a highly specialized method of propagation. Their seeds germinate into seedlings while on the parent tree and after an initial period of development, the seedlings fall down from the parent tree to the sands below. They then can either sprout or be carried with the tide to colonize other locations. Some propagules remain viable for periods of weeks or a year or more (Rabinowitz 1978).

Mangroves help to protect coastlines from erosion, storm damage, and wave action. They prevent shoreline erosion by acting as buffers and trapping alluvial materials, thus stabilizing land elevations by sediment accretion that balances sediment loss (Hogarth 1999).

Mangrove ecosystems have traditionally been utilized by local populations for the production of food, medicines, tannins, fuel wood, and construction materials. For millions of indigenous coastal residents, mangrove forests provide dependable basic livelihoods and sustain their traditional cultures (Quarto 2001).

Mangroves are almost exclusively tropical and can be found between the latitudes of 32 degrees north and 38 degrees south, along the tropical coasts of Africa, Australia, Asia, and the Americas. This distribution is an indication of a limitation by temperature and they rarely occur outside the winter position of the 20°C isotherm (Hogarth 1999).

In this study, I am particularly interested in the mangroves species found in Northeastern Brazilian State of Para, the region where the sites Lagoa A and Lagoa B are located. The main species found in at these sites are *Laguncularia racemosa*, *Avicennia germinans* and *Rhizophora mangle* and in the following sections I briefly describe these three species.

3.1.1.1 *Avicennia germinans*

Black mangrove or *Avicennia germinans* occurs in periodically immersed and fully terrestrial environments (see **Figure 3.2**). It tolerates airborne salt and a degree of water salinity, but favors fresh water environments. It prefers loamy or muddy substrates, but tolerates sand and it is also reasonably tolerant of cutting back and mild frost conditions. It does not grow on prop roots; rather it possesses pneumatophores that allow its roots to breathe even when growing in standing water. It occurs mainly in tropical Atlantic regions where it thrives on sandy and muddy shores. Like many other mangroves, it reproduces by vivipary. Their seeds are cased inside a fruit until this falls into the water to release the germinated seedling. *Avicennia* expels absorbed salt mainly from its leathery leaves. It is widely distributed along Atlantic coasts of tropical America and is found in Bermuda, the Bahamas, and the West Indies, in southeastern USA as far as northern Florida and southeastern Texas, and from northern Mexico southwards along the Atlantic Coast to Brazil. It is also found on the Pacific Coast from Mexico to Ecuador including the Galapagos Islands, and as far as northwestern Peru, and on coasts of western Africa (Little 1983, Kjerfve & Lacerda 1993, Hogarth 1999). For additional information see, **Table 3.2** and **Table 3.3**.



Figure 3.2. Black mangrove or *Avicennia germinans*.

3.1.1.2 *Rhizophora mangle*

Red mangrove or *Rhizophora mangle* (see **Figure 3.3**) can live in water and in periodically immersed environments; it also occurs as a fully terrestrial plant in well-hydrated conditions. It tolerates fresh, brackish or full seawater but cannot adapt to marked changes in salinity. It favors fine sand or muddy substrates but can survive on coarse substrates. It is the most temperature sensitive of three genera listed here. It requires warmer temperatures and is also the most sensitive to cutting back. It generally occurs in intertidal areas which are inundated daily by the tides. *Rhizophora* has a number of adaptations suited to this environment, namely propagules that allow them to breath in an anaerobic environment (Little 1983, Hogarth 1999). For additional information, see **Table 3.2** and **Table 3.3**.



Figure 3.3. Red mangrove or *Rhizophora mangle*.

3.1.1.3 *Laguncularia racemosa*

White mangrove or *Laguncularia racemosa* (see **Figure 3.4**) is a fully terrestrial plant which tolerates airborne salt, but not highly saline water. It is very tolerant of cutting back and is moderately to very tolerant of occasional frost conditions. It can be found on both coasts of tropical America, from northern Mexico to Brazil and Ecuador, including the Galapagos Islands and as far as northwestern Peru, as well as in the West Indies, Bermuda, in southern and central Florida, and in West Africa from Senegal to Cameroon (Little 1983, Hogarth 1999). For additional information, see **Table 3.2** and **Table 3.3**.

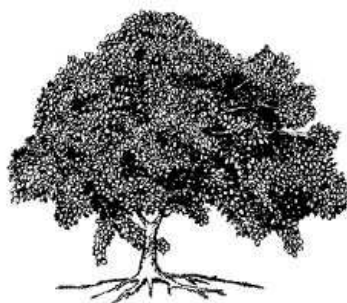


Figure 3.4. White mangrove or *Laguncularia racemosa*.

Species	Weight (g)	Length (cm)	Floating (d)	Longevity (d)
<i>Avicennia</i>	1.1	1.83	always	110S
<i>Rhizophora</i>	22.1	22.1	-	-
<i>Laguncularia</i>	0.4	2.1	23F and 31S	35S

Table 3.2. Table 3.2 Characteristics of propagules of three mangrove species (adapted from Rabinowitz 1978). (S) Salt water conditions and (F) Fresh water conditions.

Species	Shade tolerance	Salinity
<i>Avicennia</i>	Intolerant	100(MS) and <40(OG)
<i>Rhizophora</i>	Intolerant	70(MS)
<i>Laguncularia</i>	Intolerant	90(MS)

Table 3.3. Ecological Characteristics of various mangrove species. "Salinity" in ($^0/_{00}$). MS = Maximum pore water salinity measured in the fields at sites where the species was growing, OG = Salinity for optimum growth based on culture studies. Adapted from Smith III (1991).

3.1.2 Mangrove forest evolution

Early studies used a four stage model to describe the development of mangrove stands: mangrove first establish themselves during a colonization phase and continue through later phases of early development and maturity. Finally a new cycle of colonization begins during the senescence stage. The duration of a complete cycle was estimated to be about 80-100 years (Jimenez & Lugo 1985, Fromard et al. 1988). Later Duke (2001) updated this approach by considering gap dynamics explicitly.

However, recent studies in mangrove forest evolution show that the early development stage is much longer than assumed in this model. Menezes (2006) has proposed subdividing the early development stage in two stages, which he denominates "early development" and "young forest" stages (see **Table 3.4**).

Development Stage	Colonization	Early development	Young Forest	Mature Stand	Senescence
Density	low to high	very high	high	medium	low
Biomass	low	medium	medium	high	high to low
Self-thinning	minimal	high	high to moderate	moderate to low	minimal
Size distribution	normal	L-shape	L-shape	normal	J-shape

Table 3.4. A preliminary model of stand development in mangroves. The forest collapses with "senescence" when the cycle resumes with re-colonization. Adapted from Duke (2001), Silvertown & Doust (1993) and Menezes *et al.* (2004).

The colonization stage starts with the establishment of propagules in gaps and on unoccu-

ped and damaged tidal areas. Recruitment and growth is fast, self-thinning is minimal and the density of plants increases throughout this stage. *Laguncularia racemosa* is the dominant species at this stage. This occurs because *Laguncularia* presents some characteristics of pioneer species, including a low shade tolerance and a high nutrient use efficiency. For this reason, this species is often the first colonizer of newly created mud banks. Under optimal light or nutrient conditions, *Laguncularia* overtops *Avicennia* and *Rhizophora* in terms of growth rate (Lovell & Feller, 2003). As soon as the conditions become suboptimal, *Laguncularia* loses this initial advantage. This stage lasts about 4 years, until canopy closure is largely achieved (Duke 2001, Berger et al. 2006, Menezes et al. 2006).

The early development stage is characterized by very intense self-thinning and a rapid decline in density while the seedling bank is formed under the closed canopy. During this stage, the height of the stand increases more slowly until the canopy approaches "site maximal canopy height". and/or appear in the stand. (Duke 2001, Menezes et al. 2006). This stage lasts about 5 years. It should be noted that this description is derived from studies undertaken on the Acaraó Peninsula (Brazil), where the study sites Lagoa A and Lagoa B are located (Berger 2006).

In the young forest stage, the number of individuals continues to decrease due to self-thinning effects. At this point there two possibilities for the future development the stand: either a change in dominance from *Laguncularia racemosa* to *Rhizophora mangle* (Ball 1980) or a change in dominance from *Laguncularia racemosa* to *Avicennia germinans* (Berger et al. 2006).

The mature stand stage commences when the "site maximal canopy height" is achieved. At this stage the trees start to gain biomass while tree density continues to decrease due to self-thinning effects. Neighborhood competition varies between low and moderate values. The mean age of the trees varies between 30 - 60 years (Duke 2001, Menezes et al. 2006).

The senescence stage starts when large individuals begin to die standing or they fall over. At this stage, tree density is expected to be low and self-thinning minimal. (Duke 2001). During this stage, the stand is dominated by few old and large trees. There are wide gaps in the canopy and a lack of regeneration. It cannot be considered as an interval development of the stand, because in this case, the whole forest collapses (Duke 2001, Menezes 2006).

Analysis of the shape of the tree dbh histogram could provide a good indication of the stage of development a stand. Studies have shown that, initially, plant size (in this case, I am considering dbh) in dense populations generally has a normal distribution, which quickly skews to an L-shape distribution with a many small individuals and a few larger ones. As the trees grow, the mortality caused by the self-thinning may totally remove the smallest individuals, producing a more symmetrical size distribution once again. In an advanced stage of the development, the number of small trees decreases and the stand is dominated by old and large trees and their dbh distribution presents a J-shape (Silvertown & Doust 1993).

3.2 Results

3.2.1 Lagoa A

Site Lagoa A contains a total of 812 trees (including 252 dead trees) (see **Figure 3.5**).

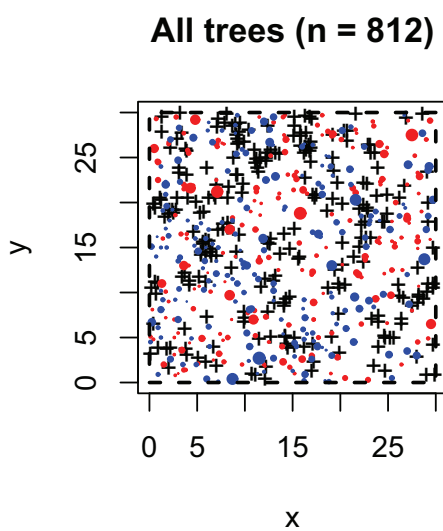


Figure 3.5. All trees at stand site Lagoa A. (black cross) dead tree, (blue dot) *Laguncularia racemosa* and (red dot) *Avicennia germinans*. The size of dot is proportional to the dbh of *Avicennia* and *Laguncularia* (there's no information about the dbh of the dead trees). (scale in meters)

Type	mean(dbh)	var(dbh)	max(dbh)	n	n/N
All	4.41*	14.11*	18.46*	812	1.000
<i>Avicennia germinans</i>	3.70	13.37	17.83	309	0.38
<i>Laguncularia racemosa</i>	5.28	13.72	18.46	251	0.31
Dead trees	-	-	-	252	0.31

Table 3.5. Short statistical summary of the mean stem diameter in breast height (dbh) for Lagoa A site. (-) There's no information about the dead trees's dbh. (*) Excluding the dead trees. (dbh in cm).

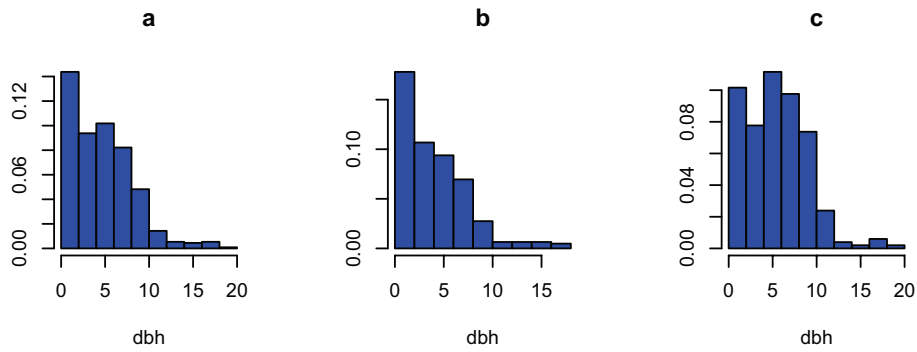


Figure 3.6. Lagoa A - Histograms showing the size class distribution of the mean stem diameter in breast height (dbh) in cm obtained for (a) all trees (excluding dead trees), (b) *Avicennia germinans* and (c) *Laguncularia racemosa*. (scale in cm)

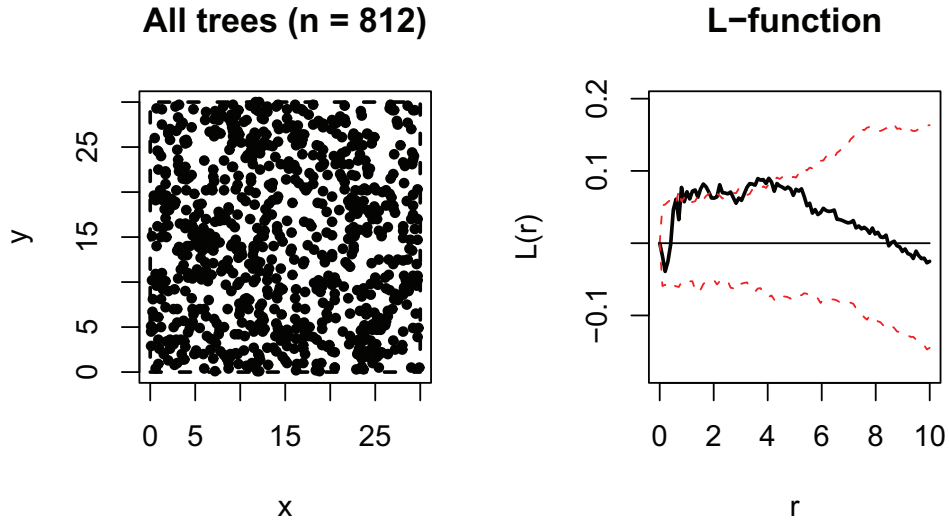


Figure 3.7. (left) Spatial point pattern relative to all trees of the stand Lagoa A and its (right) respective L-function (black) and 99% simulation envelope (dashed red). The simulation envelope was calculated via Monte Carlo method (Besag 1977) for the CSR hypothesis with 10000 simulations.

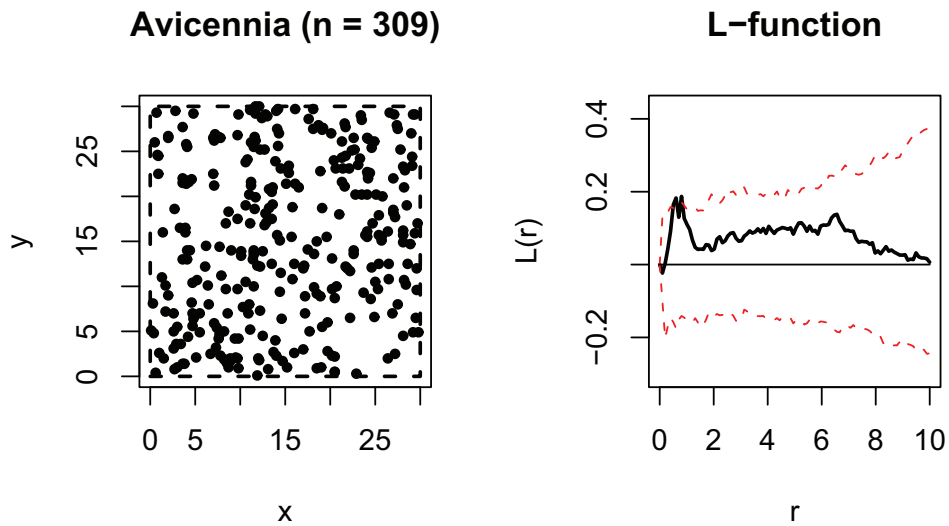


Figure 3.8. (left) Spatial point pattern relative to the species *Avicennia germinans* within stand Lagoa A. Its (right) respective L-function (black) and 99% simulation envelope (dashed red). The simulation envelope was calculated via Monte Carlo method (Besag 1977) for the CSR hypothesis with 10000 simulations.

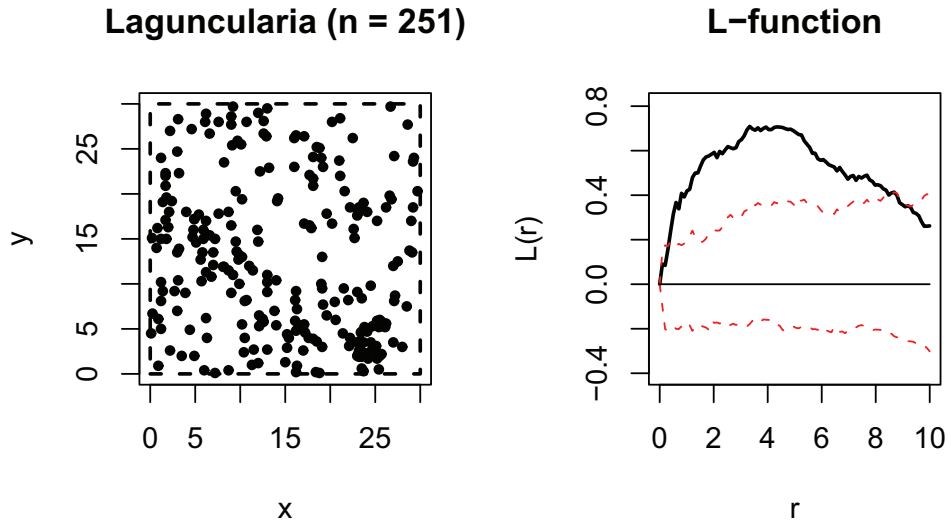


Figure 3.9. (left) Spatial point pattern relative to the species *Laguncularia racemosa* within stand Lagoa A. Its (right) respective L-function (black) and 99% simulation envelope (dashed red). The simulation envelope was calculated via Monte Carlo method (Besag 1977) for the CSR hypothesis with 10000 simulations.

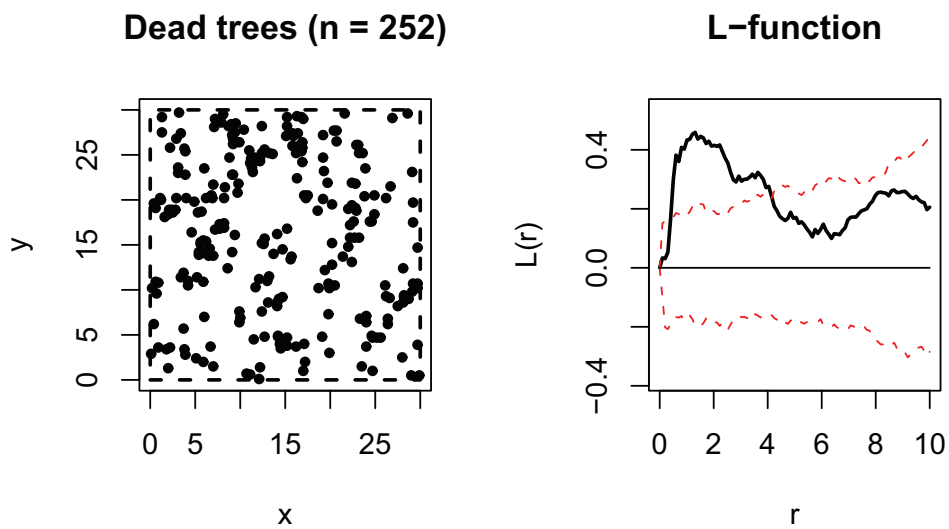


Figure 3.10. (left) Spatial point pattern relative to dead trees within stand Lagoa A. Its (right) respective L-function (black) and 99% simulation envelope (dashed red). The simulation envelope was calculated via Monte Carlo method (Besag 1977) for the CSR hypothesis with 10000 simulations.

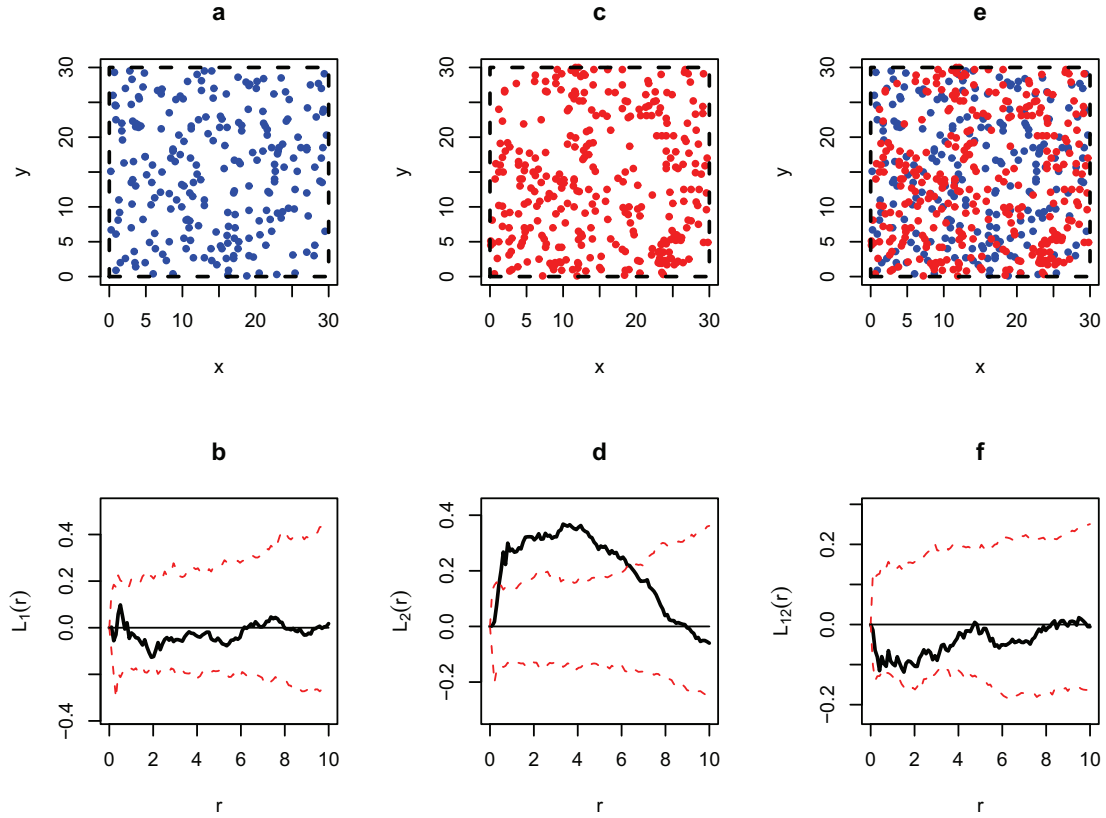


Figure 3.11. The point patterns (a) and (c) represents respectively the big trees ($n=232$) and small trees ($n=328$). (b) and (d) represents their L-function (black) and 99% simulation envelope for CSR hypothesis (dashed red) respectively. The point pattern (e) represent the large trees (blue) and small trees (red). (f) represents its bivariate L-function (black) and 99% simulation envelope for spatial independence hypothesis (dashed red). The simulation envelopes were calculated via Monte Carlo method (Besag 1977) with 10000 simulations.

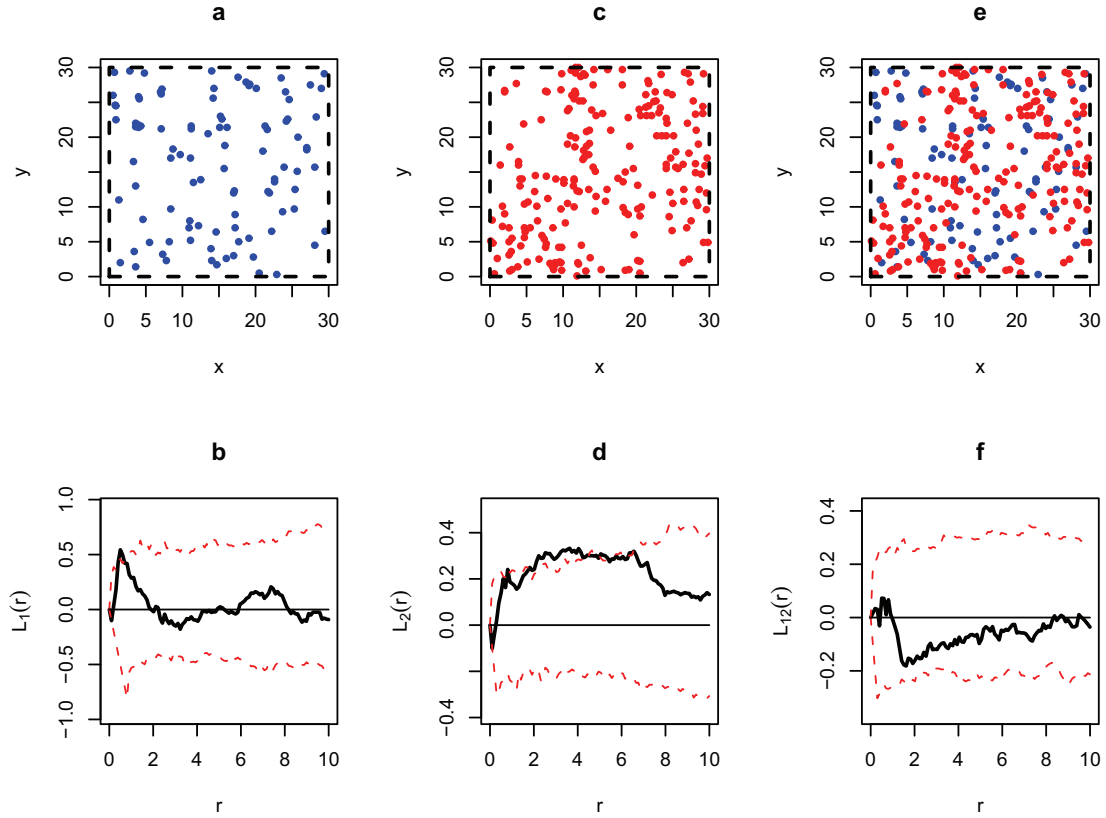


Figure 3.12. The point patterns (a) and (c) represent respectively the large *Avicennia* ($n=100$) and small *Avicennia* ($n=209$). (b) and (d) represent their L-function (black) and 99% simulation envelope for CSR hypothesis (dashed red) respectively. The point pattern (e) represents the big *Avicennia* (blue) and small *Avicennia* (red). (f) represents its bivariate L-function (black) and 99% simulation envelope for spatial independence hypothesis (dashed red). The simulation envelopes were calculated via Monte Carlo method (Besag 1977) with 10000 simulations.

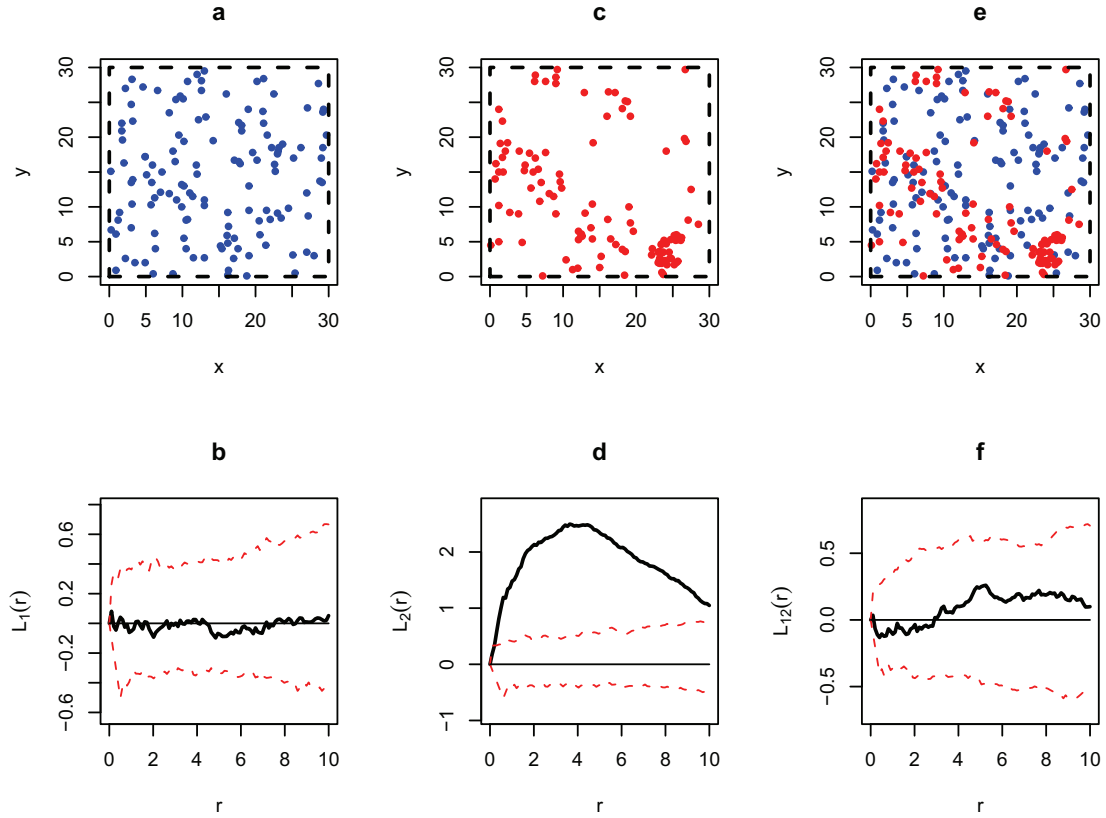


Figure 3.13. The point patterns (a) and (c) represents respectively the large Laguncularia ($n=132$) and small Laguncularia ($n=132$). (b) and (d) represents their L-function (black) and 99% simulation envelope for CSR hypothesis (dashed red) respectively. The point pattern (e) represents the big Laguncularia (blue) and small Laguncularia (red). (f) represents its bivariate L-function (black) and 99% simulation envelope for spatial independence hypothesis (dashed red). The simulation envelopes were calculated via Monte Carlo method (Besag 1977) with 10000 simulations.

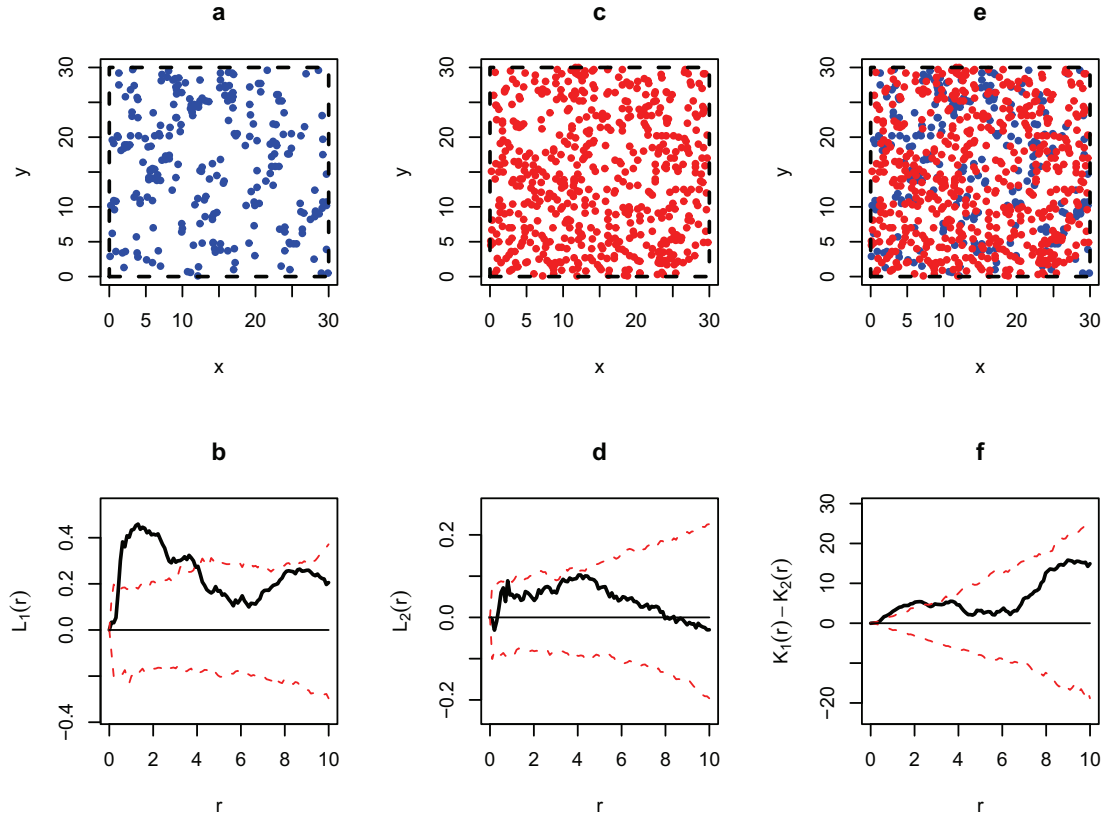


Figure 3.14. The point patterns (a) and (c) represents respectively the dead trees ($n=252$) and living trees ($n=560$). (b) and (d) represents their L-function (black) and 99% simulation envelope for CSR hypothesis (dashed red) respectively. The point pattern (e) represents the dead trees (blue) and living trees (red). (f) represents its $K_1(r) - K_2(r)$ (black) and 99% simulation envelope for random labeling hypothesis (dashed red). The simulation envelopes were calculated via Monte Carlo method (Besag 1977) with 10000 simulations.

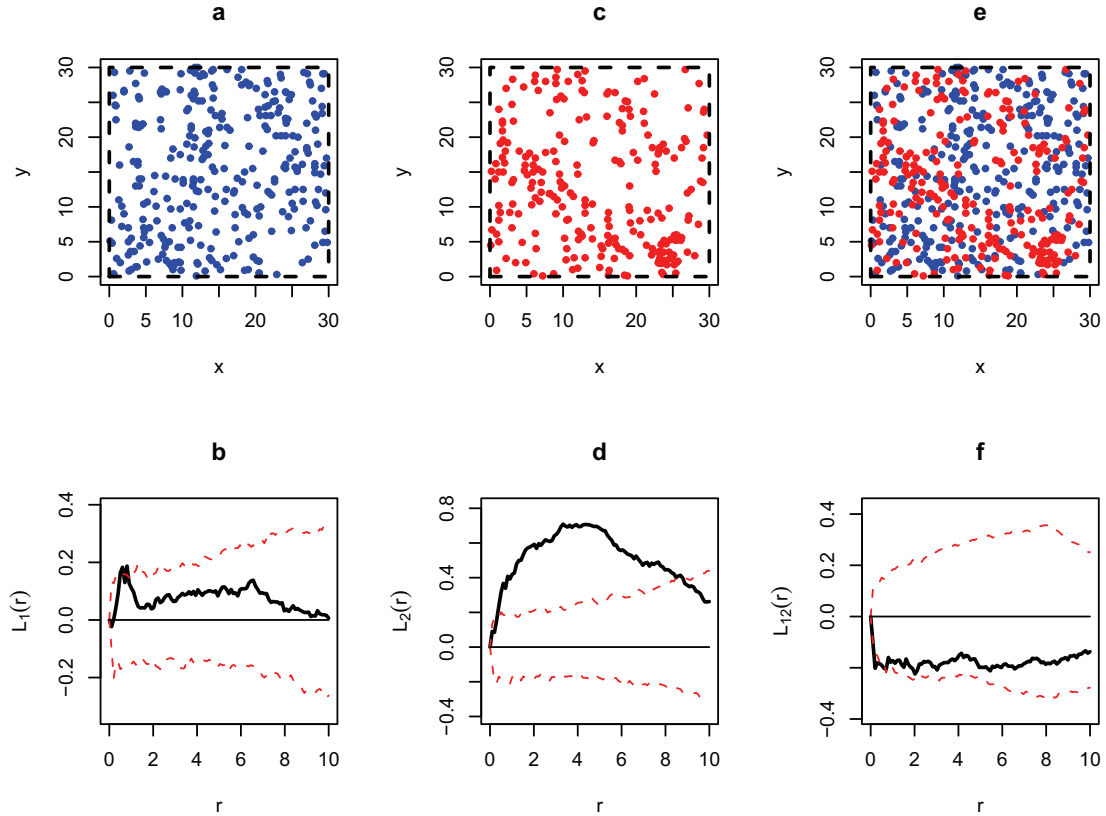


Figure 3.15. The point patterns (a) and (c) represents respectively the species *Avicennia* ($n=309$) and *Laguncularia* ($n=251$). (b) and (d) represents their L-function (black) and 99% simulation envelope for CSR hypothesis (dashed red) respectively. The point pattern (e) represents the species *Avicennia* (blue) and *Laguncularia* (red). (f) represents its bivariate L-function (black) and 99% simulation envelope for spatial independence hypothesis (dashed red). The simulation envelopes were calculated via Monte Carlo method (Besag 1977) with 10000 simulations.

All trees in Lagoa A present clustering at scales $r = 2$ m and $r = 4$ m and a certain tendency to regularity at scale $r = 0.20$ m. This pattern is probably a result of a superposition of various ecological processes that occur at different scales within the same community. Because of this, an interpretation of the overall pattern is not straightforward. More information can be obtained by analysing the patterns exhibited by different species and different groups, as follows. (see **Figure 3.7**)

Avicennia germinans trees exhibit clustering at scale $r = 0.5$ m (see **Figure 3.8**).

Laguncularia racemosa trees exhibit clustering at different scales, with a maximum at scale $r = 4$ m (see **Figure 3.9**).

Dead trees exhibit clustering at lower and intermediate scales, with maxima at scales $r = 1$ m and $r = 4$ m (see **Figure 3.10**).

Large trees generally exhibit CSR but with a tendency to regularity at scale $r = 2$ m and small trees tends to be clumped at lower and intermediate scales, in particular at scale $r = 4$ m (see **Figure 3.11**). The spatial relation between the large and small trees shows some tendency to repulsion at lower scales (see **Figure 3.11**).

Large *Avicennia* trees tend to be clumped at scale $r = 1$ m and small *Avicennia* trees tend to be clumped at scales $r = 1$ m and $r = 3$ m (see **Figure 3.12**). The spatial relation between large and small *Avicennia* trees additionally presents a tendency to repulsion at scale $r = 2$ m (see **Figure 3.12**).

Large *Laguncularia* trees tend to exhibit CSR and *Laguncularia* trees exhibit clumping at all scales (with a maximum at scale $r = 4$ m) (see **Figure 3.13**). The spatial relation between large and small *Laguncularia* trees exhibits spatial independence (see **Figure 3.13**).

Living trees exhibit clumping at scales between $r = 1$ m and $r = 4$ m (see **Figure 3.14**). The spatial relation between dead and living trees exhibits aggregation at lower scales (with a maximum at $r = 2$ m) (see **Figure 3.14**).

The spatial relation between *Laguncularia* and *Avicennia* trees exhibits a tendency to repulsion at lower scales (in particular at scale $r = 0.50$ m) (see **Figure 3.15**).

In **Table 3.6** and **Table 3.7** I present a summary of the results obtained from the spatial statistical analyses described above.

Lagoa A - Univariate Case	
Type	$L(r)$
All	Regularity ($r \simeq 0.2$ m)*
	Clumping at LS ($r \simeq 1$ m and $r \simeq 4$ m)**
Avicennia	Clumping at $r \simeq 1$ m.
Laguncularia	Clumping at all scales ($r \simeq 4$ m)**
Dead trees	Clumping at LS ($r \simeq 1$ m and $r \simeq 4$ m)**

Table 3.6. Summary of the univariate L-function analysis obtained for the site Lagoa A. (*) tendency and (**) in particular. LS (Lower Scales), IS (Intermediate Scales) and HS (Higher Scales).

Lagoa A - Bivariate Case			
Type	$L_1(r)$	$L_2(r)$	$L_{12}(r)$
1 Large trees	Regularity*	Clumping at LS	Repulsion* at LS
2 Small trees	($r \simeq 2$ m)	and IS ($r \simeq 4$ m)**	($r \simeq 2$ m)**
1 Large <i>Avi.</i>	Clumping	Clumping	Repulsion* at LS
2 Small <i>Avi.</i>	($r \simeq 1$ m)	($r \simeq 1$ m and $r \simeq 3$ m)	($r \simeq 2$ m)**
1 Large <i>Lag.</i>	Spatial	Clumping at all scales	Spatial
2 Small <i>Lag.</i>	independence	($r \simeq 4$ m)**	independence
1 Dead trees	Clumping at LS	Clumping at LS	Aggregation at LS
2 Alive trees	($r \simeq 1$ m and $r \simeq 4$ m)**	and IS ($r \simeq 4$ m)**	($r \simeq 2$ m)**
1 <i>Avi.</i>	Clumping	Clumping at all scales	Repulsion*
2 <i>Lag.</i>	($r \simeq 1$ m)	($r \simeq 4$ m)**	($r \simeq 1$ m)

Table 3.7. Summary of the univariate and bivariate L-function analysis obtained for the site Lagoa A. small = (dbh ≤ 5 cm) and large = (dbh > 5 cm).(*) tendency and (**) in particular. LS (Lower Scales), IS (Intermediate Scales) and HS (Higher Scales).

3.2.2 Lagoa B

Site Lagoa B contains a total of 543 trees (including 116 dead trees) (see **Figure 3.16**).

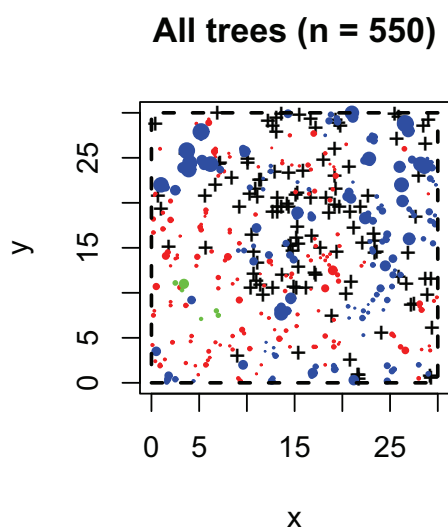


Figure 3.16. All trees of the stand Lagoa B. (black cross) dead tree, (blue dot) *Laguncularia racemosa* and (red dot) *Avicennia germinans* and (green dot) *Rhizophora mangle*. The size of dot is proportional to the dbh of *Avicennia* and *Laguncularia* (there's no information about the dbh of the dead trees).

Type	mean(dbh)	var(dbh)	max(dbh)	n	n/N
All	5.18*	25.54*	24.83*	N=550	1.000
<i>Avicennia germinans</i>	2.77	6.81	13.05	256	0.47
<i>Laguncularia racemosa</i>	8.79	31.93	24.83	171	0.31
<i>Rhizophora mangle</i>	5.73	16.79	13.69	7	0.01
Dead trees	-	-	-	116	0.21

Table 3.8. Short statistical summary of the mean stem diameter in breast height (dbh) for Lagoa B site. (-) There's no information about the dead trees's dbh. (*) Excluding the dead trees. (dbh in cm).

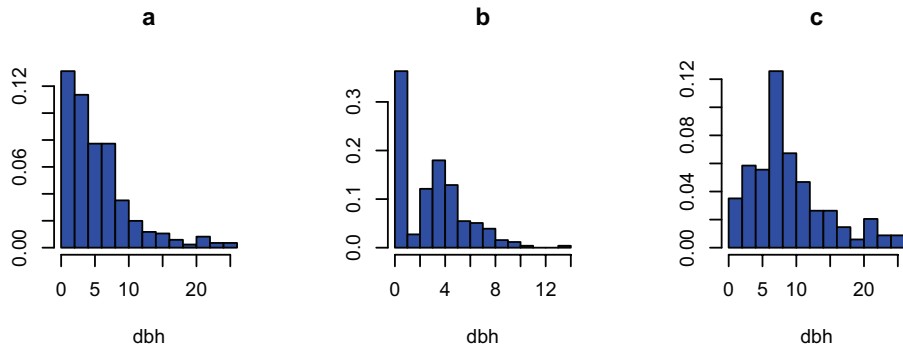


Figure 3.17. Lagoa B - Histograms showing the size class distribution of mean stem diameter in breast height (dbh) in cm obtained for (a) all trees (excluding dead trees), (b) *Avicennia germinans* and (c) *Laguncularia racemosa*.

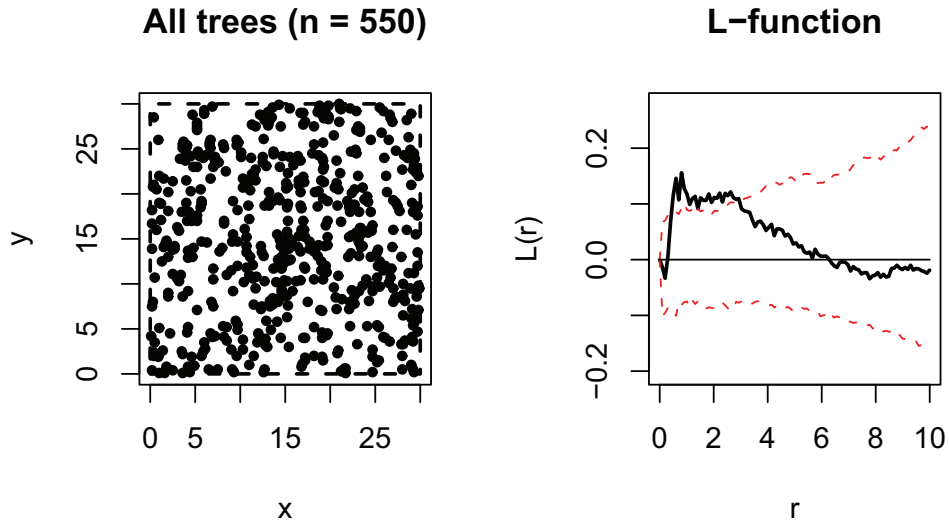


Figure 3.18. (left) Spatial point pattern relative to all trees of the stand Lagoa B and its (right) respective L-function (black) and 99% simulation envelope (dashed red). The simulation envelope was calculated via Monte Carlo method (Besag 1977) for the CSR hypothesis with 10000 simulations.

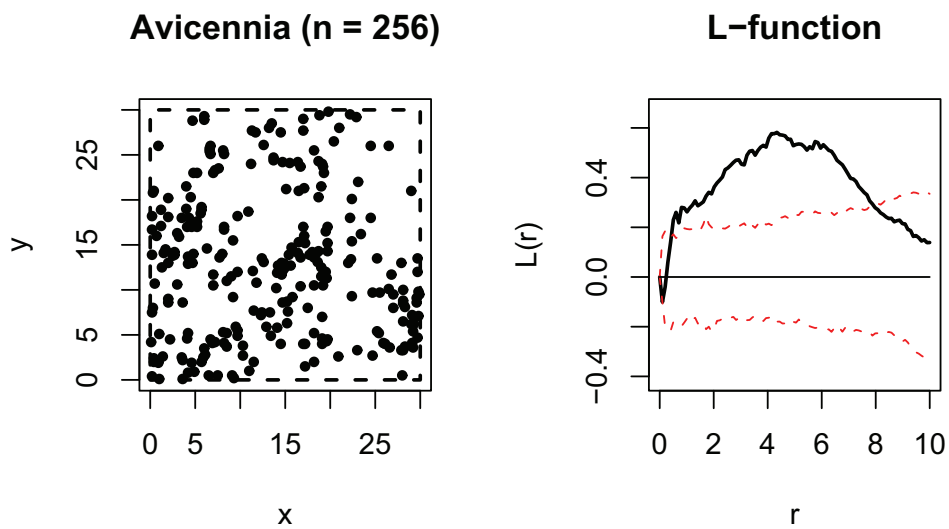


Figure 3.19. (left) Spatial point pattern relative to the species *Avicennia germinans* within stand Lagoa B. Its (right) respective L-function (black) and 99% simulation envelope (dashed red). The simulation envelope was calculated via Monte Carlo method (Besag 1977) for the CSR hypothesis with 10000 simulations.

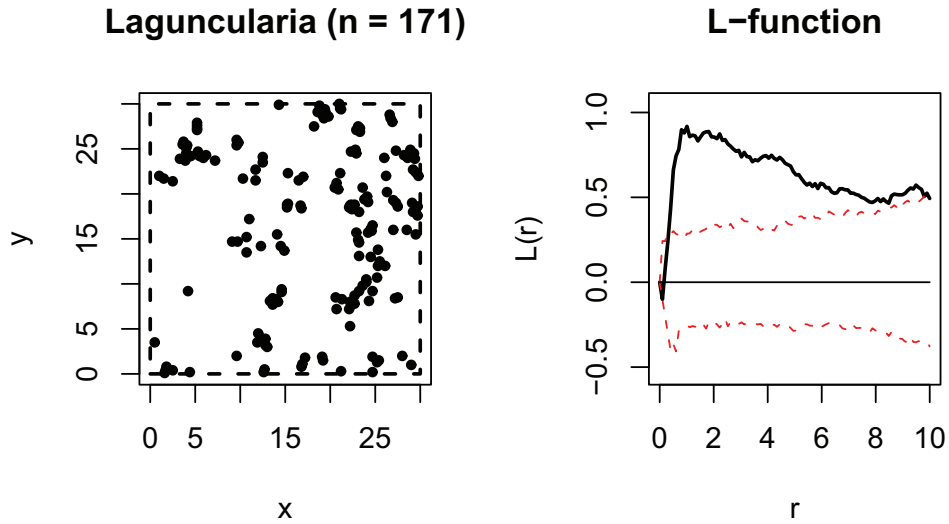


Figure 3.20. (left) Spatial point pattern relative to species *Laguncularia racemosa* within stand Lagoa B. Its (right) respective L-function (black) and 99% simulation envelope (dashed red). The simulation envelope was calculated via Monte Carlo method (Besag 1977) for the CSR hypothesis with 10000 simulations.

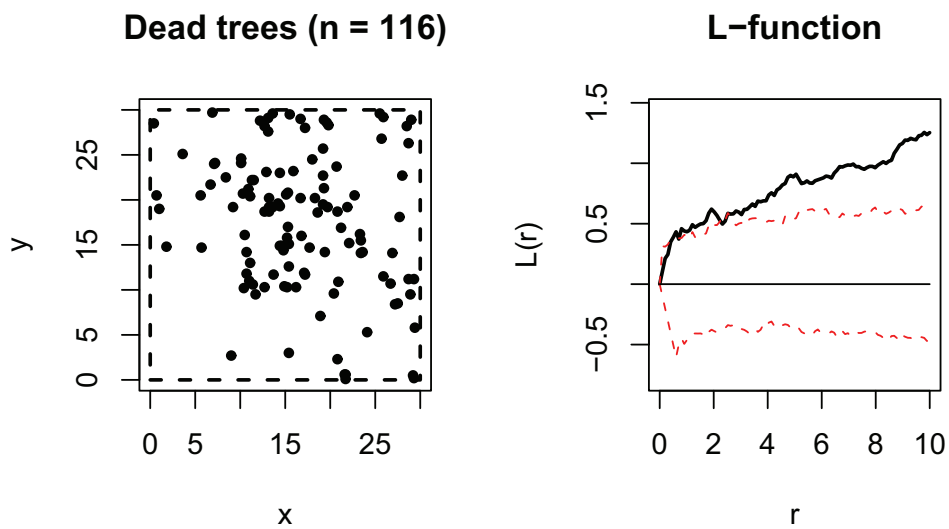


Figure 3.21. (left) Spatial point pattern relative to dead trees within stand Lagoa A. Its (right) respective L-function (black) and 99% simulation envelope (dashed red). The simulation envelope was calculated via Monte Carlo method (Besag 1977) for the CSR hypothesis with 10000 simulations.

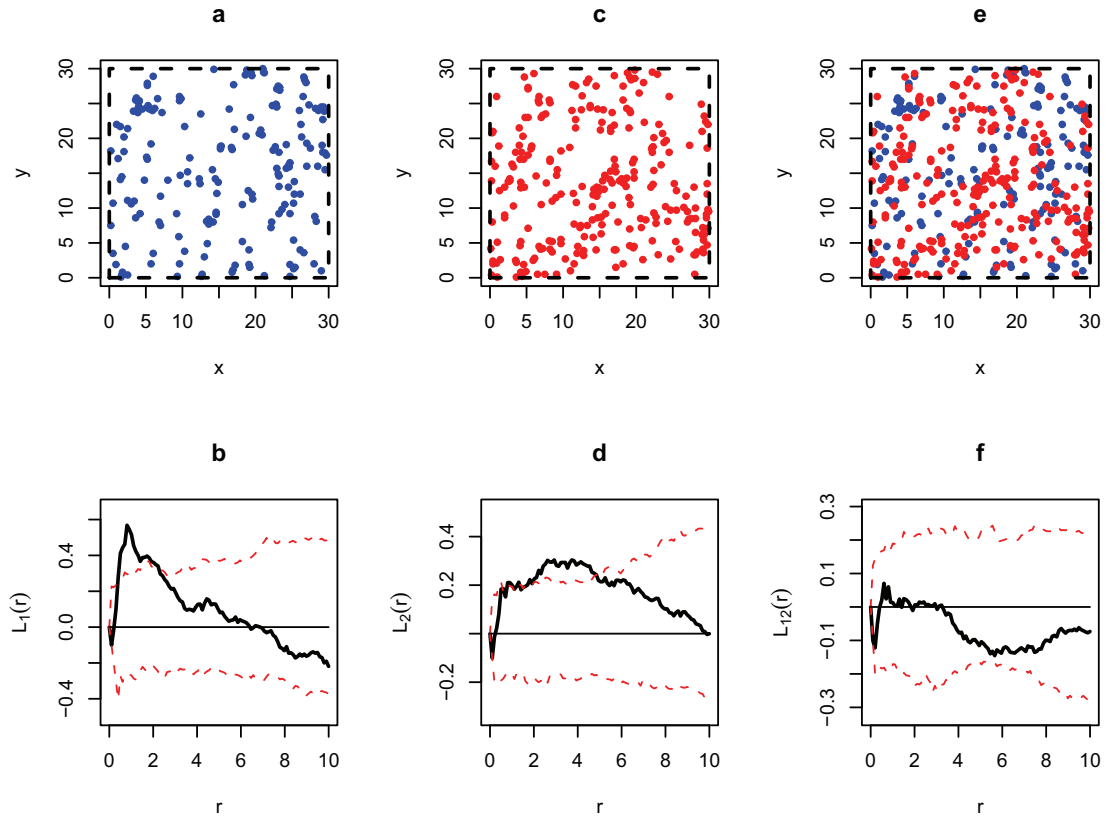


Figure 3.22. The point patterns (a) and (c) represents respectively the large trees ($n=179$) and small trees ($n=255$). (b) and (d) represents their L-function (black) and 99% simulation envelope for CSR hypothesis (dashed red) respectively. The point pattern (e) represents the big trees (blue) and small trees (red). (f) represents its bivariate L-function (black) and 99% simulation envelope for spatial independence hypothesis (dashed red). The simulation envelopes were calculated via Monte Carlo method (Besag 1977) with 10000 simulations.

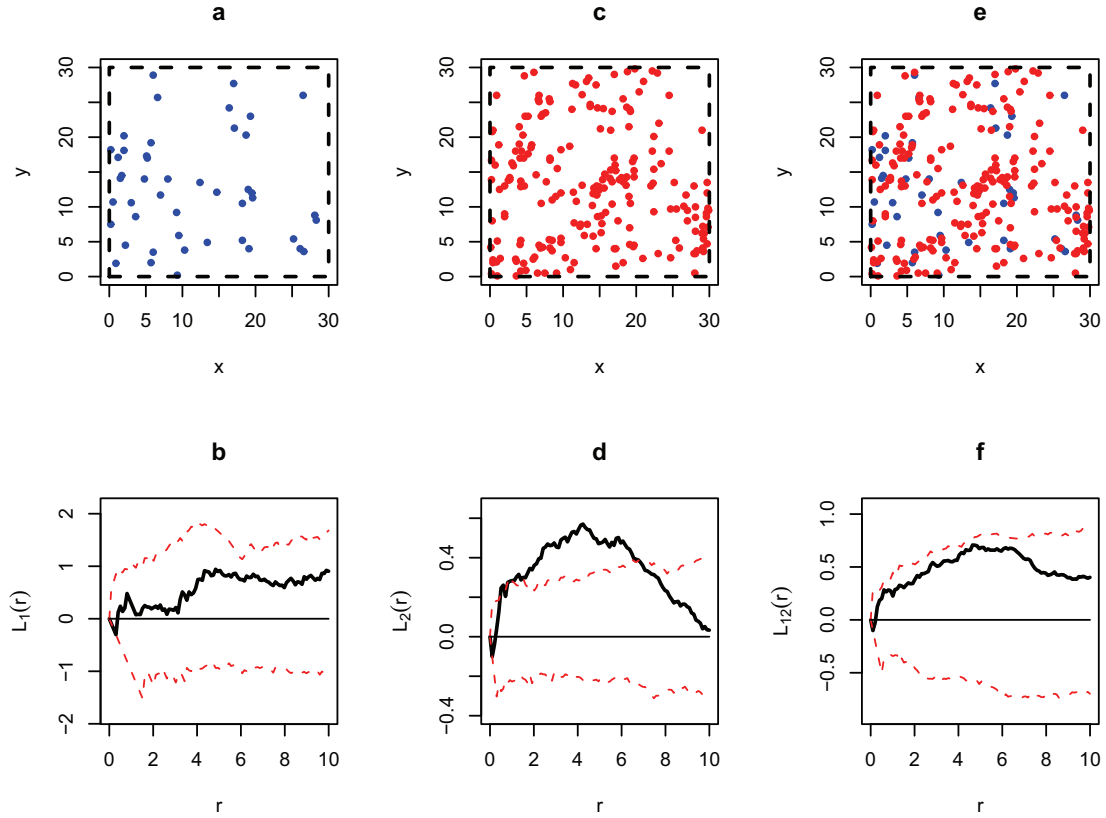


Figure 3.23. The point patterns (a) and (c) represents respectively the large *Avicennia* (n=46) and small *Avicennia* (n=210). (b) and (d) represents their L-function (black) and 99% simulation envelope for CSR hypothesis (dashed red) respectively. The point pattern (e) represents the big *Avicennia* (blue) and small *Avicennia* (red). (f) represents its bivariate L-function (black) and 99% simulation envelope for spatial independence hypothesis (dashed red). The simulation envelopes were calculated via Monte Carlo method (Besag 1977) with 10000 simulations.

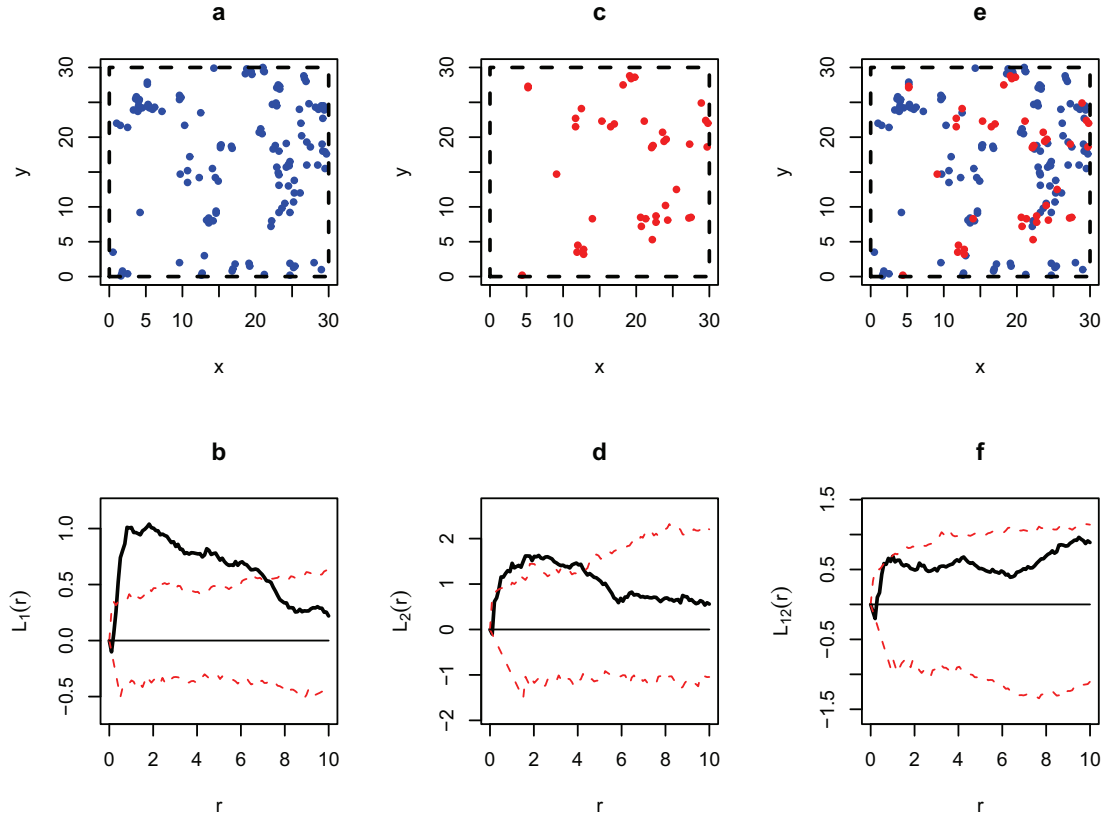


Figure 3.24. The point patterns (a) and (c) represents respectively the large *Laguncularia* ($n=129$) and small *Laguncularia* ($n=42$). (b) and (d) represents their L-function (black) and 99% simulation envelope for CSR hypothesis (dashed red) respectively. The point pattern (e) represents the big *Laguncularia* (blue) and small *Laguncularia* (red). (f) represents its bivariate L-function (black) and 99% simulation envelope for spatial independence hypothesis (dashed red). The simulation envelopes were calculated via Monte Carlo method (Besag 1977) with 10000 simulations.

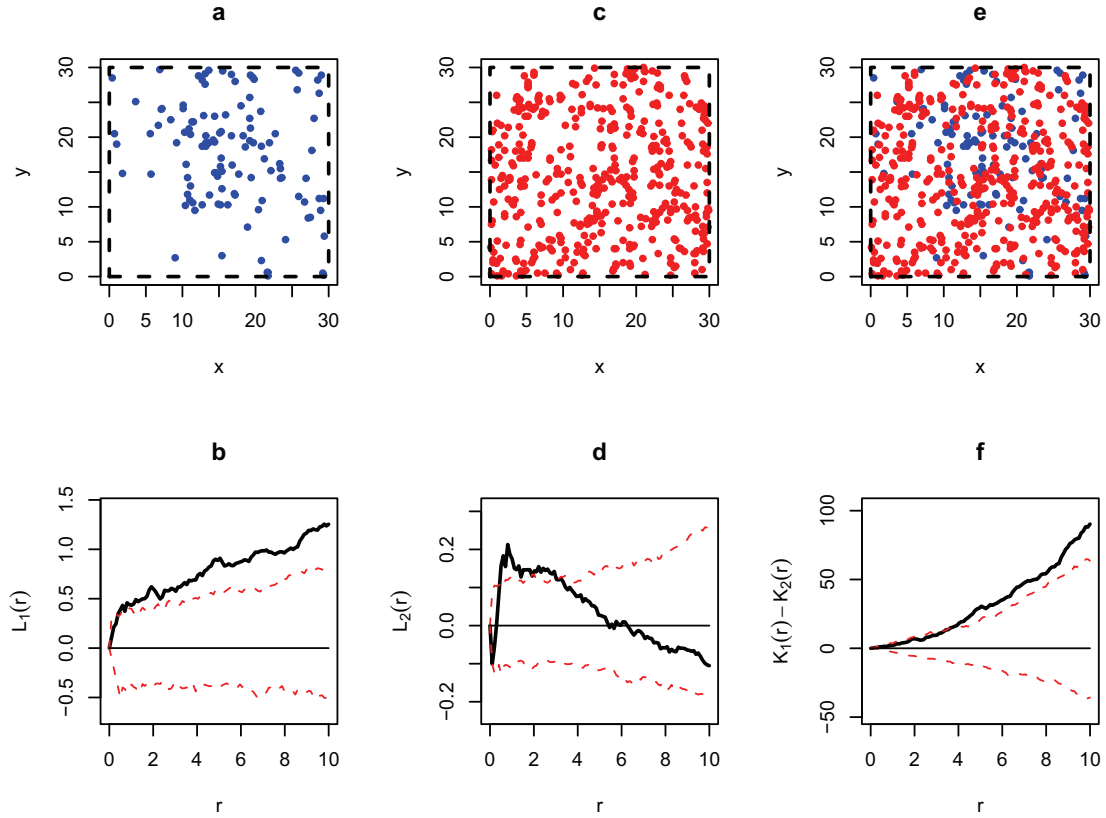


Figure 3.25. The point patterns (a) and (c) represents respectively the dead trees ($n=116$) and living trees ($n=434$). (b) and (d) represents their L-function (black) and 99% simulation envelope for CSR hypothesis (dashed red) respectively. The point pattern (e) represents the dead trees (blue) and living trees (red). (f) represents its $K_1(r) - K_2(r)$ (black) and 99% simulation envelope for random labeling hypothesis (dashed red). The simulation envelopes were calculated via Monte Carlo method (Besag 1977) with 10000 simulations.

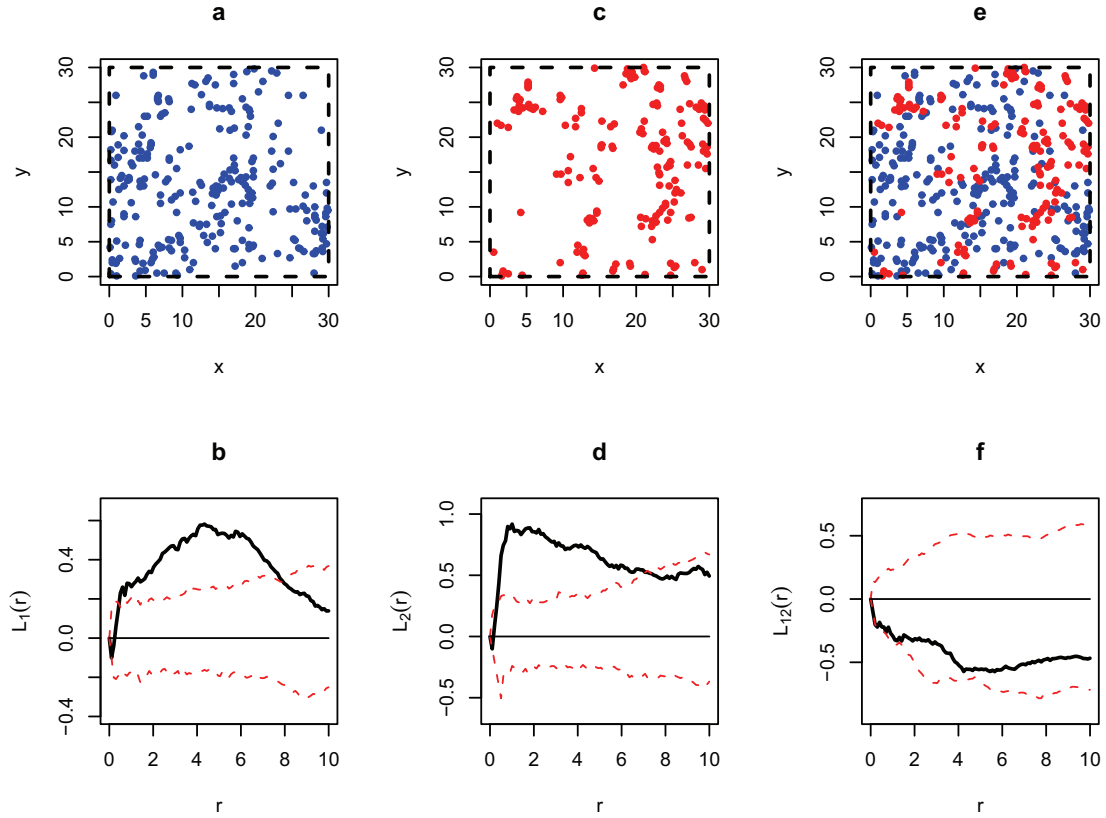


Figure 3.26. The point patterns (a) and (c) represents respectively the species *Avicennia* ($n=256$) and *Laguncularia* ($n=171$). (b) and (d) represents their L-function (black) and 99% simulation envelope for CSR hypothesis (dashed red) respectively. The point pattern (e) represents the species *Avicennia* (blue) and *Laguncularia* (red). (f) represents its bivariate L-function (black) and 99% simulation envelope for spatial independence hypothesis (dashed red). The simulation envelopes were calculated via Monte Carlo method (Besag 1977) with 10000 simulations.

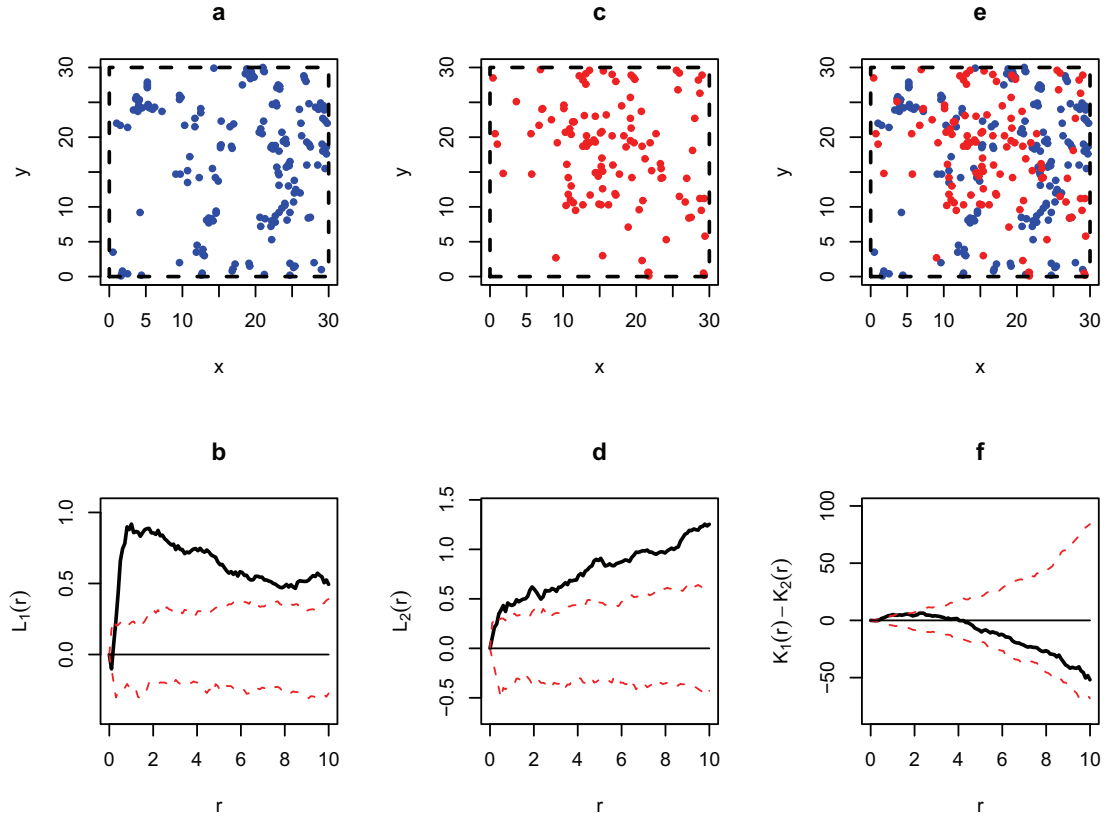


Figure 3.27. The point patterns (a) and (c) represents respectively the species *Laguncularia* ($n=171$) and dead trees ($n=171$). (b) and (d) represents their L-function (black) and 99% simulation envelope for CSR hypothesis (dashed red) respectively. The point pattern (e) represents the species *Laguncularia* (blue) and dead trees (red). (f) represents its bivariate L-function (black) and 99% simulation envelope for spatial independence hypothesis (dashed red). The simulation envelopes were calculated via Monte Carlo method (Besag 1977) with 10000 simulations.

All trees in Lagoa B exhibit clustering at lower scales (with a maximum at scale $r = 1$ m) (see **Figure 3.18**).

Avicennia germinans trees exhibit clustering at lower and intermediate scales (with a maximum at scale $r = 4$ m) (see **Figure 3.19**).

Laguncularia racemosa trees exhibit clustering at lower, intermediate and higher scales (with a maximum at scale $r = 1$ m) (see **Figure 3.20**).

Dead trees exhibit clustering at lower, intermediate and higher scales (see **Figure 3.21**).

Large trees exhibit clustering at scale $r = 1$ m and small trees exhibit clustering at intermediate scales (with a maximum at scale $r = 4$ m) (see **Figure 3.22**). The spatial relation between the large and small trees exhibits a tendency to repulsion at scale $r = 6$ m (see **Figure 3.22**).

Large *Avicennia* trees exhibit CSR. Small *Avicennia* trees exhibit clustering at intermediate scales (with a maximum at scale $r = 4$ m) (see **Figure 3.23**). The spatial relation between large and small *Avicennia* trees exhibits a tendency to aggregation at lower and intermediate scales (with a maximum at $r = 4$ m) (see **Figure 3.23**).

The spatial relation between large and small *Laguncularia* trees exhibits aggregation at scale $r = 1$ m (see **Figure 3.24**).

Living trees exhibit clustering at lower scales (with a maximum at $r = 1$ m) (see **Figure 3.25**). The spatial relation between the dead and living trees exhibits aggregation at intermediate and higher scales (see **Figure 3.25**).

The spatial relation between *Avicennia* and *Laguncularia* trees exhibits repulsion at scale $r = 1$ m and a tendency to repulsion at scale $r = 4$ m (see **Figure 3.26**).

The spatial relation between *Laguncularia* and dead trees exhibits aggregation at lower scales (see **Figure 3.27**).

In **Table 3.9** and **Table 3.10** I present a summary of the results obtained from the spatial statistical analyses described above.

Lagoa B - Univariate Case	
Type	$L(r)$
All	Clumping at lower scales ($r \simeq 1$ m)**
Avicennia	Clumping LS and IS ($r \simeq 4$ m)**
Laguncularia	Clumping at all scales ($r \simeq 1$ m)**
Dead trees	Clumping at all scales

Table 3.9. Summary of the univariate L-function analysis obtained for the site Lagoa B. (*) tendency and (**) in particular. LS (Lower Scales), IS (Intermediate Scales) and HS (Higher Scales).

Lagoa B - Bivariate Case			
Type	$L_1(r)$	$L_2(r)$	$L_{12}(r)$
1 Large trees	Clumping	Clumping at IS	Repulsion*
2 Small trees	($r \simeq 1$ m)	($r \simeq 4$ m)**	($r \simeq 6$ m)
1 Large <i>Avi.</i>	CSR	Clumping at IS	Aggregation* at LS
2 Small <i>Avi.</i>	pattern	($r \simeq 4$ m)**	and IS ($r \simeq 4$ m)**
1 Large <i>Lag.</i>	Clumping at LS	Clumping at LS	Aggregation
2 Small <i>Lag.</i>	and IS ($r \simeq 2$ m)**	($r \simeq 2$ m)**	($r \simeq 1$ m)
1 Dead trees	Clumping at	Clumping at LS	Aggregation at LS
2 Alive trees	all scales	($r \simeq 1$ m)**	and IS
1 <i>Avi.</i>	Clumping at LS	Clumping at all scales	Repulsion
2 <i>Lag.</i>	and IS ($r \simeq 4$ m)**	($r \simeq 1$ m)**	($r \simeq 1$ m)
1 <i>Lag.</i>	Clumping at all scales	Clumping at	Aggregation at LS
2 Dead trees	($r \simeq 1$ m)**	all scales	($r \simeq 1$ m)**

Table 3.10. Summary of the univariate and bivariate L-function analysis obtained for the site Lagoa B. small = (dbh ≤ 5 cm) and large = (dbh > 5 cm). (*) tendency and (**) in particular. LS (Lower Scales), IS (Intermediate Scales) and HS (Higher Scales).

3.3 Discussion

The results in **Table 3.5** and **Table 3.8** provide some important information about the probable stages of the development of mangrove forests at sites Lagoa A and Lagoa B. It should be noted that is very difficult to obtain this information about a mangroves forest. The problem is that mangroves show a high degree of plasticity in response to environmental conditions. If conditions are harsh, the trees grow more slowly. Thus, trees can be small because they are young or because of poor conditions for growth in the stand . The same argument applies to the succession stages (Hogarth 1999). Moreover I have no information about the inundation regimes and abiotic conditions at these sites. For these reasons, the

discussion presented below can be no more than a preliminary interpretation of probable underlying ecological processes occurring at sites Lagoa A and Lagoa B. Four points can be made:

First, tree density at the sites Lagoa A and Lagoa B is 0.90 ind/m² and 0.61 ind/m² respectively (see **Table 3.5** and **Table 3.8**). Silvertown & Dourt (1993) show that the density of the trees generally tends to decrease during the development of a forest stand, due to self-thinning effects.

Second, some individuals of *Rhizophora mangle* are present at Lagoa B and by contrast, none were found at Lagoa A (see **Table 3.5** and **Table 3.8**). Ball (1980) shows that *Rhizophora mangle* generally colonizes a mangrove forest only in relatively advanced stages of the development.

Third, mean(dbh) of trees at Lagoa A and Lagoa B present = 4.41 cm and 5.18 cm respectively (see **Table 3.5** and **Table 3.8**). Jimenez et al. (1985) and Fromard et al. (1988) show that, during the development of a forest stand, the mean dbh of the trees generally increases.

Finally, the sites Lagoa A and Lagoa B contain the same proportion of *Laguncularia racemosa* trees in the stands (31%). However, the proportion of *Avicennia germinans* at sites Lagoa A and Lagoa B is 38% and 47% of respectively (see **Table 3.5** and **Table 3.8**). Duke (2001) and Menezes (2006) show that, during the development of a stand, *Avicennia germinans* is the second species to establish itself.

Taken together, the results and their interpretation presented above provide a strong indication that the mangrove forest at Lagoa A is at an earlier stage of development than at site Lagoa B. Site Lagoa A contains a high proportion of *Laguncularia racemosa* and no specimens of *Rhizophora mangle* (see **Table 3.5**). The dbh histogram calculated for all trees in this site presents a L-shape distribution (see **Figure 3.6**). On this basis, I surmise that the forest at site Lagoa A could be at an early development stage (Ball 1980).

Site Lagoa B also contains a high proportion of *Laguncularia racemosa*, but in contrast to the site Lagoa A, it also contains some individuals of *Rhizophora mangle*, which is starting to colonize the stand (see **Table 3.8**). The dbh histogram calculated for all trees in this site presents a L-shape distribution. On this basis, I surmise that the forest at site Lagoa B is also at an early development stage.

In summary, the sites Lagoa A and Lagoa B seem to be in the same stage of development, but Lagoa B seems to be more advanced in relation to the site Lagoa A.

Now I move on to consider the underlying ecological processes at the two sites, basing our inferences on the statistical analysis of the spatial configuration of the trees in sites presented in **Chapter 2**. It is important to note that these methods have some limitations. They assume that the spatial patterns being analyzed are homogeneous. The hypothesis of homogeneity means that the second-order characteristics of a point pattern are invariant under translation and rotation. But it is well-known that heterogeneity is common in nature and it is unlikely that the sites Lagoa A and Lagoa B are exceptions to this rule.

The spatial configuration of all trees in sites Lagoa A and Lagoa B is probably a result of the superposition of different ecological processes occurring at different scales within the same community (see **Figure 3.7** and **Figure 3.18**). In order to try to isolate and identify these different processes, I performed univariate and bivariate L-function analyses, separating the trees into different species and groups.

In site Lagoa A, *Avicennia germinans* show clustering at lower scales (see **Figure 3.8**). This could be either a seed dispersal (Sterner et al. 1986) or a nurse-plant effect (Tielbörger & Kadmon 2000). By contrast, *Avicennia germinans* in site Lagoa B exhibits clustering at intermediate scales (see **Figure 3.19**). This could be result of environmental heterogeneity within the stand (Klaas et al. 2000).

Laguncularia racemosa in site Lagoa A exhibits clustering at higher scales (see **Figure 3.9**). On the other hand, *Laguncularia racemosa* in site Lagoa B exhibits clustering at intermediate scales (see **Figure 3.20**). These results could be the result of spatial environmental heterogeneity within the stands (Klaas et al. 2000). Although the L-function has no spatial resolution, visually it is possible to make out large regions with a high density of *Laguncularia racemosa* trees, both in Lagoa A (see **Figure 3.9**) and Lagoa B (see **Figure 3.20**). The indication of clumping at the scale $r = 4$ m in Lagoa A is result of a cluster located at the bottom right of the site (see **Figure 3.9**).

Dead trees in site Lagoa A don't exhibit heterogeneity (see **Figure 3.10**). This means that the death of trees at this site has been a homogeneous process. By contrast, dead trees of the site Lagoa B exhibit clustering at higher scales (see **Figure 3.21**). This could be a result of environmental heterogeneity (Klaas et al. 2000). Probably, the death of the trees is a process that has occurred at specific locations within this site.

The regular pattern of large trees in site Lagoa A (see **Figure 3.11**) could be a result of a competition effect (Wiegand & Moloney 2004). In contrast, the small trees present clustering (see **Figure 3.11**). The spatial relationship between the large and small trees (see **Figure 3.11**) indicates probably the existence of light gaps (Duke 2001), where the small trees tends to occupy the space that exists between the big trees. In contrast, the large trees in site Lagoa B exhibit clustering, and small trees in the Lagoa B exhibit the same spatial pattern (see **Figure 3.22**). But the spatial relationship between these large and small trees exhibits repulsion at intermediate scales (see **Figure 3.22**). In summary, in site Lagoa B, trees of the same group tends to form clusters, but there is a tendency to repulsion between trees of different groups. That could be result of a succession process (Begon et al. 1976, Connel & Slatyer 1977) or invasion by a species new to the location (Goreaud et al. 1996).

Large and small *Avicennia* in site Lagoa A exhibit clumping at lower scales (see **Figure 3.12**). But in contrast, the spatial relationship between the large and small *Avicennia* presents some tendency to repulsion at lower scales (see **Figure 3.12**). This could be a indication of intra-specific competition (Kenkel 1988). In site Lagoa B, the large *Avicennia* trees exhibit CSR (see **Figure 3.23**). On the other hand, small trees exhibit clumping at intermediate scales (see **Figure 3.23**). The spatial relationship between large and small *Avicennia* trees (see **Figure 3.23**) shows some tendency to aggregation, in particular at

an intermediate scale, providing an indication of environmental heterogeneity within the stand (Klaas et al. 2000).

In site Lagoa A, large *Laguncularia* exhibit CSR and small *Laguncularia* exhibit clumping (see **Figure 3.13**). This could be result of environmental heterogeneity in the stand (Klaas et al. 2000). Additionally, these large and small *Laguncularia* trees exhibit spatial independence at all scales (see **Figure 3.13**). In site Lagoa B, large *Laguncularia* exhibit clustering at intermediate scales (see **Figure 3.24**). This could be indication of environmental heterogeneity within the stand (Klaas et al. 2000). Large and small *Laguncularia* presents aggregation at lower scales (see **Figure 3.24**). This could be an indication of nurse-plant effect (Tielbörger & Kadmon 2000) or a seed-dispersion effect (Sternier 1986).

In site Lagoa A, dead and living trees present clumping pattern at lower scales (see **Figure 3.14**). But the spatial relationship between dead and living trees shows aggregation at lower scales (see **Figure 3.14**). The death of the trees has probably occurred homogeneously within this site. In site Lagoa B, dead and living trees (see **Figure 3.25**) show indications of environmental heterogeneity within the stand (Klaas et al. 2000). In contrast with site Lagoa A, the death of the trees has not occurred homogeneously within this site. Visually, it is easy to notice that dead trees seem to occur more frequently in areas with a high density of *Laguncularia* trees (see **Figure 3.27**). The spatial relation between *Laguncularia* and dead trees shows aggregation at lower scales, confirming our hypothesis.

In the sites Lagoa A and Lagoa B, the spatial relationship between the species *Avicennia germinans* and *Laguncularia racemosa* exhibits a tendency to repulsion at lower and intermediate scales (see **Figure 3.15** and **Figure 3.26** respectively). This could be an indication of inter-specific competition occurring within the stand (Barot et al. 1999), succession (Begon et al. 1976, Connel & Slatyer 1977) or evidence of invasion by a new species (Goreaud et al. 1996).

In summary, analysis of the spatial configuration of individual trees at the sites Lagoa A and Lagoa B shows few similarities between the two sites, despite the short distance between them (about 15 m). This could be a result of the different inundation conditions occurring at these sites. The frequency of inundation is presumably lower at Lagoa A than at Lagoa B, due to its lower basin (Harum 2006).

There are more indications of spatial heterogeneity at site Lagoa B than at Lagoa A. This could be an indication of greater environmental heterogeneity at Lagoa B (Klaas et al. 2000). This hypothesis is difficult to prove, because I have no information about the abiotic conditions at the study sites Lagoa A and Lagoa B, but the spatial configuration exhibited by the trees could be a indication of environmental heterogeneity and so I cannot exclude this possibility.

The results provide an indication of a probable succession process (Begon et al. 1976, Connel & Slatyer 1977) occurring among the *Avicennia* and *Laguncularia* trees within sites Lagoa A and Lagoa B. If I consider that mangrove forests are in a continuous process of growth and constantly establishing and renewing themselves (Duke 2001), the hypothesis of succession occurring among the individuals of species *Avicennia* and *Laguncularia* within

the stands is a plausible one. The results suggest a certain tendency among *Laguncularia* and *Avicennia* trees to occupy specific regions of the stand (i.e they exhibit repulsion). But the Ripley K-function cannot detect this because it has no spatial resolution. That is a limitation of the Ripley K-function. The method provides information about the scales which the ecological processes occur, but no information about where these processes occur.

Despite the heterogeneity presented within sites Lagoa A and Lagoa B and the inability of the Ripley K-function (hypothesis of heterogeneity) to provide information about this, the Ripley K-function did provide important information about the underlying ecological processes occurring in these stands.

Later in Chapter 4, I present a methodology that can be used in combination with the standard spatial statistical methods applied to spatial pattern analysis (Ripley K-function, for example), in order to overcome these limitations and provide, under certain conditions, scale-spatial information about the ecological processes that occur in the stand.

Chapter 4

Object Pattern Analysis

4.1 Introduction

In plant ecology, each individual plant is mapped as a point with the Cartesian coordinates (x, y) representing the center of their stems. But, depending on the dimensions of the individuals in relation to the scale that I want to analyze, this transformation can cause problems. To analyze the spatial configuration of individuals (trees, coral, etc...) using traditional statistical spatial methods (quadrat counts and the Ripley K-function, for example), each individual within the study site Ω is represented as a point $(x, y) \in \Omega \subset \mathbb{R}^2$, for the two dimensional case. Problem can arise due to the loss of information during the transformation, which involves the following steps: The first step T_1 represents a three dimensional plant individual as a two dimensional abstraction, representing only its stem and crown. The second step T_2 transforms this two dimensional representation into a single point (see **Figure 4.1**).

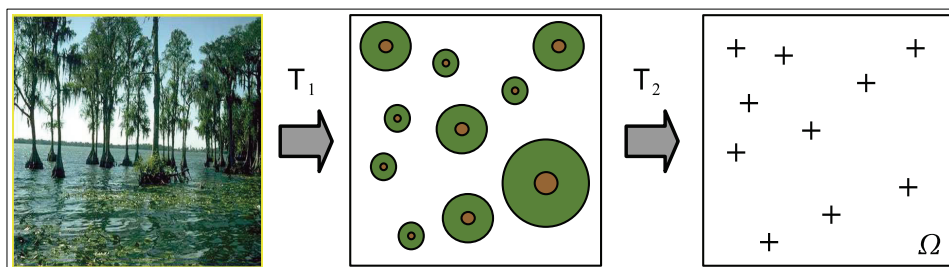


Figure 4.1. Steps of a transformation of a tridimensional object (tree) into a point. **(left)** Real trees, **(middle)** bidimensional abstraction of a real tree with crown (green) and stem (brown) and **(right)** point pattern representing the bidimensional abstraction.

The limitations of this procedure which considers a three dimensional plant individual as a point, affect the interpretation of results obtained via standard spatial methods, which can not correspond to what is really happening at the study site. For example, this procedure can indicate regularity at lower scales instead of a significant small-scale aggregation (Simberloff 1979, Prentice & Werger 1983) (see **Figure 4.2**).

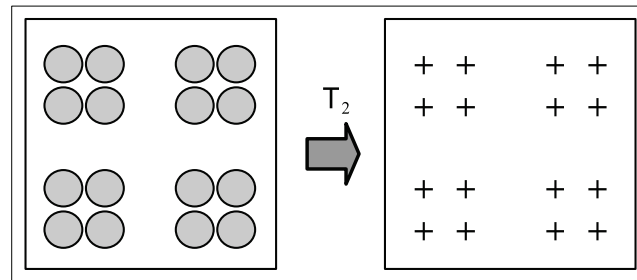


Figure 4.2. The circle-to-point transformation T_2 indicates regularity at lower scales, instead of small-scale aggregation.

One way of minimizing the effects of this limitation, could be to utilize the definition of functional scale^{4.1} adopted by Malkinson *et al.* (2003). The lower boundary of the functional scale can be estimated by calculating the mean plant rbh of the plants in the community. Then, only the ecological processes that occur above this scale should be considered. For example, tree interactions would be considered as occurring at distances of between one and ten meters (Stoyan & Penttinen 2000). However this can lead to information being lost due to the failure to take of account of information about interactions at smaller scales.

Furthermore, Wiegand *et al.* (2006) proposed a methodology, based on a grid-based approach, to perform the analysis of spatial configuration of objects of finite size and irregular shape. The method basically consists to discretize each individual in a grid and utilizes grid-based versions of the bivariate functions $K_{12}(r)$, $L_{12}(r)$ and $g_{12}(r)$ (Wiegand & Moloney 2004) to analyze the spatial relationship of these tree individuals within a study site.

Similarly, the main objective of this chapter is to provide a suitable method to perform spatial analysis of individuals, considering these individuals as a circular objects, rather than points. The idea behind the method is to approximate each individual as a circle and to perform the spatial analysis considering these individuals as circular objects.

There exists at least two basic differences among the method proposed by Wiegand *et al.* (2006) and the method proposed in this chapter. The first discretizes the individuals in a grid and do not permits the overlapping among these individuals. On the other hand, our method represents each individual analytically as a circle and permits the overlapping between these objects. Of course, these method is only applicable if the shape of the analysed individuals are approximately circular.

The methodology was applied to the stand sites Lagoa A and Lagoa B and compared with the results obtained in the **Chapter 2**.

Additionally, I want to know if the method has sufficient sensibility to detect a probable succession process occurring among the trees of species *Avicennia germinans* and *Laguncularia racemosa* within these stands.

4.1. The scales at which interactions among plants occur in each study site.

4.2 Method

The idea was to adapt the Ripley K-function to analyze the spatial pattern of objects (circles, in our case). This procedure considers the spatial distribution of circular objects, rather than points. Here $c_i(r_i)$ and $c_j(r_j)$ are defined respectively as a circle of radius r_i centered at a point p_i and a circle of radius r_j centered at a point p_j and $c_i(r)$ is a search circle with radius r centered at a point p_i . These circles are located inside a study region Ω . (see **Figure 4.3**).

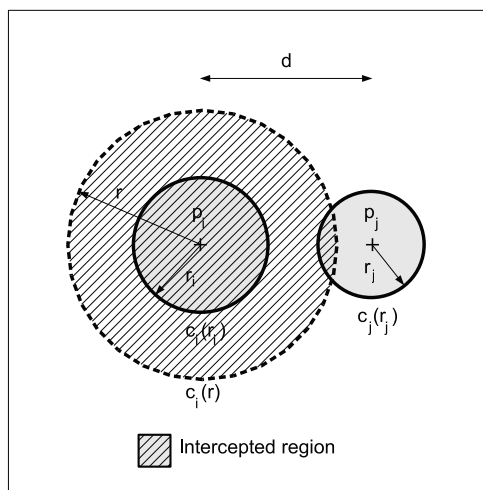


Figure 4.3. Two circular objects $c_i(r_i)$ and $c_j(r_j)$ and a search circle $c_i(r)$ inside a study region Ω .

4.2.1 Univariate Analysis

I define $K_c(r)$, a function adapted to perform spatial analysis of circular objects, as

$$K_c(r) = \mu^{-1} \mathbb{E}[A_{ij}(r)] = \mu^{-1} \frac{1}{n} \sum_{i=1}^n w_i(r) \sum_{j=1}^n A_{ij}(r), \quad (4.1)$$

where $w_i(r)$ is an edge effect correction factor based on area. The parameter μ is the specific area. It is the area of the circular objects per unit of area of the study region under consideration (Cressie 1991). It is defined as

$$\mu = \frac{A_c}{A_\Omega}, \quad (4.2)$$

where A_c is the area of all circles inside the study region Ω and A_Ω is the area of the study region Ω . The function $A_{ij}(r)$, is the area of the interception between the search circles $c_i(r)$ and the circular object $c_j(r_j)$, separated by a distance d , and it is defined as

$$A_{ij}(r) = r_j^2 \cos^{-1} \left(\frac{d^2 + r_j^2 - r^2}{2dr_j} \right) + r^2 \cos^{-1} \left(\frac{d^2 + r^2 - r_j^2}{2dr} \right) - \frac{1}{2} \sqrt{(-d + r_j - r)(d + r_j - r)(d - r_j + r)(d + r_j + r)} \quad . \quad (4.3)$$

The idea of the method is to estimate the area of the objects contained within a distance r of an arbitrary circular object inside region Ω and compare this result with the expected area, considering that μ is homogeneous inside Ω or $\mu(x, y) = \mu, \forall (x, y) \in \Omega$ (see **Figure 4.4**).

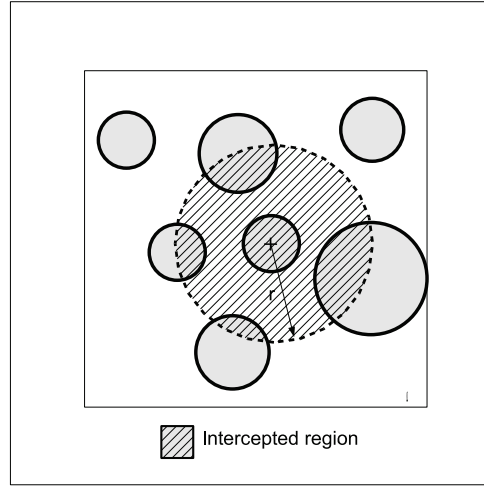


Figure 4.4. Estimating the expected specific area within a distance r of an arbitrary circular object of the study region Ω .

The expected intercepted area within a circle of radius r is

$$E[A_{ij}(r)] = \pi r^2 \mu. \quad (4.4)$$

Substituting equation (4.4) in the equation (4.1) I obtain

$$E[K_c(r)] = \mu^{-1} E[A_{ij}(r)] = \mu^{-1} \pi r^2 \mu = \pi r^2. \quad (4.5)$$

If the estimated area for a fixed scale r is greater than the expected area, the circular objects exhibit aggregation at this scale. If the area for a fixed r is smaller than the expected area, they exhibit repulsion.

The interpretation of the $K_c(r)$ is show in **Table 4.1**.

$K_c(r) = \pi r^2$	$K_c(r) > \pi r^2$	$K_c(r) < \pi r^2$
CSR	Clustering	Repulsion

Table 4.1. Interpretation of the $K_c(r)$ function.

Now I propose a modified function $L_c(r)$ to normalize the function $K_c(r)$. It is defined as

$$L_c(r) = \sqrt{\frac{K_c(r)}{\pi}} - r, \quad (4.6)$$

and the interpretation is shown in **Table 4.2** below.

$L_c(r) = 0$	$L_c(r) > 0$	$L_c(r) < 0$
CSR	Clustering	Repulsion

Table 4.2. Interpretation of the $L_c(r)$ function.

Several studies show that the classical cumulative Ripley K-function can confuse effects at large distances with effects at short distances (Getis & Franklin 1987, Condit *et al.* 2000, Revilla & Palomares 2002). The function $K_c(r)$ has the same limitation. One way of avoiding this problem is to use rings, rather than circles (Wiegand & Moloney, 2004).

Then I define a function $R_\varepsilon(r)$ (hereinafter object ring method) as

$$R_\varepsilon(r) = \mu^{-1} \frac{1}{n} \sum_{i=1}^n \sum_{j=1}^n w_i(r + \varepsilon/2) A_{ij}(r + \varepsilon/2) - w_i(r - \varepsilon/2) A_{ij}(r - \varepsilon/2), \quad (4.7)$$

where μ is the specific area, n is the number of circular objects, w_i is an edge effect correction factor based on area and A_{ij} is the function defined in equation (4.3).

The expected intercepted area for the ring in **Figure 4.5** is defined as

$$\begin{aligned} E[A_{ij}(r + \varepsilon/2) - A_{ij}(r - \varepsilon/2)] &= [\pi(r + \varepsilon/2)^2 - \pi(r - \varepsilon/2)^2] \mu = \\ &= \pi \mu (r^2 + r\varepsilon + \varepsilon^2/4 - r^2 + r\varepsilon - \varepsilon^2/4) = 2\pi \mu r \varepsilon, \end{aligned} \quad (4.8)$$

and substituting in the equation (4.5) I obtain

$$E[R_\varepsilon(r)] = \mu^{-1} \pi 2 \mu r \varepsilon = 2\pi \varepsilon r. \quad (4.9)$$

The interpretation of the $R_\varepsilon(r)$ function is shown in **Table 4.3** below.

$R_\varepsilon(r) = 2\pi\varepsilon r$	$R_\varepsilon(r) > 2\pi\varepsilon r$	$R_\varepsilon(r) < 2\pi\varepsilon r$
CSR	Clustering	Regularity

Table 4.3. Interpretation of the function $R_\varepsilon(r)$.

The normalization of the function $R_\varepsilon(r)$ is obtained as

$$\bar{R}_\varepsilon(r) = \frac{R_\varepsilon(r)}{2\pi r \varepsilon}, \quad (4.10)$$

and its interpretation is shown in **Table 4.4**.

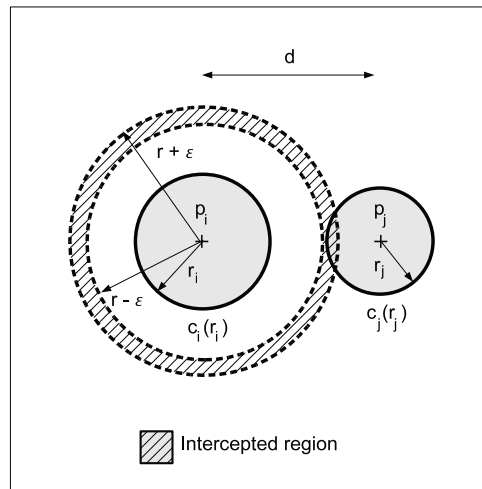


Figure 4.5. Estimating the expected specific area inside a ring.

$\bar{R}_\varepsilon(r) = 1$	$\bar{R}_\varepsilon(r) > 1$	$\bar{R}_\varepsilon(r) < 1$
CSR	Clustering	Regularity

Table 4.4. Interpretation of the function $\bar{R}_\varepsilon(r)$.

The function $\bar{R}_\varepsilon(r)$ is similar to the pair-correlation $g(r)$ associated to the K-Ripley function $K(r)$ and it can be defined also as

$$\bar{R}_\varepsilon(r) = \frac{1}{2\pi r} \frac{dK_c(r)}{dr}. \quad (4.11)$$

4.2.2 Bivariate Analysis

In a similar way, I define the bivariate version of the function $R_\varepsilon(r)$. First of all, I have to define the function $R_\varepsilon^{12}(r)$. This function estimates the area of the objects of type 2 contained within a distance r of an arbitrary circular object of type 1 inside region Ω . It is defined as

$$R_\varepsilon^{12}(r) = \mu_2^{-1} \frac{1}{n_1} \sum_{i=1}^{n_1} \sum_{j=1}^{n_2} w_i(r + \varepsilon/2) A_{ij}(r + \varepsilon/2) - w_i(r - \varepsilon/2) A_{ij}(r - \varepsilon/2), \quad (4.12)$$

where n_1 and n_2 are the number of objects of type 1 and type 2 respectively, w_i is an edge correction factor based on area, A_{ij} is the function defined in the equation (4.3) and μ_2 is the specific area of the objects of type 2. It is defined as

$$\mu_2 = \frac{A_c^2}{A_\Omega}, \quad (4.13)$$

where A_c^2 and A_Ω are the area of the circles of type 2 and the area of the study site respectively.

Similarly, I define the function $R_\varepsilon^{21}(r)$. This function estimates the area of the objects of type 1 contained within a distance r of an arbitrary circular object of type 2 inside region Ω . It is defined as

$$R_\varepsilon^{21}(r) = \mu_1^{-1} \frac{1}{n_2} \sum_{i=1}^{n_2} \sum_{j=1}^{n_1} w_i(r + \varepsilon/2) A_{ij}(r + \varepsilon/2) - w_i(r - \varepsilon/2) A_{ij}(r - \varepsilon/2), \quad (4.14)$$

where n_1 and n_2 are the number of objects of type 1 and type 2 respectively, w_i is an edge correction factor based on area, A_{ij} is the function defined in the equation (4.3) and μ_1 is the specific area of the objects of type 1. It is defined as

$$\mu_1 = \frac{A_c^1}{A_\Omega}, \quad (4.15)$$

where A_c^1 and A_Ω are the area of the circles of type 1 and the area of the study site respectively. Now I define the bivariate version of the $R_\varepsilon(r)$ function as

$$\hat{R}_\varepsilon^B = \frac{n_1 R_\varepsilon^{21} + n_2 R_\varepsilon^{12}}{n_1 + n_2}, \quad (4.16)$$

where n_1 and n_2 are the number of objects of type 1 and type 2 respectively. The interpretation of the functions \hat{R}_ε^B is similar to the function $R_\varepsilon(r)$ and its normalization is obtained by

$$\bar{R}_\varepsilon^B(r) = \frac{\hat{R}_\varepsilon^B(r)}{2\pi r \varepsilon}, \quad (4.17)$$

and its interpretation is shown in **Table 4.5**.

$\bar{R}_\varepsilon^B(r) = 1$	$\bar{R}_\varepsilon^B(r) > 1$	$\bar{R}_\varepsilon^B(r) < 1$
CSR	Aggregation	Repulsion

Table 4.5. Interpretation of the function $\bar{R}_\varepsilon^B(r)$.

It is interesting to notice that the expected values of the functions $R_\varepsilon(r)$ and \hat{R}_ε^B do not depend on the value of the parameters μ , μ_1 and μ_2 .

4.2.3 Simulations Envelope

In order to detect if a tendency to clustering/aggregation or regularity/repulsion is statistically significant, I have to compare the observed function value observed with an adequate null model.

Now I define the ZOI (Zone of influence) of each tree as a circular zone surrounding each tree, within which a tree influences its neighbors and is influenced by its neighbors (Berger & Hildenbrandt 2000). The equation that defines the radius of the ZOI is

$$R_{ZOI} = a * rbh^b, \quad (4.18)$$

where rbh stands for the stem radius at breast height in meters. The parameters a and b are scaling parameters specific for each specie of tree. In this case, I use the same parameters, $a = 7.113$ and $b = 0.654$, for both species *Avicennia germinans* and *Laguncularia racemosa*, following Berger & Hildenbrandt (2000).

The object pattern model used to obtain the simulation envelope via Monte Carlo method (Besag 1977) for the univariate case is very similar to a soft core model (Tomppo 1986). First I have to simulate a CSR point pattern with the same number of objects as the study site and the radii of the objects having a normal distribution $N(\overline{R_{ZOI}}, \text{var}(R_{ZOI}))$, where $\overline{R_{ZOI}}$ and $\text{var}(R_{ZOI})$ are respectively the mean R_{ZOI} and the variance of R_{ZOI} for the observed object pattern (Goreaud *et al.* 1996). Hereinafter, I define this model as Model I.

The simulation of the envelope in the bivariate case is very similar and it is obtained by simulating a CSR point pattern with the same number of the objects of type 1 and type 2.

The radii of type 1 objects has normal distribution $N(\overline{R_{ZOI_1}}, \text{var}(R_{ZOI_1}))$ and the radii of type 2 objects has a normal distribution $N(\overline{R_{ZOI_2}}, \text{var}(R_{ZOI_2}))$, where $\overline{R_{ZOI_1}}$ and $\overline{R_{ZOI_2}}$ are the means R_{ZOI} of type 1 and type 2 objects and $\text{var}(R_{ZOI_1})$ and $\text{var}(R_{ZOI_2})$ are the variances of R_{ZOI} of type 1 and type 2 objects respectively. Hereinafter, I define this model as Model II.

Information about the parameters used for the calculation of the simulation envelopes can be found at the **Table 4.6** and **Table 4.7**.

4.3 Results

Now I apply the methodology to the datasets Lagoa A and Lagoa B, obtained from the study sites which have already been described in **Chapter 2**. But in this case, I consider only the trees with $\text{dbh} > 0$. I also exclude the dead trees, because lack of information about the dbh for group. It is also important to note that, for this analysis of these two study sites, I applied only the ring functions $\bar{R}_\varepsilon(r)$ and $\bar{R}_\varepsilon^B(r)$.

4.3.1 Lagoa A

The **Table 4.6** and **Figure 4.6** provides a summary of the basic statistics and shows the resulting histogram for each group analyzed in this simulation experiment.

Group	n	\bar{R}_{ZOI}	$\text{var}(R_{ZOI})$	$\min(R_{ZOI})$	$\max(R_{ZOI})$
All	402	0.71	0.05	0.24	1.50
Small	171	0.51	0.01	0.24	0.63
Large	231	0.86	0.03	0.64	1.50
Avic.	201	0.67	0.05	0.30	1.46
Lag.	201	0.74	0.05	0.24	1.50
Small Avic.	101	0.51	0.01	0.30	0.62
Small Lag.	70	0.52	0.01	0.24	0.63
Large Avic.	100	0.85	0.04	0.64	1.46
Large Lag.	131	0.86	0.03	0.64	1.49

Table 4.6. Basic statistics for Lagoa A. \bar{R}_{ZOI} , $\min(\bar{R}_{ZOI})$ and $\max(\bar{R}_{ZOI})$ in m and $\text{var}(\bar{R}_{ZOI})$ in m^2 .

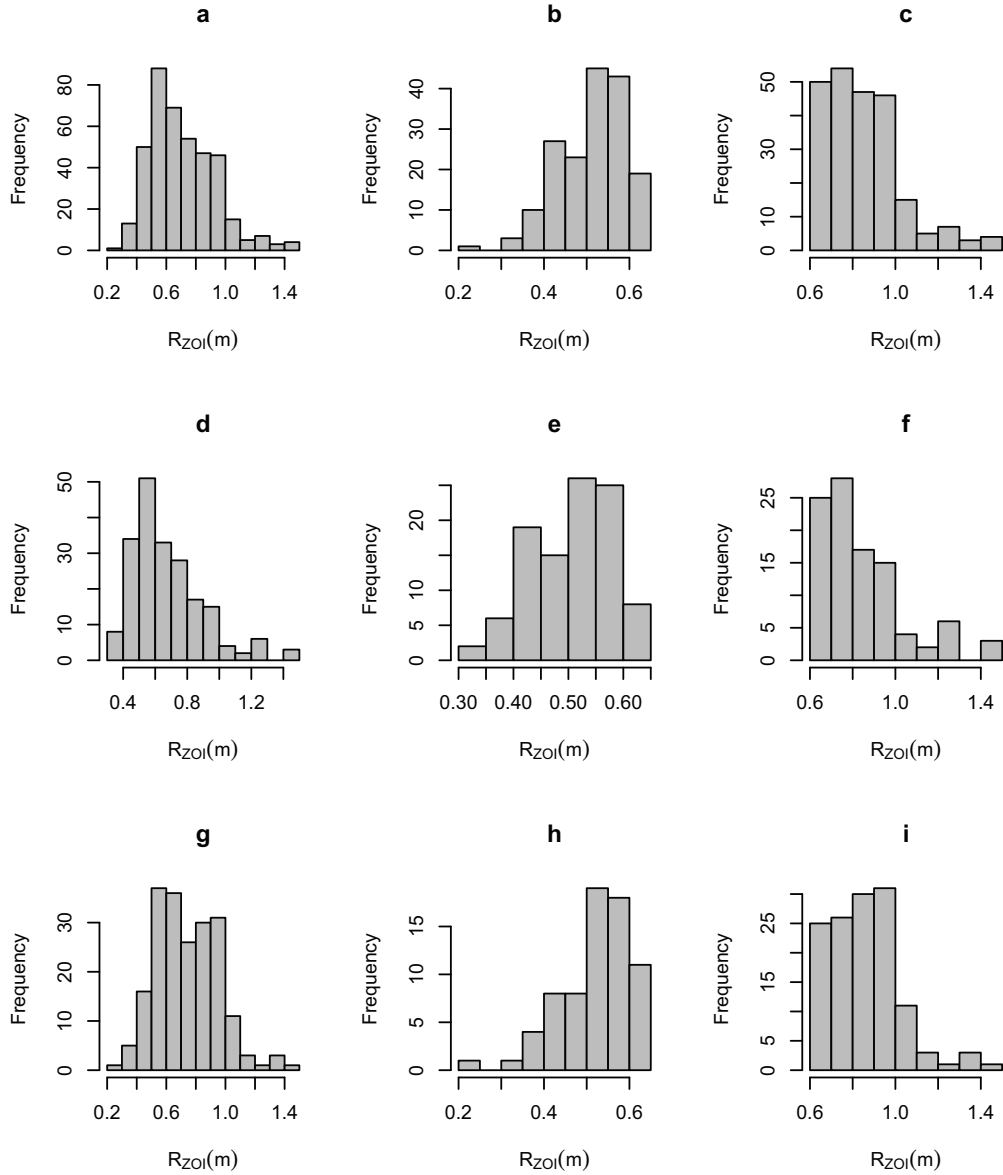


Figure 4.6. Histogram calculated for the R_{ZOI} distribution relative to (a) all trees, (b) small trees (dbh < 5 cm), (c) large trees (dbh \geq 5 cm), (d) *Avicennia germinans*, (e) small *Avicennia* (dbh < 5 cm), (f) large *Avicennia* (dbh \geq 5 cm), (g) *Laguncularia racemosa*, (h) small *Laguncularia* (dbh < 5 cm) and (i) large *Laguncularia* (dbh \geq 5 cm).

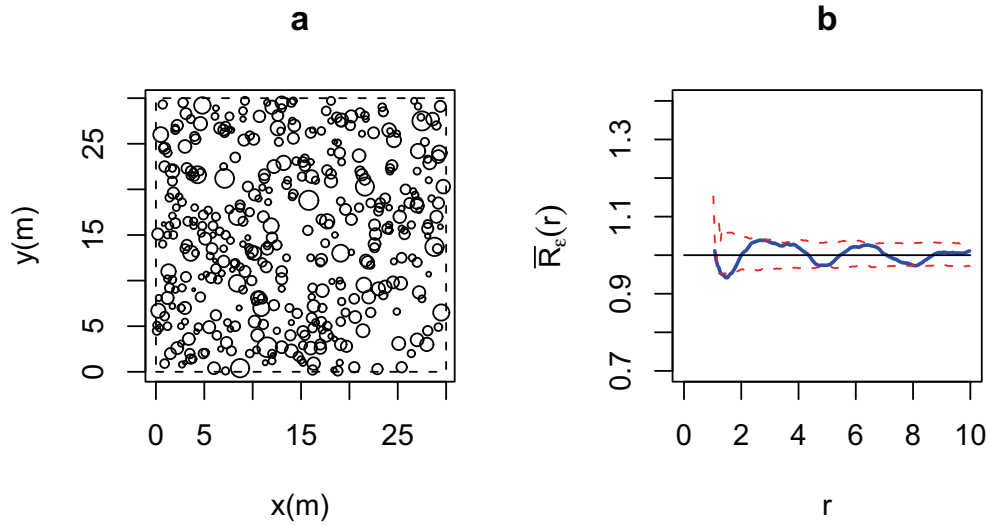


Figure 4.7. (a) Object pattern relative to all trees within study site Lagoa A. (b) Object ring analysis (blue) and respective 90% simulation envelope (red) obtained via Monte Carlo Method (Besag 1977) for the Model I hypothesis with 200 simulations.

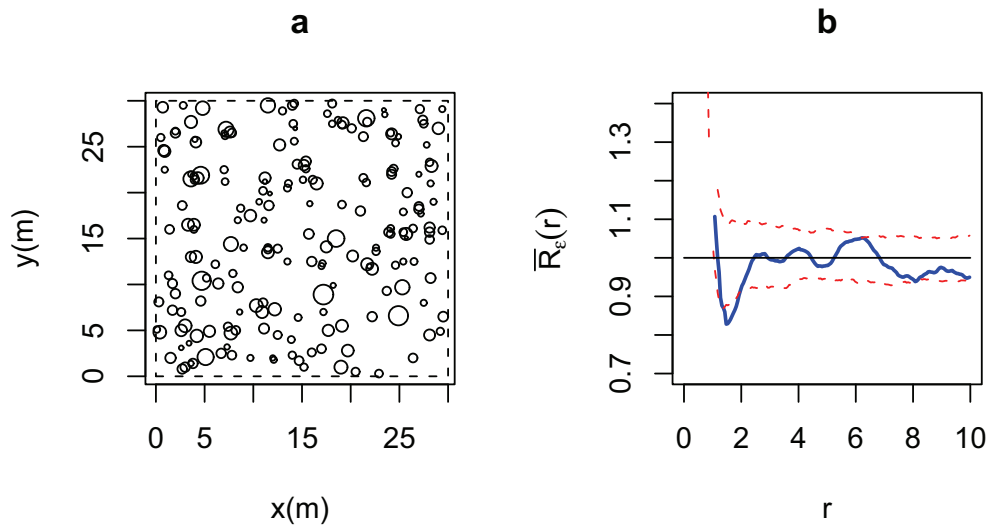


Figure 4.8. (a) Object pattern relative to *Avicennia germinans* within study site Lagoa A. (b) Object ring analysis (blue) and respective 90% simulation envelope (red) obtained via Monte Carlo Method (Besag 1977) for the Model I hypothesis with 200 simulations.

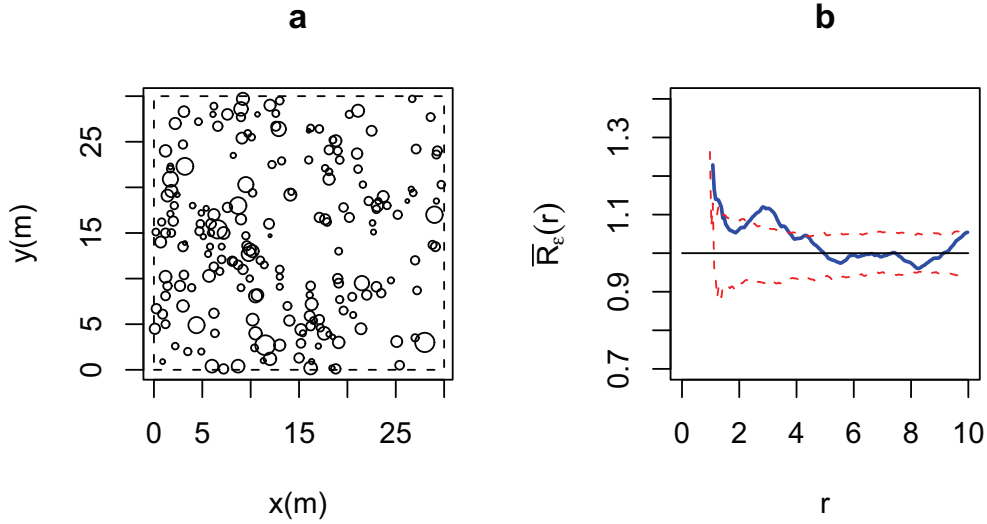


Figure 4.9. (a) Object pattern relative to *Laguncularia racemosa* within study site Lagoa A. (b) Object ring analysis (blue) and respective 90% simulation envelope (red) obtained via Monte Carlo Method (Besag 1977) for the Model I hypothesis with 200 simulations.

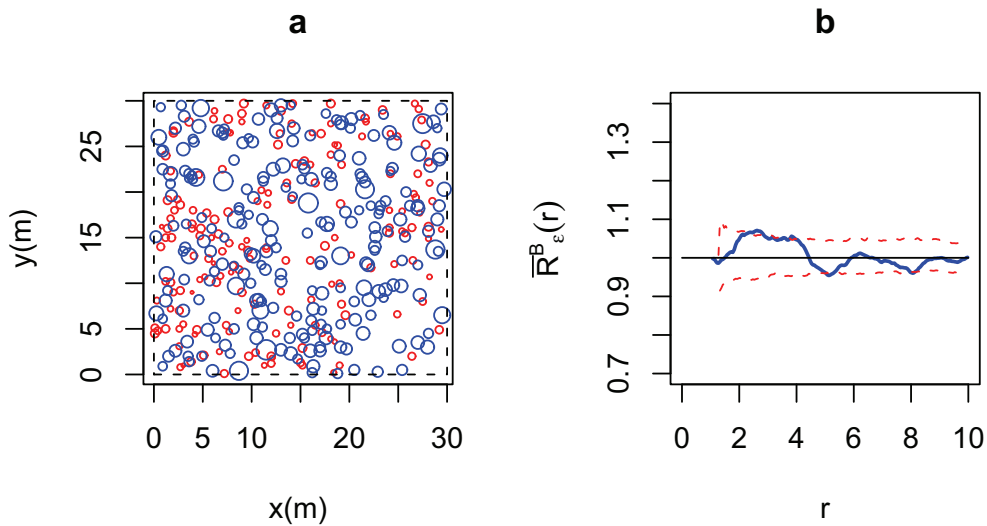


Figure 4.10. (a) Object pattern relative to small (dbh < 5 cm) (red) and large (dbh ≥ 5 cm) (blue) trees within study site Lagoa A. (b) Bivariate object ring analysis (blue) and respective 90% simulation envelope (red) obtained via Monte Carlo Method (Besag 1977) for the Model II hypothesis with 200 simulations.

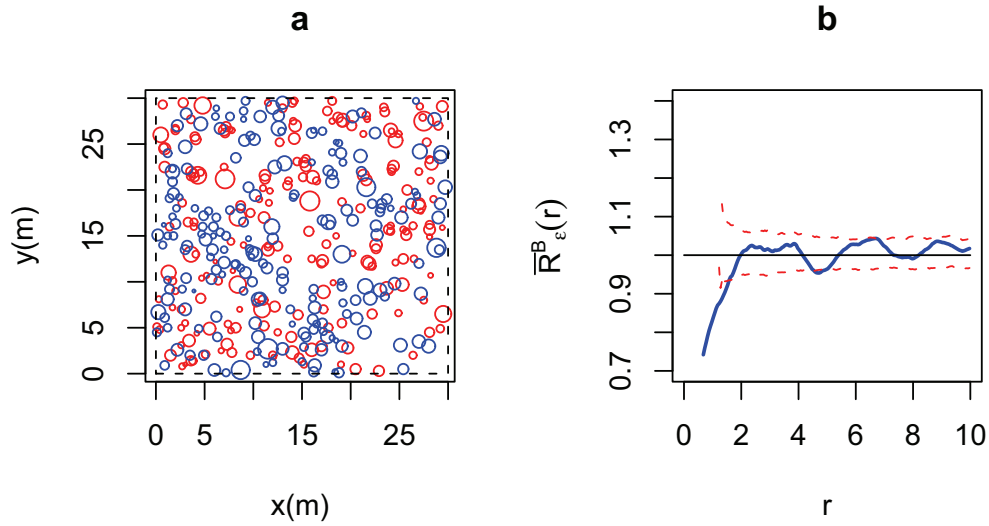


Figure 4.11. (a) Object pattern relative to *Avicennia germinans* (red) and *Laguncularia racemosa* (blue) trees within study site Lagoa A. (b) Bivariate object ring analysis (blue) and respective 90% simulation envelope (red) obtained via Monte Carlo Method (Besag 1977) for the Model II hypothesis with 200 simulations.

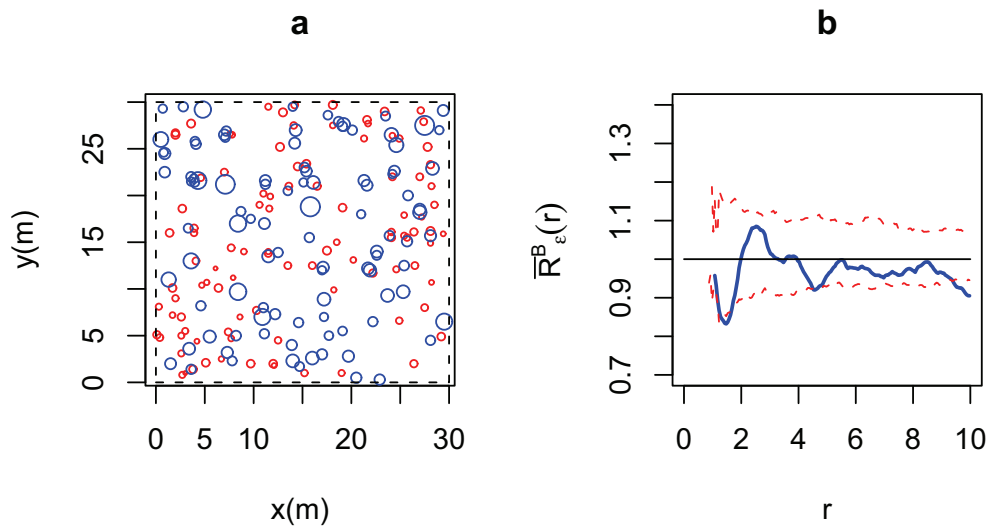


Figure 4.12. Object pattern relative to small (dbh < 5 cm) (red) and large (dbh ≥ 5 cm) (blue) *Avicennia* trees within study site Lagoa A. (b) Bivariate object ring analysis (blue) and respective 90% simulation envelope (red) obtained via Monte Carlo Method (Besag 1977) for the Model II hypothesis with 200 simulations.

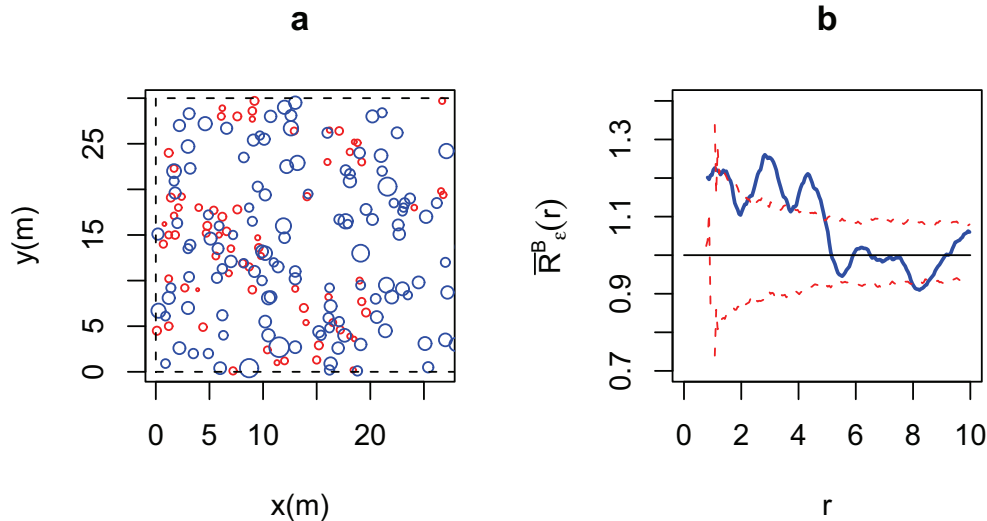


Figure 4.13. Object pattern relative to small ($\text{dbh} < 5$ cm) (red) and large ($\text{dbh} \geq 5$ cm) (blue) *Laguncularia* trees within study site Lagoa A. (b) Bivariate object ring analysis (blue) and respective 90% simulation envelope (red) obtained via Monte Carlo Method (Besag 1977) for the Model II hypothesis with 200 simulations.

The pattern presented by all trees shows a tendency to regularity at scales $r \simeq 1, 5$ and 8 m. However they show a tendency to clustering at loIr and intermediate scales (see **Figure 4.7**).

The pattern presented by the group *Avicennia germinans* shows regularity at scale $r \simeq 2$ m. This regular pattern at loIr scales could be associated with competition between the trees (King & Woodel 2004) (see **Figure 4.8**).

The pattern presented by the group *Laguncularia racemosa* shows clustering at scale $r \simeq 3$ m and at larger scales. This result could be an indication of environmental heterogeneity (Klass *et al.* 2000) (see **Figure 4.9**).

The spatial relation between individuals of groups of small ($\text{dbh} < 5$ cm) and large ($\text{dbh} \geq 5$ cm) trees exhibits some tendency to clustering at lower scales. However, the pattern shows some tendency to repulsion at scales $r \simeq 5$ and 8 m. This could be an indication of intraspecific competition (Kenkel 1998) and/or light gaps (Duke 2001) (see **Figure 4.10**).

The spatial relation between individuals of species *Avicennia germinans* and *Laguncularia racemosa* exhibits repulsion at scales $r \simeq 5$ m. Again, this could be a indication of succession (Begon *et al.* 1976) and/or interspecific competition (Begon *et al.* 1976, Connel & Slattier 1977) (see **Figure 4.11**).

The spatial relation between individuals of groups of small ($\text{dbh} < 5$ cm) and large ($\text{dbh} \geq 5$ cm) *Avicennia germinans* exhibits some tendency to repulsion at scales $r \simeq 2$ and 4 m. This could be an indication of intra-specific competition (Kenkel 1988) (see **Figure 4.12**).

The spatial relation between individuals of groups of small ($\text{dbh} < 5 \text{ cm}$) and large ($\text{dbh} \geq 5 \text{ cm}$) *Laguncularia racemosa* exhibits aggregation at intermediate scales and repulsion at large scales. This result could be a indication of either intra-specific competition (Kenkel 1988) and/or environmental heterogeneity (Klass *et al.* 2000).

4.3.2 Lagoa B

The **Table 4.7** and **Figure 4.14** present a summary of the basic statistics and the histogram calculated of each analyzed groups at this experiment respectively.

Group	n	\bar{R}_{ZOI}	$\text{var}(R_{ZOI})$	$\min(R_{ZOI})$	$\max(R_{ZOI})$
All	330	0.75	0.10	0.30	1.82
Small	151	0.49	0.01	0.30	0.62
Large	179	0.96	0.08	0.64	1.81
Avic.	163	0.57	0.03	0.30	1.19
Lag.	161	0.93	0.12	0.30	1.82
Small Avic.	117	0.49	0.01	0.30	0.62
Small Lag.	32	0.50	0.01	0.30	0.62
Large Avic.	46	0.78	0.01	0.64	1.19
Large Lag.	129	1.03	0.09	0.64	1.82

Table 4.7. Basic statistics for Lagoa B. \bar{R}_{ZOI} , $\min(\bar{R}_{ZOI})$ and $\max(\bar{R}_{ZOI})$ in m and $\text{var}(\bar{R}_{ZOI})$ in m^2 .

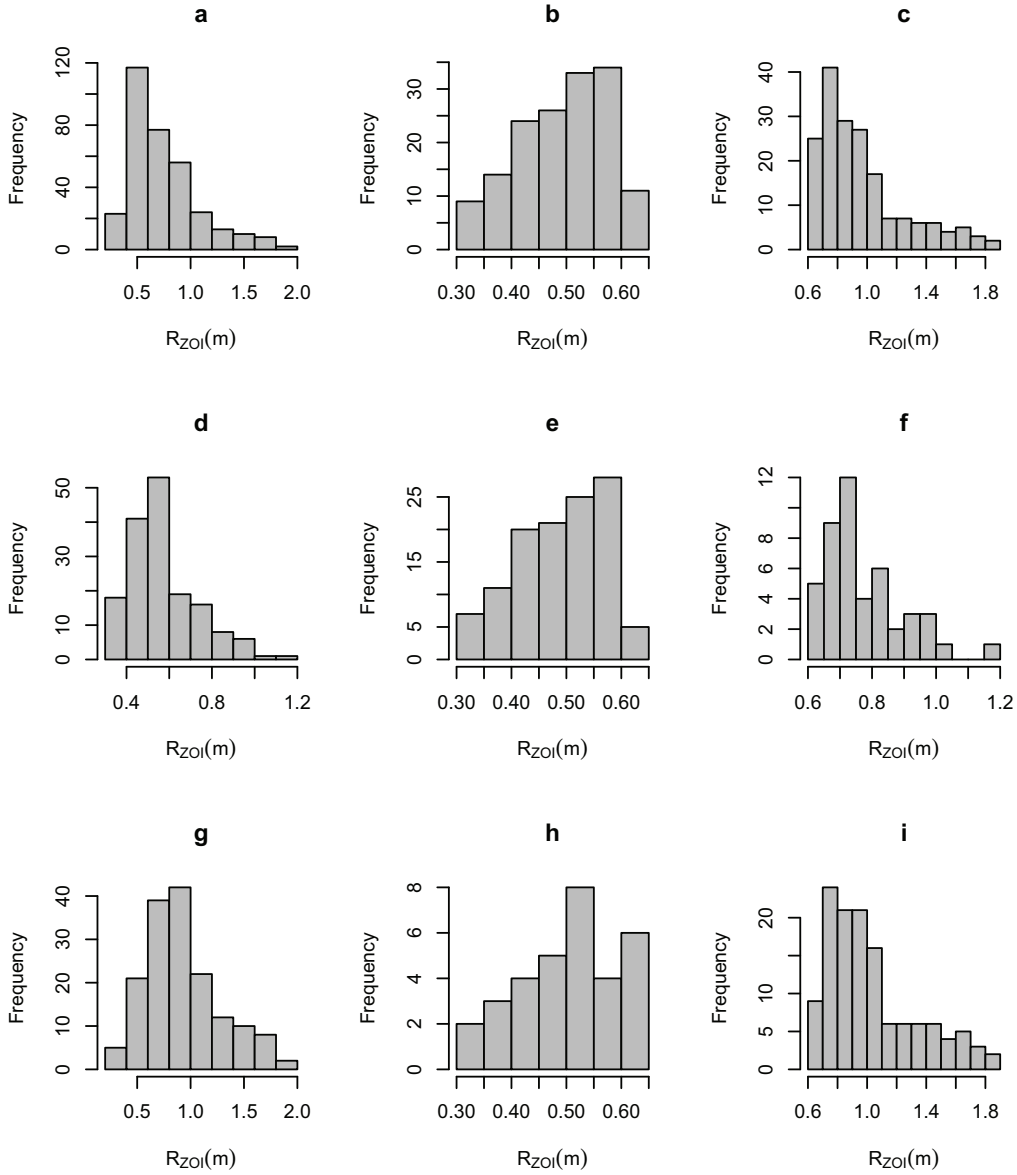


Figure 4.14. Histogram calculated for the R_{ZOI} distribution relative to (a) all trees, (b) small trees ($dbh < 5$ cm), (c) large trees ($dbh \geq 5$ cm), (d) *Avicennia germinans*, (e) small *Avicennia* ($dbh < 5$ cm), (f) large *Avicennia* ($dbh \geq 5$ cm), (g) *Laguncularia racemosa*, (h) small *Laguncularia* ($dbh < 5$ cm) and (i) large *Laguncularia* ($dbh \geq 5$ cm).

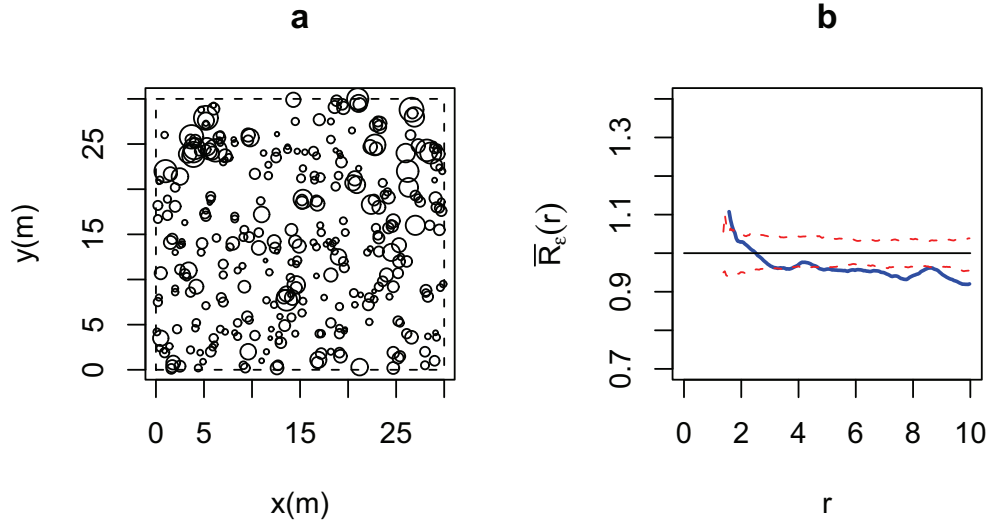


Figure 4.15. (a) Object pattern relative to all trees within study site Lagoa B. (b) Object ring analysis (blue) and respective 90% simulation envelope (red) obtained via Monte Carlo Method (Besag 1977) for the Model I hypothesis with 200 simulations.

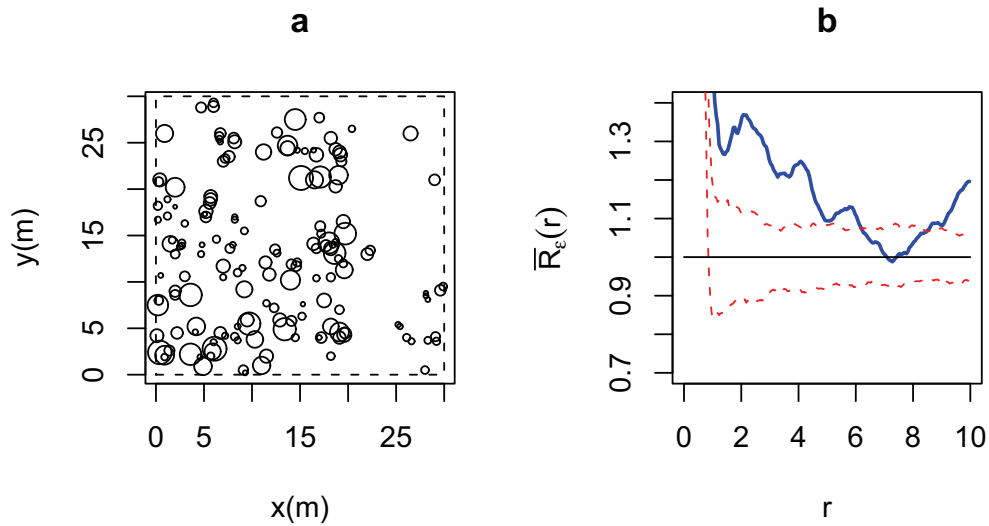


Figure 4.16. (a) Object pattern relative to *Avicennia germinans* within study site Lagoa B. (b) Object ring analysis (blue) and respective 90% simulation envelope (red) obtained via Monte Carlo Method (Besag 1977) for the Model I hypothesis with 200 simulations.

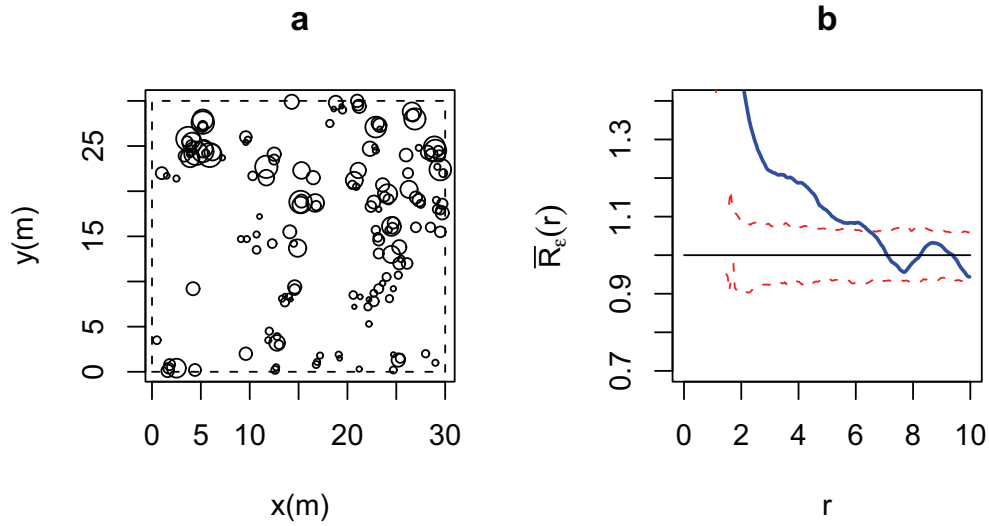


Figure 4.17. (a) Object pattern relative to *Laguncularia racemosa* within study site Lagoa B. (b) Object ring analysis (blue) and respective 90% simulation envelope (red) obtained via Monte Carlo Method (Besag 1977) for the Model I hypothesis with 200 simulations.

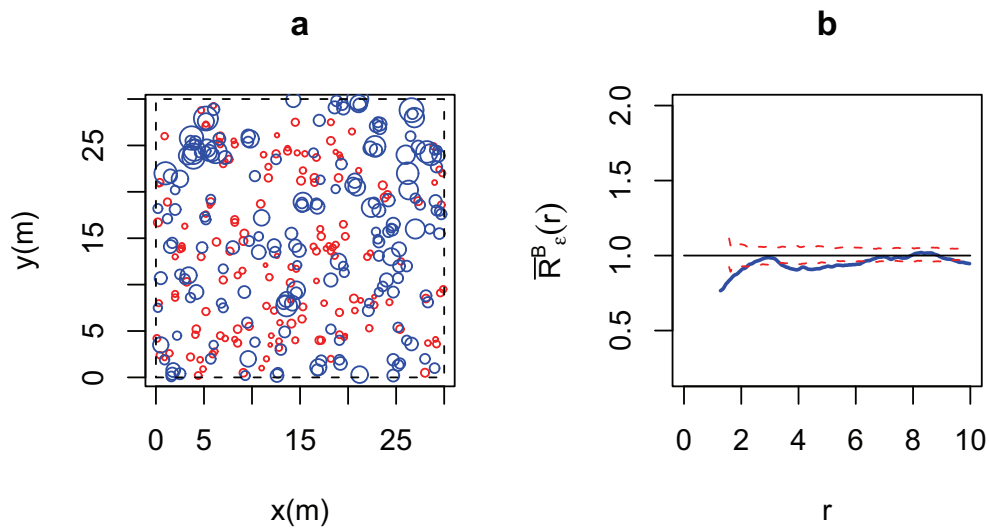


Figure 4.18. (a) Object pattern relative to small (dbh < 5 cm) (red) and large (dbh ≥ 5 cm) (blue) trees within study site Lagoa A. (b) Bivariate object ring analysis (blue) and respective 90% simulation envelope (red) obtained via Monte Carlo Method (Besag 1977) for the Model II hypothesis with 200 simulations.

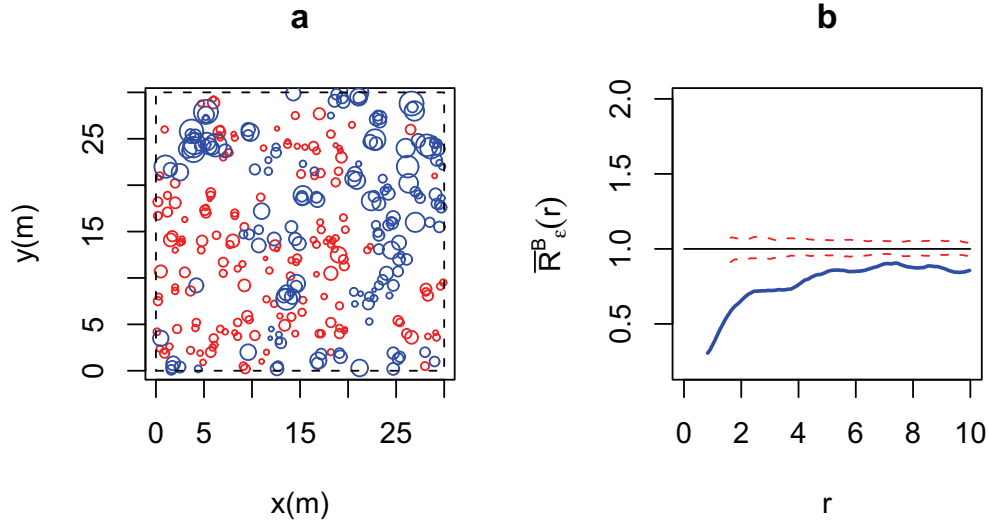


Figure 4.19. (a) Object pattern relative to *Avicennia germinans* (red) and *Laguncularia racemosa* (blue) trees within study site Lagoa A. (b) Bivariate object ring analysis (blue) and respective 90% simulation envelope (red) obtained via Monte Carlo Method (Besag 1977) for the Model II hypothesis with 200 simulations.

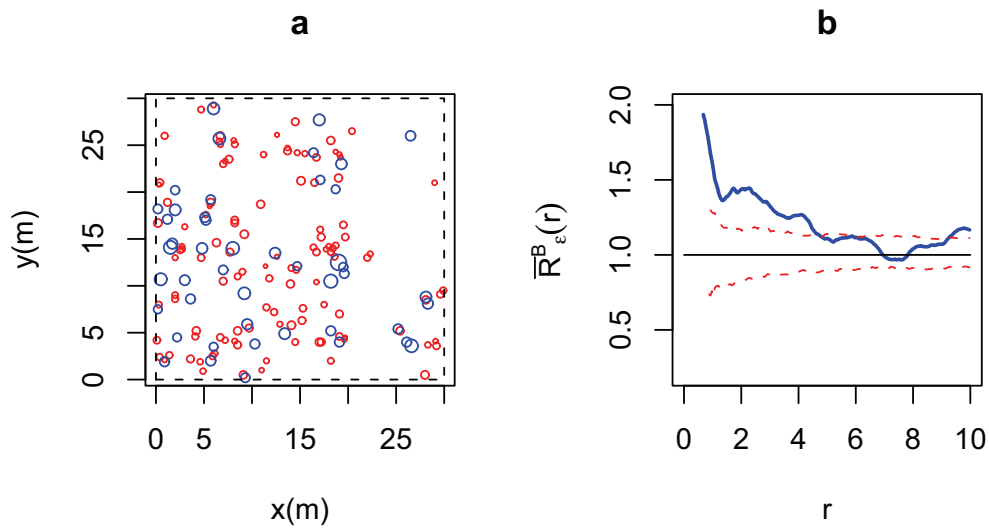


Figure 4.20. Object pattern relative to small ($\text{dbh} < 5$ cm) (red) and large ($\text{dbh} \geq 5$ cm) (blue) *Avicennia* trees within study site Lagoa A. (b) Bivariate object ring analysis (blue) and respective 90% simulation envelope (red) obtained via Monte Carlo Method (Besag 1977) for the Model II hypothesis with 200 simulations.

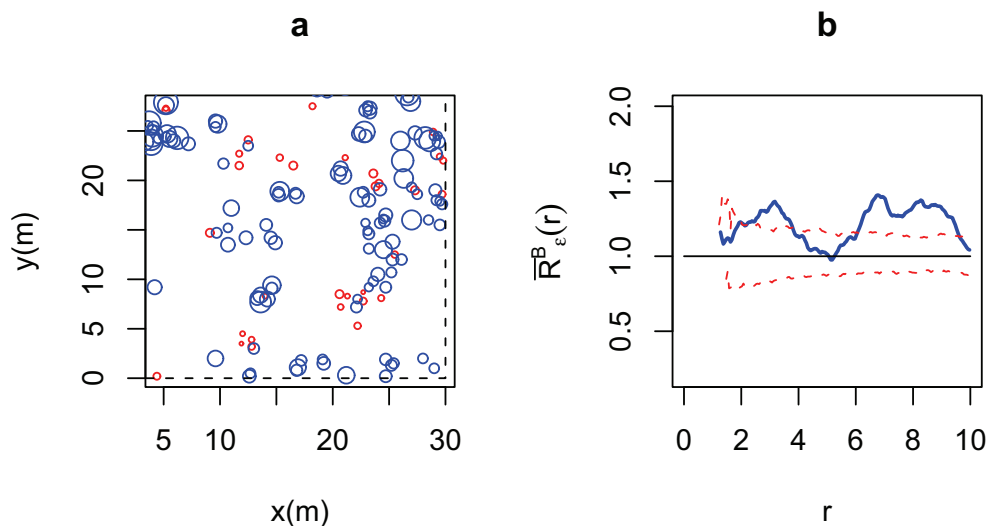


Figure 4.21. Object pattern relative to small ($\text{dbh} < 5$ cm) (red) and large ($\text{dbh} \geq 5$ cm) (blue) *Laguncularia* trees within study site Lagoa A. **(b)** Bivariate object ring analysis (blue) and respective 90% simulation envelope (red) obtained via Monte Carlo Method (Besag 1977) for the Model II hypothesis with 200 simulations.

The spatial relation presented by all trees exhibits regularity at intermediate and larger scales. This pattern could be result of environmental heterogeneity (Klass *et al.* 2000) (see **Figure 4.15**).

The trees of group *Avicennia germinans* exhibits clustering at lower, intermediate and higher scales. This could be an indication of either environmental heterogeneity within the stand (Klass *et al.* 2000) (see **Figure 4.16**).

The trees of group *Laguncularia racemosa* shows clustering at lower and intermediate scales. This could be an indication of environmental heterogeneity (Klass *et al.* 2000) (**Figure 4.17**).

The spatial relation between individuals of groups of small ($\text{dbh} < 5$ cm) and large ($\text{dbh} \geq 5$ cm) trees exhibits repulsion at small, intermediate and large scales. This could be an indication of either environmental heterogeneity (Klass *et al.* 2000) and/or succession (Begon *et al.* 1976) (**Figure 4.18**).

The spatial relation between individuals of species *Avicennia germinans* and *Laguncularia racemosa* shows repulsion at all range of scales. This could be an indication of either environmental heterogeneity (Klass *et al.* 2000) or succession (Begon *et al.* 1976) (**Figure 4.19**).

The spatial relation between small ($\text{dbh} < 5 \text{ cm}$) and large ($\text{dbh} \geq 5 \text{ cm}$) *Avicennia racemosa* exhibits aggregation at lower scales. That could be an indication of either seed dispersal (Barot *et al.* 1999) and/or nurse-plant effects (Tielbörger & Kadmon 2000). Additionally, they also show clustering at larger scales. This could be a indication of either succession (Begon *et al.* 1976) or environmental heterogeneity (Klass *et al.* 2000) (**Figure 4.20**).

The spatial relation between small ($\text{dbh} < 5 \text{ cm}$) and large ($\text{dbh} \geq 5 \text{ cm}$) *Laguncularia racemosa* presents aggregation at scale $r \simeq 3 \text{ m}$ and at large scales. This could be a result of either succession (Begon *et al.* 1976) or environmental heterogeneity (Klass *et al.* 2000) (**Figure 4.21**).

4.4 Discussion

It is very difficult to compare the results described in this chapter with the results in **Chapter 3** and there are at least two reasons for this.

First, I applied a different analytical approach. Secondly, the dataset is completely different, because I excluded the trees with $\text{dbh} > 0$ and the dead trees from the analysis. This procedure significantly reduced the number of individuals compared to our original dataset. But despite the differences between the two methods (Ripley K-function and object ring function $\bar{R}_\varepsilon(r)$), some of the results obtained were equivalent in qualitative sense.

The analysis was applied to different groups of trees in the sites Lagoa A and Lagoa B. The main aim of our study was to see whether the object ring function $\bar{R}_\varepsilon(r)$ is sufficiently sensitive to detect the spatial interactions occurring between trees of species *Laguncularia racemosa* and *Avicennia germinans* within these study sites. A particular interest was to see whether the method could provide indirect evidence of the succession processes that are probably occurring in these stands.

The spatial relation between trees of species *Laguncularia racemosa* and *Avicennia germinans* exhibits repulsion at intermediate scale in Lagoa A and repulsion at all scales in Lagoa B (**Figure 4.11** and **Figure 4.19** respectively). These results are equivalent to the results observed in **Figure 3.15** and **Figure 3.26** of the **Chapter 3** respectively. These results shows only a tendency to repulsion between the species *Laguncularia* and *Avicennia*.

The result in **Figure 4.19**, shows that the ring method displays greater sensitivity in detecting the repulsion process between trees of species and within the sites Lagoa A and Lagoa B. These patterns could be a result of either succession (Begon *et al.* 1976) or environmental heterogeneity (Klass *et al.* 2000).

The hypothesis of environmental heterogeneity is difficult to prove, because I have no information about abiotic conditions in the two studies sites Lagoa A and Lagoa B; however the spatial heterogeneity exhibited by the trees could be a indication of environmental heterogeneity and so I cannot exclude this possibility.

Mangroves forests are in a continuous process of growth and constantly establishing and renewing themselves (Duke 2001). Therefore, the hypothesis of succession occurring among the individuals of species and in the stands is a plausible one.

It's important to emphasize that both hypotheses could be correct and the spatial distribution of the trees could be a result of their combined action.

The main characteristic of the ring function $\bar{R}_\varepsilon(r)$ is that it considers individual trees as circles, rather than points. This procedure overcomes the problems associated with the reduction of a three dimensional individual into a point, minimizing the loss of information caused by the transformation step T2. It is important to note the method can only be applied when the shape of the individuals considered by the analysis is approximately circular. Otherwise, the method can not to be applied.

I considered just two simple models to simulate the spatial distribution of circular objects and to generate the simulation envelope using the Monte Carlo method (Besag 1977). Other null models could be used to test other hypothesis, but at this stage this is no more than an idea for future work.

Finally, the object ring method, like the Ripley K-function, has the limitation that although it can provide information about the scale of processes occurring in the stands, it does not provide information where these processes are occurring; or in other words, neither method has spatial resolution. In the next chapter, I present a method that can provide spatial-scale information, (under certain conditions) about the processes that are occurring in a study site.

Chapter 5

Wavelet Transform applied to Ecology

5.1 Introduction

Traditional spatial statistical methods, such as the Ripley K-function, provide information about whether individual plants exhibit clumped, regular or randomly distribution in the plot and at which scale these patterns occur. However, this information is insufficient when the location of certain distribution patterns has to be taken into account, because these methods have no spatial-scale resolution.

The majority of spatial statistical methods used to analyze spatial point patterns (including the Ripley K-function) were developed to deal with homogeneous point patterns, but spatial heterogeneity^{5.1} is a common feature of natural ecosystems (Kolasa & Pickett 1991). The use of such methods to analyze a heterogeneous point pattern can thus lead to misinterpretation of the spatial point process that occurs in a study area (Pelissier & Goreaud 2001).

Spatial heterogeneity in plant distribution can occur when abiotic factors (soil, climate, nutrients, etc) vary significantly from one location to another (Pelissier & Goreaud 2001). Additionally, natural processes (birth, development, reproduction, competition, predation and senescence) can also produce spatial heterogeneity in ecological populations (Sternier *et al.* 1986, Kenkel 1988, Forget 1994, Blate *et al.* 1998, Couteron 1998, Desouhant *et al.* 1998).

The analysis of spatial variations of point locations depends on the scale of observation in relation to the size of the study site. In this study, I consider spatial variations in point position occurring at higher scales as spatial heterogeneity, whereas lower and intermediate scale variations can be considered as elements of the structure (Wiens 1989, Kolasa & Rollo

5.1. If a spatial point pattern varies from location to location, it is thus called heterogeneous (Ripley 1981).

1991, Holling 1992, He *et al.* 1994, Goreaud 2000). For example, the patchy distribution of individual trees can give rise repeated structures in a study area, whereas a single patch can display heterogeneity at a finer scale (Pelissier & Goreaud 2001).

In this chapter, I consider a number of possible approaches to the statistical analysis of spatial heterogeneity. One possible would be to apply a multiresolution method to analyze and decompose a spatial point pattern at different scales. A possibility is to apply the well known Fourier Transform method (**FT** hereinafter) to obtain this multiscale representation of a spatial point pattern. This method represents a signal as the sum of a serie of sines and cosines. It permits all the frequencies present in a time-series to be detected, but does not provide information about the location of the frequencies. That is the main limitation of this method. It has only frequency resolution and no time resolution and therefore the **FT** can be only used for decomposition of stationary signals. But ecological and environmental time series observed in nature are typically aperiodic, noisy and transient and the analysis of such time series by means of **FT** can lead to problems in the interpretation of the results. For example, **Figure 5.5** shows two different signals (**Figures 5.5a** and **5.5b**) and their respective **FT** analysis (**Figures 5.5c** and **5.5d**). The results show that the **FT** is not able to differentiate the signals and only provides information about the existence of two frequencies that in these signals.

To overcome these limitations of the **FT** method, the natural choice would be to apply the Multiresolution Decomposition Analysis (hereinafter **MDA**) obtained via the Wavelet Transform method (hereinafter **WT**). The **WT** method is a mathematical tool that permits spatial information to be obtained about the structures contained within an image at different scales. The method decomposes an image into various maps and each map represents a range of scales contained in the original image.

The **MDA** is obtained via **DWT** (Discrete Wavelet Transform), the discrete version of the **WT** method. The main advantage of this method in comparison to other spectral methods, such as Fourier Transform (hereinafter **FT**), is its spatial-scale resolution.

Subject to certain restrictions (connected with the Heisenberg uncertainty principle^{5.2}), the **MDA** provides information about the scale of the point processes occurring in the study site and their respective spatial-location. This singular capability permits allows the method to be used to analyze the scale and positions of heterogeneous point pattern configurations.

But it is important to mention that the **MDA** method can not be directly applied to a spatial point pattern. The first step required is to transform this spatial point pattern into a density map (an image) using a Kernel Density Estimation Method (hereinafter **KDE**). This density map provides spatial information about the density of the points over the study site (see **Figure 5.1**).

5.2. The uncertainty principle states that the time-position and frequency cannot both be measured, exactly, at the same time (Werner Heisenberg 1901-1976).

The second and final step is to decompose the density map obtained via **KDE** method at different scales using the **MDA** obtained via **WT** method (see **Figure 5.1**). This enables us to obtain spatial information about the density of the points within the study site at different scales and positions.

Additionally, I calculate the variogram to verify the decomposition of the density map during each step of the **MDA**. The variogram is a geostatistical that provides information about the scales of the structures contained in an image.

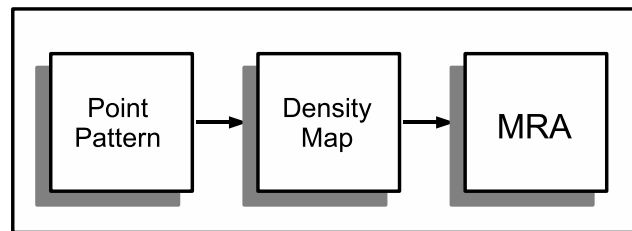


Figure 5.1. Representation of the steps of our methodology. (left) Point Pattern \Rightarrow (middle) Density Map \Rightarrow (right) Multiresolution Analysis.

I perform three applications of the methodology. The first methodology is applied to decompose a heterogeneous study area into smaller homogeneous regions that can subsequently be analyzed individually using classical spatial statistical methods that require a hypothesis of homogeneity.

A second application is performed to see if the method is sufficiently sensitive to detect the repulsive spatial pattern between the trees of species *Laguncularia* and *Avicennia* within Lagoa A and Lagoa B that was detected by the spatial statistical methods presented in **Chapter 2** and **Chapter 3**.

The idea behind the final application is to obtain scale-position information about the spatial point processes occurring at heterogeneous study site and use this information to simulate spatial point patterns using an inhomogeneous Poisson process.

5.2 Methods

The first step of the methodology (see **Figure 5.2**) is to transform a spatial point pattern that represents the spatial structure of a forest stand into a density map using a Kernel Density Estimation (Diggle, 1985). This first step is required, because is not possible to apply the **MDA** directly to spatial point patterns.

5.2.1 Kernel Density Estimation Method

Consider (s_1, s_2, \dots, s_n) the spatial position of $n = N(A)$ events in a study region $\Omega \subset \mathbb{R}^d$. The **KDE** method (Cressie 1993) is generally defined as

$$\hat{\lambda}_h(\mathbf{s}) = \frac{1}{p_h(\mathbf{s})} \left\{ \sum_{i=1}^n \kappa_h(\mathbf{s} - \mathbf{s}_i) \right\}, \mathbf{s} \in \Omega, \quad (5.1)$$

where $\kappa_h(\cdot)$ is a kernel function symmetrical about the origin, $h > 0$ is the kernel bandwidth which determines the amount of smoothing of the density map and $p_h(\mathbf{s}) = \int_{\Omega} \kappa_h(\mathbf{s} - \mathbf{u}) d\mathbf{u}$ is an edge correction factor (Diggle 1985).

The selection of an appropriate h depends on the estimation of $\lambda(\cdot)$ (Silverman 1978). But it is important to notice, that the choice of an appropriated kernel bandwidth h is also directly related to the scales that I want to analyze and will depend on the level of decomposition I want to achieve using the **MDA** via **WT** method.

To analyze structures with dimension scale s , the discretization of our density map must be at least equal to $s/2$ (Nyquist frequency).

Additionally, if our density map is a matrix with dimensions $2^d \times 2^d$, the maximal level of decomposition that is achievable is d . In this case, I consider that the algorithm used to perform the **MDA** is dyadic (Mallat 1988).

In this study, I consider the Quartic Kernel defined in two dimensions as $\kappa_h = \rho_h(u_1) \cdot \rho_h(u_2)$, where

$$\rho_h(u) = \begin{cases} 0.9375h^{-1}[1 - (u/h)^2]^2, & -h \leq u \leq h, \\ 0, & \text{otherwise.} \end{cases} \quad (5.2)$$

In **Figure 5.1**, I present an application of the method. It shows a density map obtained from a spatial point pattern via **KDE** method using a Quartic Kernel.

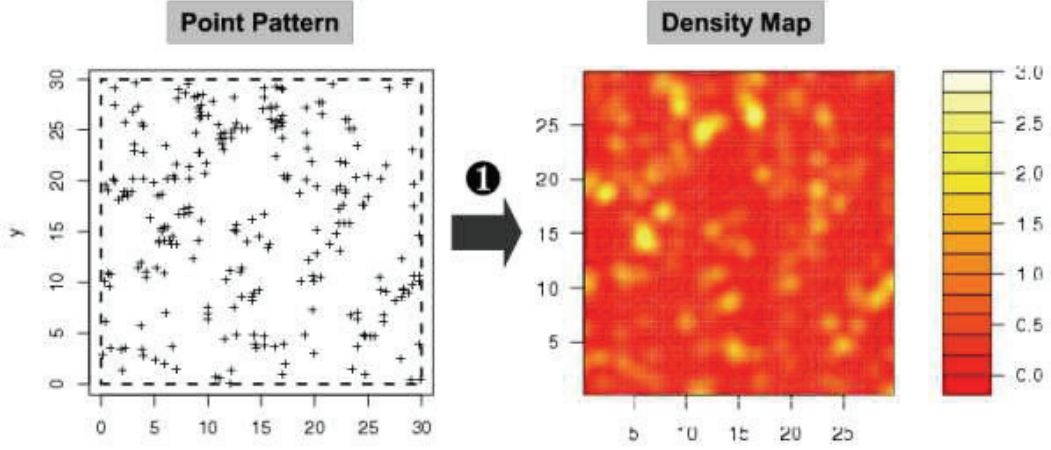


Figure 5.2. The Kernel Density Estimation method transforms a spatial point pattern (left) into a density map (right). The scale of the study site is provided in m and of the unity of the density map is points/ m^2 .

5.2.2 Variogram Analysis

The variogram^{5.3} function $\gamma(\mathbf{h})$ calculated for the density map and for each step in the decomposition of the density map obtained via **MDA**. This function provides an indication of the spatial correlation between measurements taken at sample locations. It is a crucial parameter in geostatistics (Matheron 1963) and is commonly represented as a function that shows the variance in measurements of distance between all pairs in sampled locations. The classical estimator of the Variogram function is defined as

$$\hat{\gamma}(\mathbf{h}) \equiv \frac{1}{2|N(\mathbf{h})|} \sum_{N(\mathbf{h})} (Z(\mathbf{u}) - Z(\mathbf{u} + \mathbf{h}))^2, \quad (5.3)$$

where \mathbf{u} is the vector of spatial coordinates (a point on the density map), $Z(\mathbf{u})$ is the variable under consideration as a function of spatial location (in this case, density), $Z(\mathbf{u} + \mathbf{h})$ is the lagged version of the variable under consideration, \mathbf{h} is the lag vector representing the separation between two spatial locations and $N(\mathbf{h})$ is the number of pairs separated by lag \mathbf{h} .

The main characteristics of a variogram function are presented below:

- **Sill** is the semivariance value at which the variogram levels off (C_∞).
- **Range** is the lag distance at which the semivariogram (or semivariogram component) reaches the sill value. Presumably, autocorrelation is essentially zero beyond the range.
- **Nugget** is the semivariogram value at the origin (C_0). In theory this value at the origin (0 lag) should be zero. If it is significantly different from zero for lags very close to zero, then this semivariogram value is referred to as the nugget. The nugget

5.3. Hereinafter I define the classical semivariogram as variogram.

represents variability at distances smaller than the typical sample spacing, including measurement error.

These characteristics are represented grafically in **Figure 5.3**.

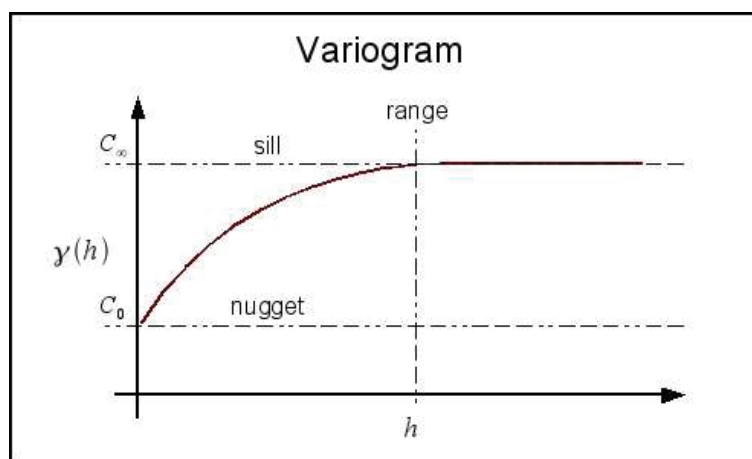


Figure 5.3. Characteristics of a Variogram.

5.2.3 Wavelet Transform

The second step of the methodology (**Figure 5.4**) is to use the **MDA** obtained via **WT** method in order to decompose an image (the density map generated by the **KDE** method) at different “scales”.

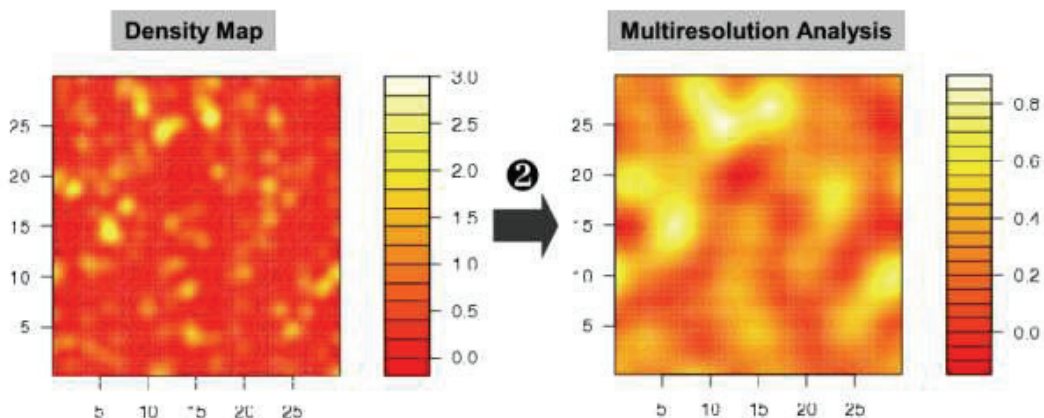


Figure 5.4. The Multiresolution Decomposition Analysis performed to decompose a density map (left) in different scales (right). The unit of the study site is provided in m and of the density map is points/ m^2 .

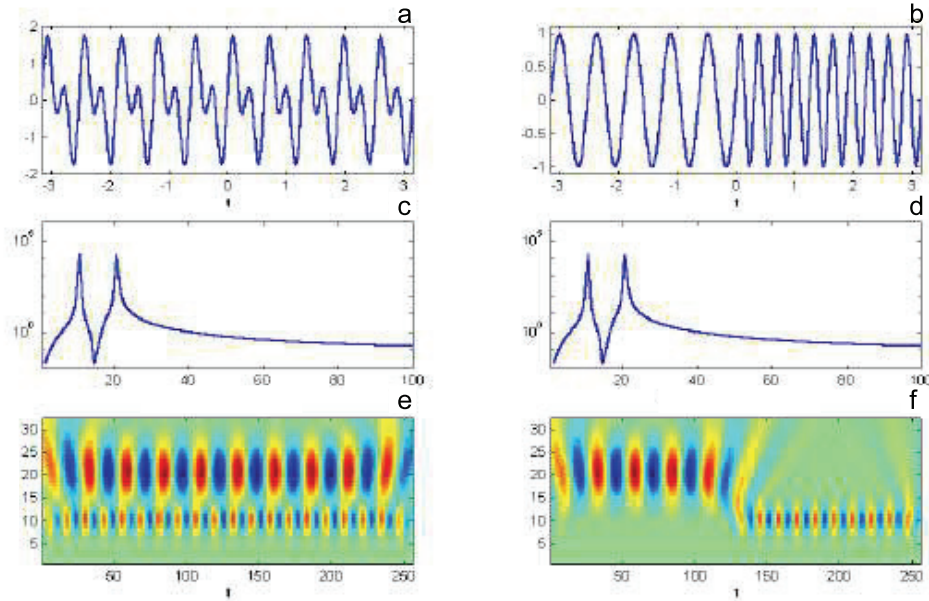


Figure 5.5. The graphic (a) represents a time series that contains a superposition of a low frequency signal ($\sin 10t$) and a high frequency signal ($\sin 20t$). The graphic (b) represents a time series that contains a low frequency signal ($\sin 10t$) in the first half and a signal with high frequency signal ($\sin 20t$) in the second half. The graphics (c) and (d) represent the response of the **FT** to the time series represented at the graphics (a) and (b) respectively. The graphics (e) and (f) are represent the response of the **WT** to the time series represented at graphics (a) and (b) respectively.

5.2.3.1 Continuous Wavelet Transform

The **WT** method was developed to investigate and analyze the temporal development of a non-stationary time-series. It is able to perform a time-frequency analysis of a time series and to estimate the spectral characteristics of the signal as a function of time (Meyers 1993, Torrence & Compo 1998). The main advantage of the **WT** in relation to other spectral analysis methods (like **FT**, for example), is its capacity to detect the frequencies that exist in the signal and their respective temporal-localization. In summary, **WT** uses a multiresolution technique to analyze different frequencies at different resolutions.

The **WT** method is an integral transformation whose integration kernels are called *wavelets* (Chi 1992, Daubechies 1992, Mallat 1998). These *wavelets* have the properties of being located in time and frequency (space and wave number if I are considering the spatial case), which permits us to analyze signals that contain non-stationary power at different frequencies (Daubechies 1990). The **WT** decomposes a signal $f(x)$ using scaled

and shifted versions of a function called *mother wavelet* and it is generally defined as

$$Wf(\lambda, t) = \int_{-\infty}^{+\infty} f(u)\psi_{\lambda,t}(u) du, \quad (5.4)$$

where $f(t)$ is the signal to be analyzed and $\psi_{\lambda,t}(u)$ is a family of functions defined as

$$\psi_{\lambda,t}(u) = \frac{1}{\sqrt{\lambda}}\psi\left(\frac{u-t}{\lambda}\right), \quad (5.5)$$

and λ is a scale parameter (related to the frequency), t is a shifting parameter (related to time position) and $\psi(u)$ is a *mother wavelet*.

The choice of a wavelet function $\psi(t)$ is not arbitrary and it has to satisfy two conditions: that the function $\psi(t)$ is normalized or $\int |\psi(t)|^2 dt = 1$ and $\int \psi(t) dt = 0$. The factor $\sqrt{\lambda}$ maintains the variance of the shifted and scaled wavelet identical to those of the *mother wavelet*.

Changes in the values of scale parameter λ modify the wavelet width. Large values of λ dilate the wavelet width, while small values of λ compress the wavelet width. Compressed versions of the *mother wavelet* are used to detect high frequency components (or low scale features) contained within the analyzed signal and dilated version of the *mother wavelet* are used to detect low frequency components (or high scale features) that are contained within the analyzed signal (see **Figure 5.6**). The parameter t controls the shifting of the *mother wavelet* over the entire signal $f(x)$ (see **Figure 5.7**). In summary, it controls the position of the wavelet in the signal.

Further features of the **WT** are that the method preserves the variance of the analyzed signal $f(t)$, or

$$\int_{-\infty}^{+\infty} |f(t)|^2 dt = \frac{1}{C_g} \int_{-\infty}^{+\infty} \int_0^{\infty} |W_f(\lambda, t)|^2 \psi_{\lambda,t}(u) du \frac{d\lambda}{\lambda^2}, \quad (5.6)$$

and that the original signal $f(t)$ can be recovered by the inverse wavelet transform defined as

$$f(t) = \frac{1}{C_g} \int_{-\infty}^{+\infty} \int_0^{\infty} \frac{1}{\lambda^2} W_f(\lambda, t) \psi_{\lambda,t}(u) dt d\lambda, \quad (5.7)$$

where

$$C_g = \int_{-\infty}^{+\infty} \frac{|\hat{\psi}(f)|^2}{f} df, \quad (5.8)$$

and

$$\hat{\psi}(f) = \int_{-\infty}^{+\infty} \psi(t) e^{-i2\pi ft} dt. \quad (5.9)$$

There is a relation between frequency (or pseudo-frequency) and scale (Abry 1997) defined as

$$F_a = \frac{\Delta F_c}{a}, \tag{5.10}$$

where a is the scale of the wavelet, Δ is the sample period, F_c is the central frequency in Hz of the wavelet (that value is specific for each wavelet family) and F_a is the pseudo-frequency associated with the scale a in Hz.

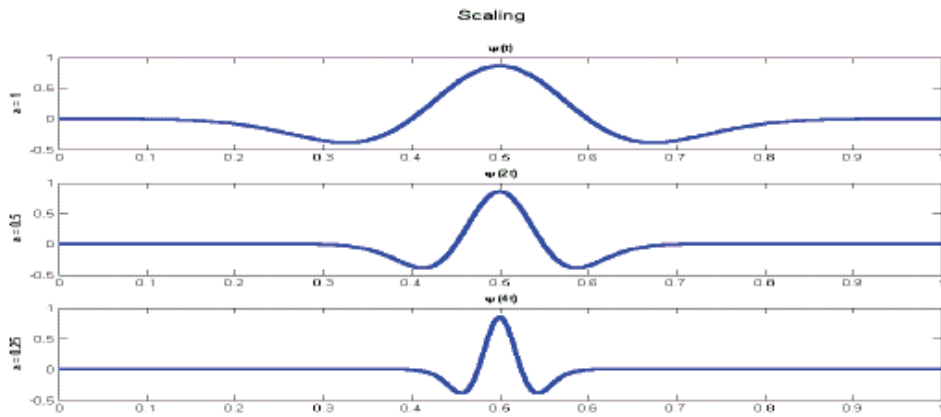


Figure 5.6. The graphics (a),(b) and (c) represent the same *mother wavelet* with parameter $\lambda = 1$, $\lambda = 0.5$ and $\lambda = 0.25$ respectively.

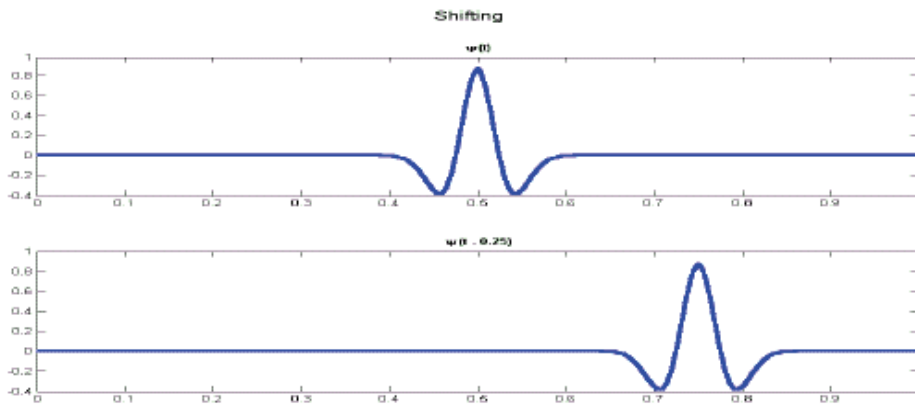


Figure 5.7. The graphics (a) and (b) represent the same *mother wavelet* with parameter $t = 0$ and $t = -0.25$ respectively.

The coefficients $Wf(\lambda, t)$ measure the match between the signal and the wavelet at the position t and scale λ . In summary, large values of $Wf(\lambda, t)$ indicate a high degree of similarity between the wavelet ψ with scale λ and the signal $f(x)$ at the position t . In

contrast, low values of $Wf(\lambda, t)$ indicate a low degree of similarity between the wavelet ψ with scale λ and the signal $f(x)$ at the position t and finally, negative values of $Wf(\lambda, t)$ indicates an out-of-phase association between the wavelet ψ with scale λ and the signal $f(x)$ at the position t .

The **WT** computed over a continuous range of values t and λ is called Continuous Wavelet Transform (hereinafter **CWT**) and the result is a three dimensional surface $Wf(\lambda, t)$ called as scalogram.

5.2.3.2 Discrete Wavelet Transform

The **WT** computed over a discrete range of parameters λ and t is called **DWT**. The **DWT** will provide us with the **MDA**, the multiscale decomposition of an image at different scales. It is a special case of the **WT** and it provides a compact representation of a signal in time and frequency that can be computed efficiently. In this case the scale parameter is $\lambda = \lambda_0^m$, where m is an integer and λ_0 is a fixed scale parameter greater than 1, and the shifting parameter is assumed to be $t = n t_0 \lambda_0^m$, where $t_0 > 0$ and depends on $\psi(t)$ and n is an integer. Then, I can define the **CWT** applied to a signal $f(t)$ as

$$Wf(\lambda, t) = \int f(t) \psi_{m,n}(t) dt, \quad (5.11)$$

where

$$\psi_{m,n}(t) = \lambda_0^{-0.5m} \psi(\lambda_0^{-m} t - n t_0). \quad (5.12)$$

In practice, the **DWT** is performed considering the parameters $\lambda_0 = 2$ and $t_0 = 1$ (Orthogonal Wavelet Transform). Then I have

$$\psi_{m,n}(t) = 2^{-0.5m} \psi(2^{-m} t - n). \quad (5.13)$$

It is possible to construct a class of orthogonal wavelets $\psi_{m,n}(t)$ satisfying the following condition

$$\int \psi_{j,k}(t) \psi_{m,n}(t) dt = \delta_{jm} \delta_{kn}, \quad (5.14)$$

where δ_{ij} is the Kronecker Delta function defined as

$$\delta_{ij} = \begin{cases} 1, & \text{if } i = j \\ 0, & \text{otherwise} \end{cases}. \quad (5.15)$$

Now I can approximate a function $f(t)$ with a linear combination of orthogonal wavelets $\psi_{m,n}(t)$ (Kumar & Fourfola 1988) as

$$f(t) = \sum_{m=-\infty}^{+\infty} \sum_{n=-\infty}^{+\infty} D_{m,n} \psi_{m,n}(t), \quad (5.16)$$

where m and n are the scale and temporal index respectively, with

$$D_{m,n} = \int f(t) \psi_{m,n}(t) dt. \quad (5.17)$$

Supposing now there are intermediate scales m_1 and m_2 , I can redefine the equation 5.15 as

$$\begin{aligned} f(t) = & \sum_{m=m_2+1}^{+\infty} \sum_{n=-\infty}^{+\infty} D_{m,n} \psi_{m,n}(t) + \sum_{m=m_1}^{m_2} \sum_{n=-\infty}^{+\infty} D_{m,n} \psi_{m,n}(t) + \\ & + \sum_{m=-\infty}^{m_1-1} \sum_{n=-\infty}^{+\infty} D_{m,n} \psi_{m,n}(t), \end{aligned} \quad (5.18)$$

that represents the decomposition of the signal $f(t)$ at three range scales: the first summation represents the higher scales characteristics of the signal ($r > m_2$), the second one represents the intermediate scales characteristics ($m_2 \leq r \leq m_1$) and the final one represents the lower scale characteristics ($r < m_1$).

In practice, the **MDA** of a signal at different scales is performed by successive use of lowpass and highpass filters. In this case, the function $\phi(t)$ or scale function corresponds to the discrete lowpass filter, that retains the low frequencies features of the signal and the function $\psi(t)$ corresponds to the discrete highpass filter, that retains the high frequencies of the signal (Daubechies & Mallat 1998).

In summary, the **MDA** is performed by decomposing the original signal into two parts: a part named “detail” that contains the high frequency features (**D**) of the signal and another one named “approximation” that contains the low frequencies features (**A**) of the signal.

The **MDA** generally (depending on the type of the filter used at the decomposition) permits a perfect reconstruction (Mallat 1998) of the original signal $f(t)$. The **MDA** at one level (see **Figure 5.8**) can be defined as

$$f(t) = A_0 = A_1 + D_1, \quad (5.19)$$

where A_0 is the original signal $f(t)$, A_1 and D_1 are respectively approximation and detail at level 1.

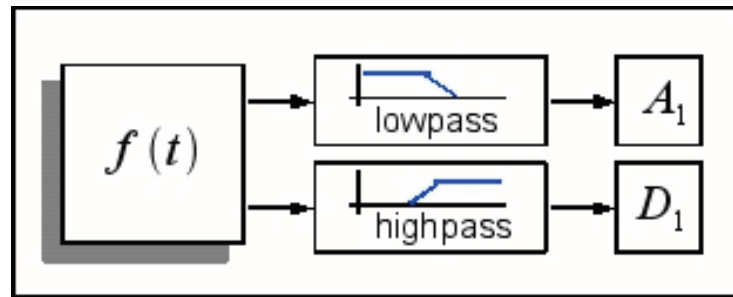


Figure 5.8. **MDA** applied to a signal $f(t)$. A_1 is the approximation at level 1 and D_1 is the detail at level 1.

The same decomposition process can be repeated with the approximation A_1 (see **Figure 5.9**). Thus, I have

$$A_1 = A_2 + D_2, \tag{5.20}$$

where A_2 and D_2 are respectively approximation and detail at level 2.

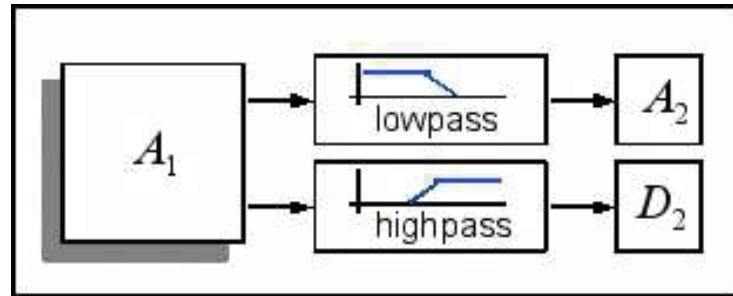


Figure 5.9. MDA applied to A_1 . A_2 is the approximation at level 2 and D_2 is the detail at level 2.

Then combining **Equation 5.18** and **Equation 5.19**, I obtain

$$f(t) = A_0 = A_2 + D_1 + D_2, \tag{5.21}$$

and by induction, a decomposition performed at level n can be represented as

$$f(t) = A_0 = A_n + D_1 + \dots + D_n = A_n + \sum_{i=1}^n D_i, \tag{5.22}$$

where A_n is the approximation at level at level n and D_i is the detail at level i . In summary, to decompose an image at level n I need to apply the highpass and lowpass filters to the image successively n times (see **Figure 5.10**).

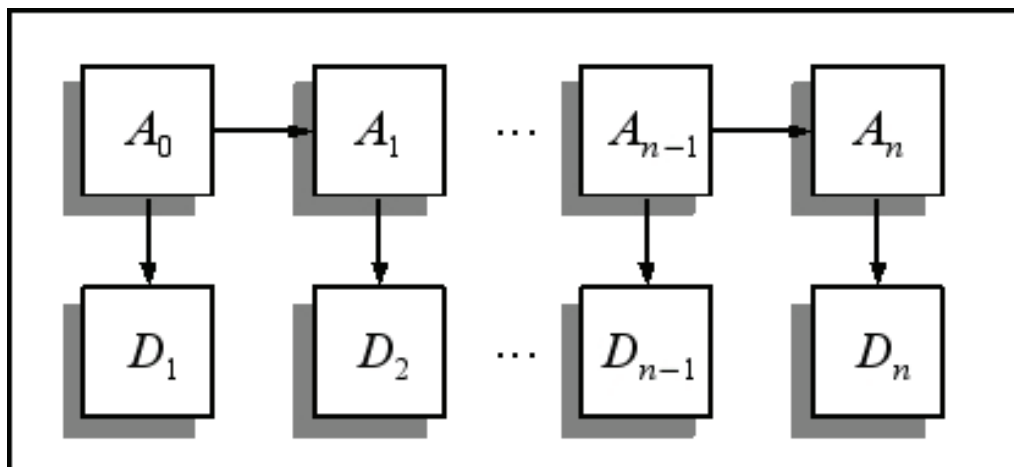


Figure 5.10. MDA at level n applied to a signal $f(t) = A_0$.

It is important to note that the methodology can be also applied to a 2D signal (Image) without loss of generality. For more details, see Mallat (1998).

Figure 5.11 shows an example of an image decomposition performed by **MDA** at level two (higher, intermediate and lower scales). This decomposition can be represented as

$$\text{Original Image} = A_0 = A_2 + D_1 + D_2, \quad (5.23)$$

where A_2 , D_2 and D_1 contains the higher, intermediate and lower scale characteristics of the original image. In fact, the **Equation 5.22** is equivalent to **Equation 5.15**.

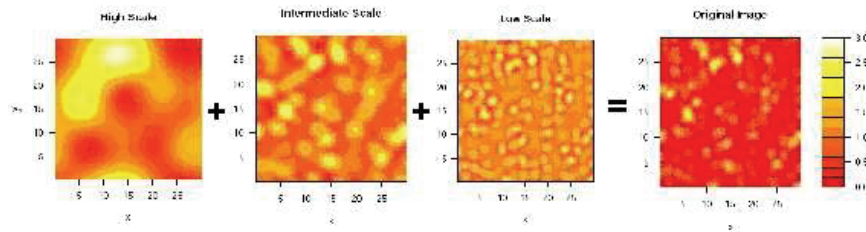


Figure 5.11. **MDA** applied to an image (density map). The original image (a density map) was decomposed at its higher, intermediate and lower scale components.

5.2.4 Inhomogeneous Poisson Process

The classical K-function requires the assumption that the point pattern is spatially homogeneous (stationary and/or isotropic). It supposes that the first order intensity over the entire area Ω is constant: that is, it is the same for all locations, or formally that $\lambda(x, y) \equiv \lambda, \forall(x, y) \in \Omega$. The problem occurs when the point pattern does not show homogeneity and then the analysis of this pattern obtained via the classical K-function can lead sometimes to a misinterpretation of the spatial point processes that occur inside the study area (Pelissier & Goreaud 2001).

A possibility way to analyze an inhomogeneous point pattern is to use the inhomogeneous K-function, a semi-parametric method that supposes that the point pattern was generated by a inhomogeneous Poisson process (Baddeley *et al* 2000). This method assumes that the first order intensity $\lambda(x, y)$ over the entire study area Ω is a function that depends on the location (x, y) . Formally the inhomogeneous K-function is defined as

$$K_i(r) = \frac{1}{A} \sum_{i=1}^n w_i(r) \sum_{j=1}^n \delta_{ij}(r) \frac{1}{\lambda_i \lambda_j}, \quad (5.24)$$

where A is the area of the study region Ω , $w_i(r)$ is an area based edge correction factor, $\delta_{ij}(r)$ is an indicator function defined as

$$\delta_{ij}(r) = \begin{cases} 1, & \text{if } d_{ij} \leq r \\ 0, & \text{otherwise} \end{cases}, \quad (5.25)$$

with

$$d_{ij} = \sqrt{(x_i - x_j)^2 + (y_i - y_j)^2}, \quad (5.26)$$

as the Euclidian distance between the points of the point pattern (x_i, y_i) and (x_j, y_j) and λ_i and λ_j are the local densities calculated at the locations (x_i, y_i) and (x_j, y_j) respectively.

To simulate a point pattern inside a study area Ω and subject to a first order intensity $\lambda(x, y)$, I have first to define the constant

$$\lambda_0 = \max_{(x,y) \in \Omega} (\lambda(x, y)), \quad (5.27)$$

and I then simulate a point (x, y) following a classical homogeneous Poisson process inside the area Ω and I accept this point as the location of a tree with probability $\frac{\lambda(x, y)}{\lambda_0}$ (Diggle 1983, Tomppo 1986). The information about the local density $\lambda(x, y)$ is obtained using the **MDA** method.

5.2.5 Density Map Generation

To generate the density map, I applied a **KDE** method to the spatial point pattern using a Quartic Kernel. I computed the local density with a kernel bandwidth of $h = 1$ m at the nodes of a 0.47 m x 0.47 m systematic grid covering the whole stand in order to obtain a density map with 64 x 64 cells. This enables us to decompose the density map at 7 levels using the **MRA** method.

The kernel bandwidth was chosen in order to preserve structures with scales greater than or equal to 2 m (Nyquist frequency).

In order to decompose the density map generated at different scales, I applied a classical **MDA** method using an algorithm implemented in the **software R**, a language and environment for statistical computing and graphics. The multiresolution analysis of the density maps are based on a Daubechies D8 wavelet performed using the **R package Waveslim**. The multiresolution decomposition was obtained up to level 4. This corresponds to filters out all the structures with scales up to 12 m. It corresponds to 40% of the dimensions of our study sites Lagoa A and Lagoa B.

5.3 Results

5.3.1 Heterogeneity detection

First I apply the **MDA** method in order to decompose a heterogeneous site into smaller homogeneous subplots that can be analyzed using classical statistical methods. In this case, I am considering heterogeneity as a deviance of the point pattern from a CSR pattern at large scales.

5.3.1.1 *Laguncularia racemosa* - Lagoa A

The results obtained from the L-function (**Figure 3.9**) show that the spatial configuration of the trees of species *Laguncularia racemosa* within stand Lagoa A exhibit clustering at large scales ($r \leq 10$ m). This could be an indication of heterogeneity in the stand (Goreaud & Pelissier 2001).

The first step of the methodology was to transform this point pattern (**Figure 3.9**) into a density map (**Figure 5.12**) using the **KDE** method. The variogram calculated (**Figure 5.12**) indicates that the density map shows structures with scales greater than 2 meters. It is interesting to note, that the density of the point pattern inside this stand is $\lambda_p = 0.279$, while the mean value obtained for the density map is $\lambda_d = 0.281$. This means that the transformation performed by the KDE preserved the global density of the stand.

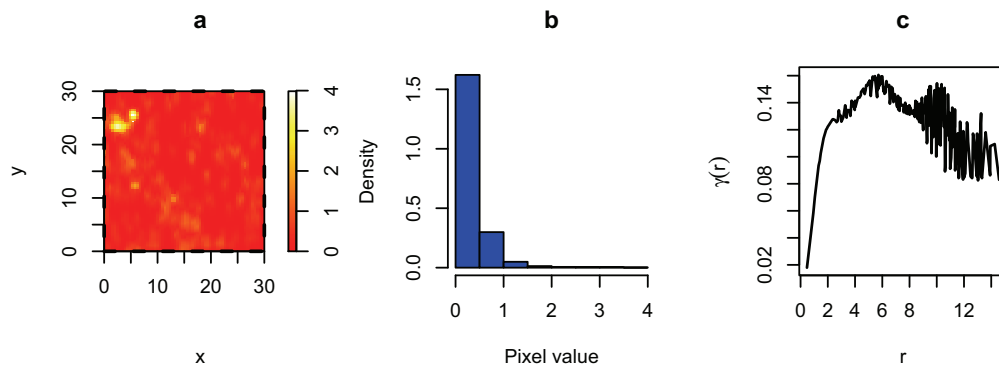


Figure 5.12. (a) Density map obtained from spatial point pattern relative to *Laguncularia racemosa* within stand Lagoa A. (b) and (c) are respectively the Histogram and the Variogram obtained from this density map in (a).

The second step was to decompose the density map into different scales using the **MDA** method. I applied the decomposition up to level 4 and in the following I describe the steps of the decomposition.

The approximation **A1** obtained at the first step of the decomposition shows no visible changes in the variogram (**Figure 5.13**). The mean density calculated for the image **A1** is $\lambda_d = 0.281$.

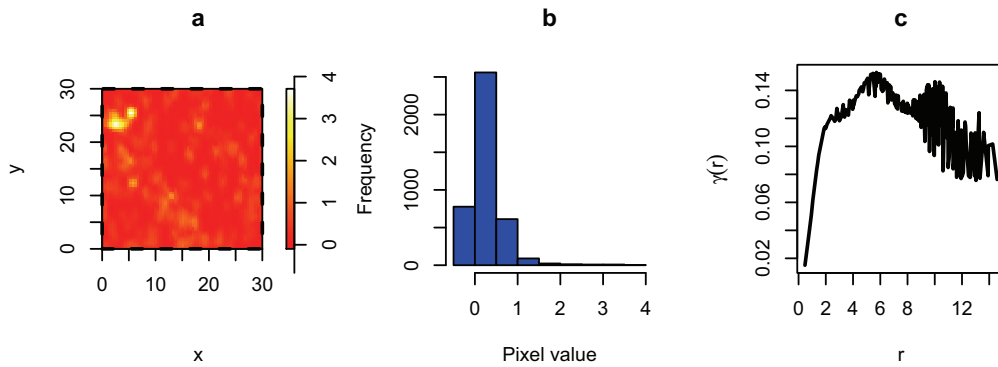


Figure 5.13. (a) Approximation **A1** relative to the density map at the **Figure 5.13**. (b) and (c) are respectively the Histogram and the Variogram obtained from this density map in (a).

The approximation **A2** obtained at the second step of the decomposition now presents changes in the variogram (**Figure 5.14**). This shows that the decomposition filtered all structures with scales smaller than or equal to 3 meters out of the density map. The mean density calculated for the image **A2** is $\lambda_d = 0.281$.

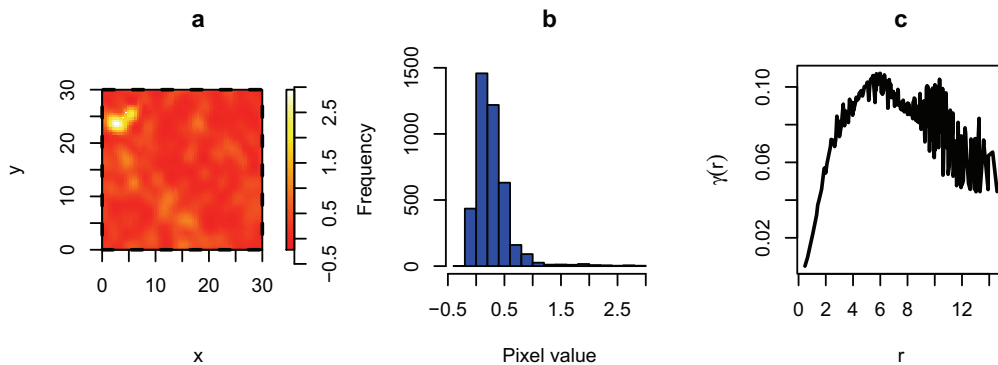


Figure 5.14. (a) Approximation **A2** relative to the density map at the **Figure 5.13a**. (b) and (c) are respectively the Histogram and the Variogram obtained from this density map in (a).

The variogram calculated for the approximation **A3** (**Figure 5.15**) shows that the decomposition filtered out all structures with scales smaller than or equal to 6 meters. The mean density calculated for the image **A3** is $\lambda_d = 0.281$.

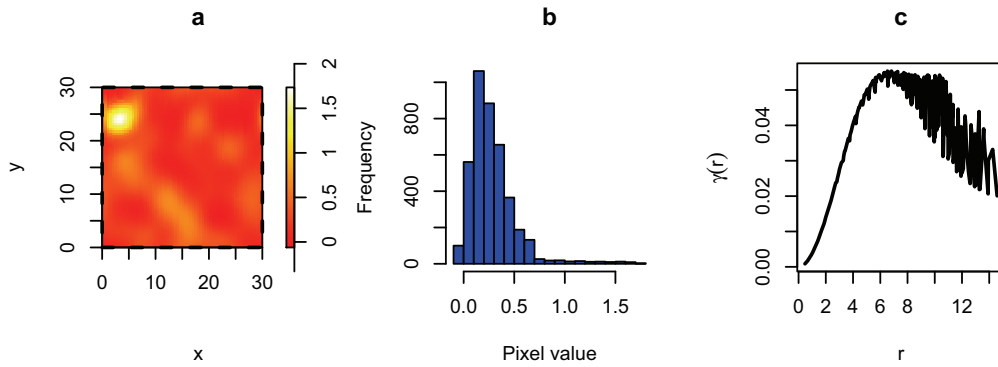


Figure 5.15. (a) Approximation **A3** relative to the density map at the **Figure 5.13**. (b) and (c) are respectively the Histogram and the Variogram obtained from this density map in (a).

The variogram calculated for the approximation **A4** shows that the decomposition filtered out all structures with scale smaller than or equal to 10 meters (**Figure 5.18**). That is the scale of our interest and the decomposition stops here. The mean density calculated for the image **A4** is $\lambda_d = 0.281$.

Visually I can see from the image **A4** (**Figure 5.16**) that there is a large region located at the left side of the stand with a high density of trees. The density cutoff chosen to separate this region from the rest of the stand was $\lambda_{\text{cutoff}} = 0.353$. The **Figure 5.17** shows the study site Lagoa A divided into two regions.

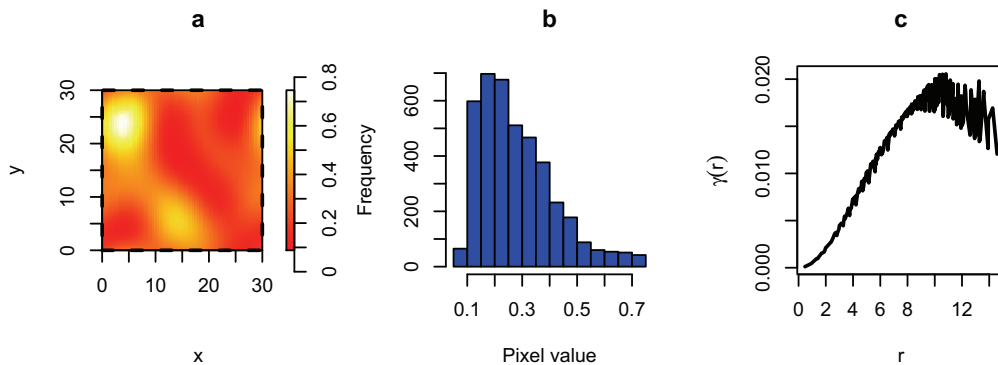


Figure 5.16. (a) Approximation **A4** relative to the density map at the **Figure 5.13a**. (b) and (c) are respectively the Histogram and the Variogram obtained from this density map in (a).

To complete the analysis, I calculated the L-function for the points contained within the red and yellow regions (**Figure 5.17**) separately. The result obtained for the L-function calculated for the point pattern within the red region (**Figure 5.17**) shows clustering at lower scales ($r \leq 5$ m). It is interesting to note that the point pattern contained within the yellow region exhibits a CSR pattern.

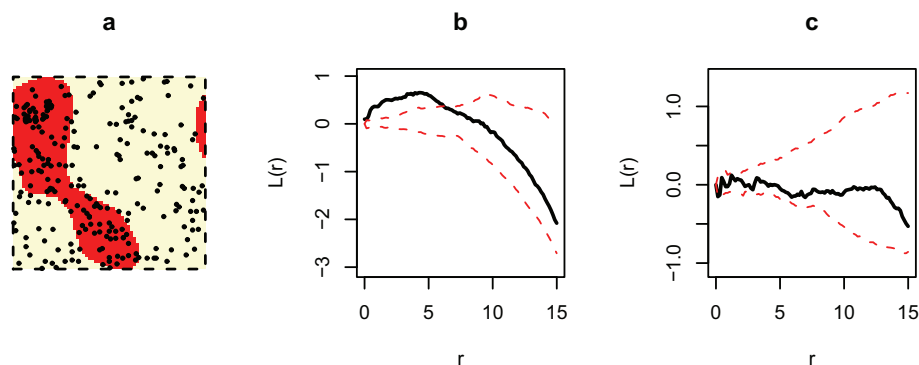


Figure 5.17. (a) Point pattern relative to *Laguncularia racemosa* whit-in stand Lagoa A, now divided at two regions (red and yellow). (b) and (c) represent the L-function (black) and 99% simulation interval (dashed red) calculated for the point pattern inside the red and yellow regions respectively. The simulation interval was calculated via Monte Carlo method (Besag 1977) for the CSR hypothesis with 10000 simulations.

Considering that low and intermediate scale variations in the structures of the study site can be considered as elements of the structure (Wiens 1989, Kolasa & Rollo 1991, Holling 1992, He *et al.* 1994, Goreaud 2000). I can affirm that I divided the whole stand site with a strong indication of heterogeneity into two subsets that exhibited homogeneity.

5.3.1.2 *Laguncularia racemosa* - Lagoa B

The trees of the species *Laguncularia racemosa* within the stand Lagoa B also exhibit clustering at larger scales (see **Figure 3.20**). This could be an indication of heterogeneity in the stand (Pelissier and Goreaud 2001). I applied the same methodology described above with this group of trees, but in the following I do not describe all the intermediate steps, just the final result.

The variogram in **Figure 5.18** shows that the density map presents structures with scales greater than 3 meters. The density calculated for the point pattern inside this stand is $\lambda_p = 0.190$, while the mean value obtained for the density map is $\lambda_d = 0.191$.

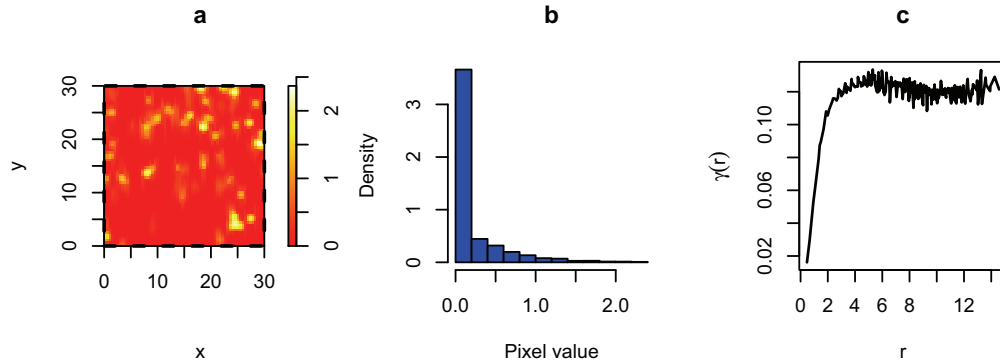


Figure 5.18. (a) Density map obtained from spatial point pattern relative to *Laguncularia racemosa* within stand Lagoa B. (b) and (c) are respectively the Histogram and the Variogram obtained from this density map in (a).

The variogram relative to the approximation **A4** shows that the decomposition filtered out all structures with scale smaller than or equal to 12 meters (**Figure 5.19**). The mean density calculated for the image **A4** remains $\lambda_d = 0.191$. Visually I can see from the image **A4** (**Figure 5.19**) that there are some areas in the stand with a high density of trees. The cutoff, chosen visually to divide the stand, was $\lambda_{\text{cutoff}} = 0.249$ and the **Figure 5.20** shows the study site Lagoa B divided into two distinct regions.

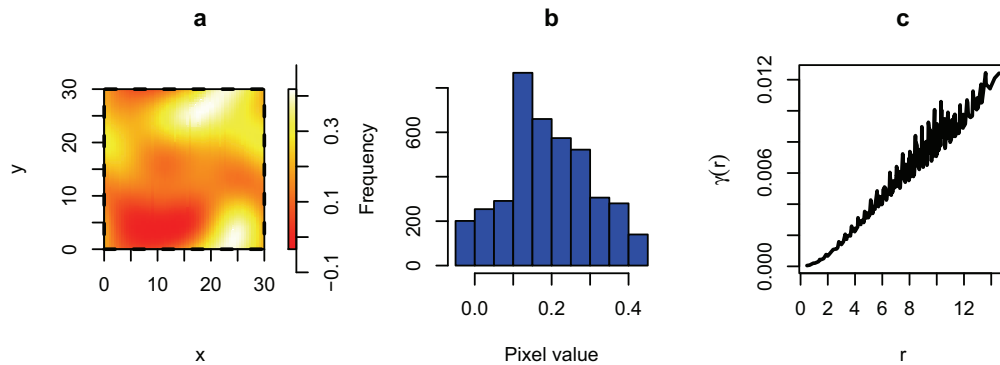


Figure 5.19. (a) Approximation **A4** relative to the density map at the **Figure 5.18**. (b) and (c) are respectively the Histogram and the Variogram obtained from this density map in (a).

The result obtained for the L-function calculated for the point pattern within the red region (**Figure 5.20**) presents clustering at lower scales ($r \leq 1$ m). The point pattern contained within the yellow region (**Figure 5.20**) presents clustering at lower scales ($r \leq 5$ m). Again, I separated a large region that presents heterogeneity at two regions that presents some homogeneity.

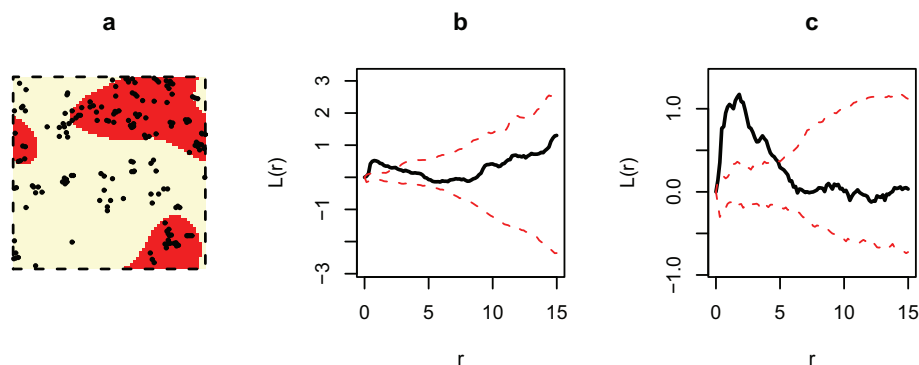


Figure 5.20. (a) Point pattern relative to *Laguncularia racemosa* whit-in stand Lagoa B, now divided at two regions (red and yellow). (b) and (c) represents the the L-function (black) and 99% simulations interval (dashed red) calculated for the point pattern inside the red and yellow respectively. The simulations interval was calculated via Monte Carlo method (Besag 1977) for the CSR hypothesis with 10000 simulations.

5.3.1.3 Dead Trees - Lagoa B

The dead trees within stand Lagoa B (**Figure 3.21**) also exhibit clustering at larger scales. This could be an indication of heterogeneity in the stand (Pelissier and Goreaud 2001).

The variogram in **Figure 5.21** indicates that the density map shows structures with scales greater than 2 meters. The density calculated for the point pattern inside this stand is $\lambda_p = 0.128$, while the mean value obtained for the density map is $\lambda_d = 0.129$. Again the transformation performed by the KDE preserved the global density of the stand.

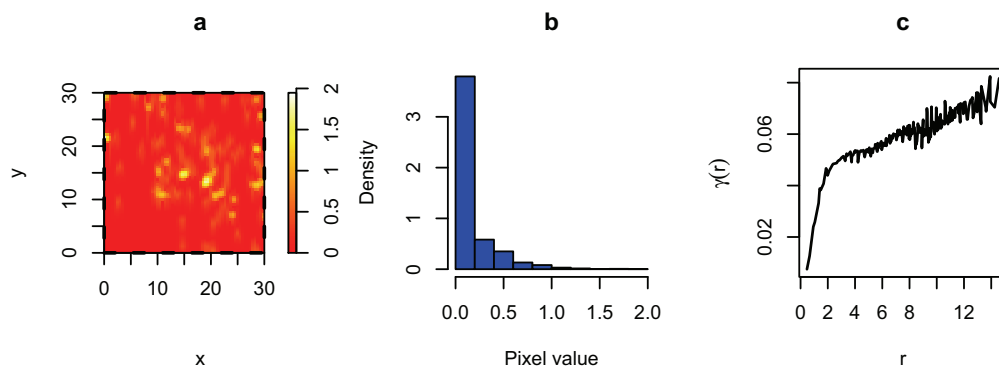


Figure 5.21. (a) Density map obtained from spatial point pattern relative to dead trees within stand Lagoa A. (b) and (c) are respectively the Histogram and the Variogram obtained from this density map in (a).

The variogram relative to the approximation **A4** shows that the decomposition filtered out all structures with scale smaller than or equal to 12 meters (**Figure 5.22**). The mean density calculated for the image **A4** remains $\lambda_d = 0.128$. Visually I can see from the image **A4** (**Figure 5.22**) that there are some area in the stand with a high density of dead trees. The cutoff chosen was $\lambda_{\text{cutoff}} = 0.152$ and the **Figure 5.23** shows the study site Lagoa B divided into two regions.

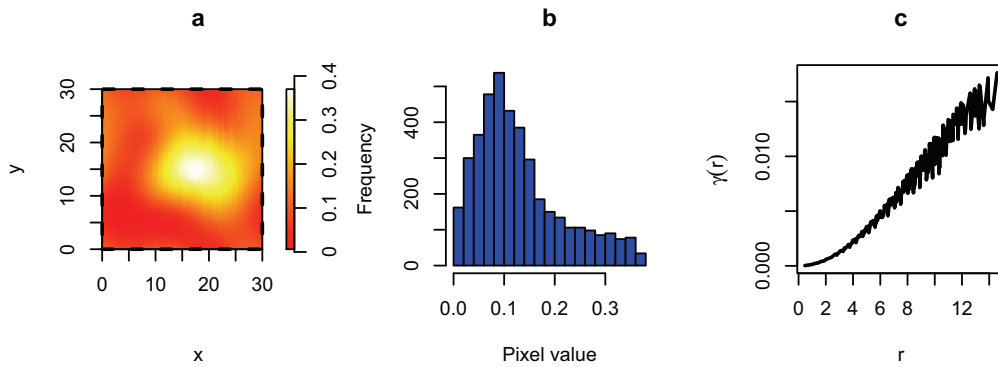


Figure 5.22. (a) Approximation **A4** relative to the density map at the **Figure 5.25a**. (b) and (c) are respectively the Histogram and the Variogram obtained from this density map in (a).

The result obtained for the L-function calculated for the point pattern within the red region (**Figure 5.26**) exhibits a CSR pattern. The point pattern in the yellow region (**Figure 5.22**) exhibits clustering at lower scales ($r \simeq 1$ m) and regularity at intermediate scales ($r \simeq 5$ m). Again I divided a large region that shows heterogeneity into two regions that exhibit some homogeneity.

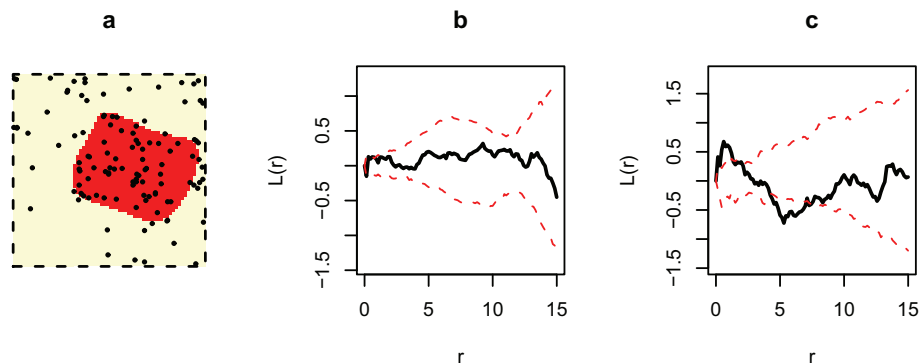


Figure 5.23. (a) Point pattern relative to dead trees whit-in stand Lagoa B, now divided at two regions (red and yellow). (b) and (c) represents the the L-function (black) and 99% simulations interval (dashed red) calculated for the point pattern inside the red and yellow respectively. The simulations interval was calculated via Monte Carlo method (Besag 1977) for the CSR hypothesis with 10000 simulations.

5.3.2 Spatial-Scale Resolution

Now the main objective of this experiment is try to provide evidence from spatial patterns of the probable succession processes occurring among the trees of species *Laguncularia racemosa* and *Avicennia germinans* within studies sites Lagoa A and Lagoa B.

5.3.2.1 Spatial relationship between *Laguncularia racemosa* and *Avicennia germinans* - Lagoa A

The results presented at **Figure 3.15** show that *Avicennia* trees tends to be clumped at scales $r \simeq 1$ m. *Laguncularia* trees exhibit clumping at all scales, with a maximum at scale $r \simeq 4$ m. The spatial relation between the *Avicennia* and *Laguncularia* trees exhibits a tendency to repulsion at lower scales, in particular at scale $r \simeq 0.50$ m.

The variogram presented in **Figure 5.24** (*Avicennia germinans*) indicates that the density map presents structures with scales greater than 2 meters. The density calculated for the point pattern inside this stand is $\lambda_p = 0.343$, while the mean value obtained for the density map is $\lambda_d = 0.345$.

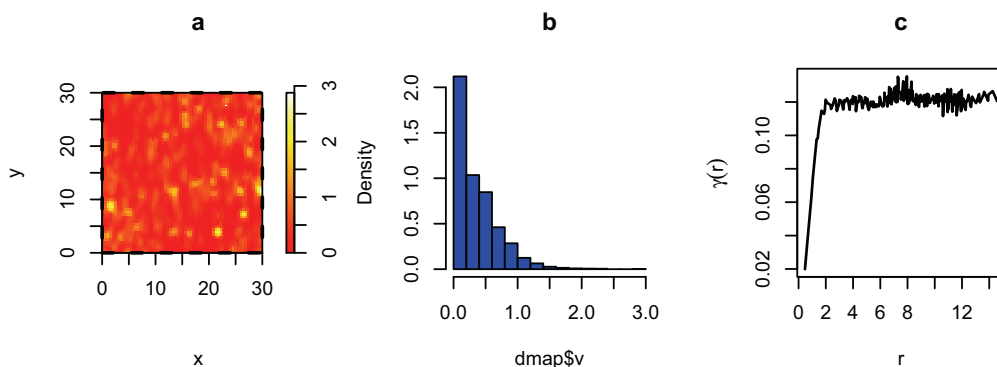


Figure 5.24. (a) Density map obtained from spatial point pattern relative to *Avicennia germinans* within stand Lagoa A. (b) and (c) are respectively the Histogram and the Variogram obtained from this density map in (a).

The variogram presented in **Figure 5.25** (*Laguncularia racemosa*) indicates that this density map also shows structures with scales greater than 2 meters. The density calculated for the point pattern inside this stand is $\lambda_p = 0.279$, while the mean value obtained for the density map is $\lambda_d = 0.281$.

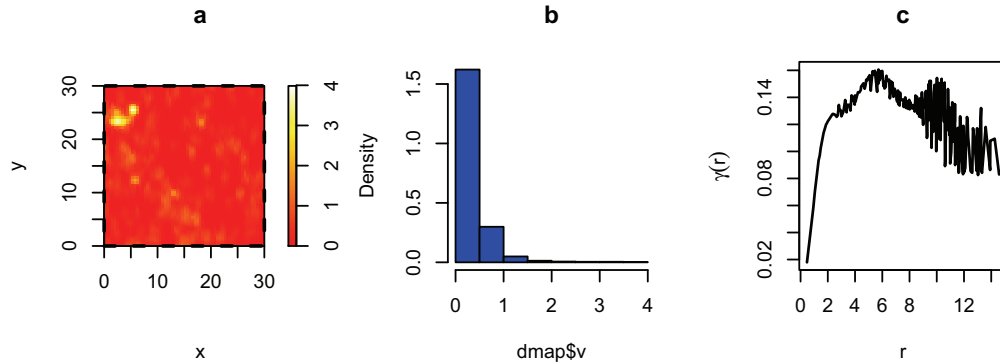


Figure 5.25. (a) Density map obtained from spatial point pattern relative to *Laguncularia racemosa* within stand Lagoa A. (b) and (c) are respectively the Histogram and the Variogram obtained from this density map in (a).

The variogram relative to the approximation **A4** shows that the decomposition filtered out all structures with scales smaller than or equal to 12 meters (**Figure 5.26**). The mean density calculated for the image **A4** remains $\lambda_d = 0.345$. Visually I can see from the image **A4** (**Figure 5.26**) that there are some areas in of the stand with a high density of trees of species *Avicennia germinans*.

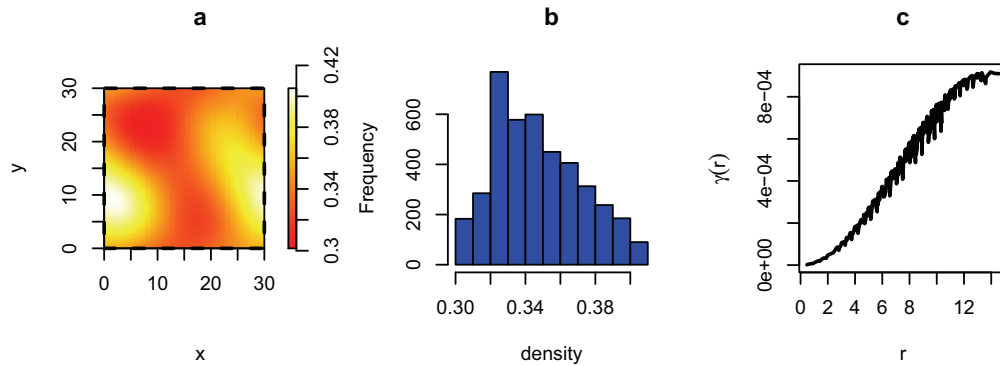


Figure 5.26. *Avicennia germinans* (a) Approximation **A4** relative to the density map at the **Figure 5.24**. (b) and (c) are respectively the Histogram and the Variogram obtained from this density map in (a).

The variogram relative to the approximation **A4** shows that the decomposition filtered out all structures with scales smaller than or equal to 12 meters (**Figure 5.27**). The mean density calculated for the image **A4** remains $\lambda_d = 0.281$. Visually I can see from the image **A4** (**Figure 5.37**) that there are some area in the stand with a high density of trees of species *Laguncularia racemosa*.

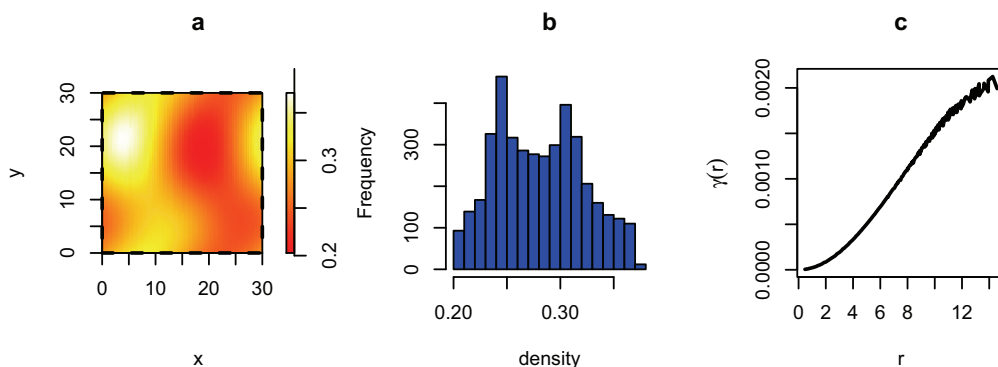


Figure 5.27. *Laguncularia racemosa* (a) Approximation **A4** relative to the density map at the **Figure 5.25**. (b) and (c) are respectively the Histogram and the Variogram obtained from this density map in (a).

The result presented in **Figure 5.28** shows a repulsive spatial pattern at larger scales exhibited by trees of species *Laguncularia* and *Avicennia*. Visually, it can be clearly observed that there is a high density of *Laguncularia* trees in places with a low density of *Avicennia* trees and vice-versa.

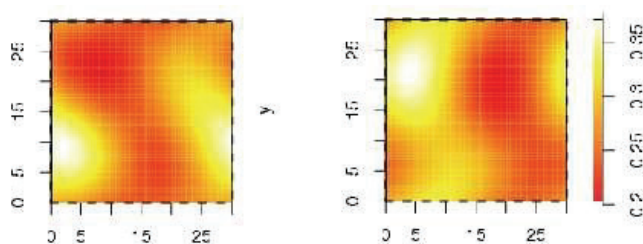


Figure 5.28. (a) Approximation **A4** relative to the density map obtained for the *Avicennia germinans* and (b) Approximation **A4** relative to the density map obtained for the *Laguncularia racemosa* within Lagoa A.

5.3.2.2 Spatial relationship between *Laguncularia racemosa* and *Avicennia germinans* - Lagoa B

The result shows that *Avicennia* trees exhibit clustering at lower and intermediate scales, with a maximum at $r \simeq 4$ m. The *Laguncularia* trees exhibit clumping at lower and intermediate scales, in with a maximum at $r \simeq 1$ m. The spatial relation between *Avicennia* and *Laguncularia* trees exhibits repulsion at scale $r \simeq 1$ m and a tendency to repulsion at scale $r \simeq 4$ m (see **Figure 3.26**).

The variogram in **Figure 5.29** indicates that the density map shows structures with scales greater than 2 meters. The density calculated for the point pattern inside this stand is $\lambda_p = 0.284$, while the mean value obtained for the density map is $\lambda_d = 0.286$. Again the transformation performed by the KDE preserved the global density of the stand.

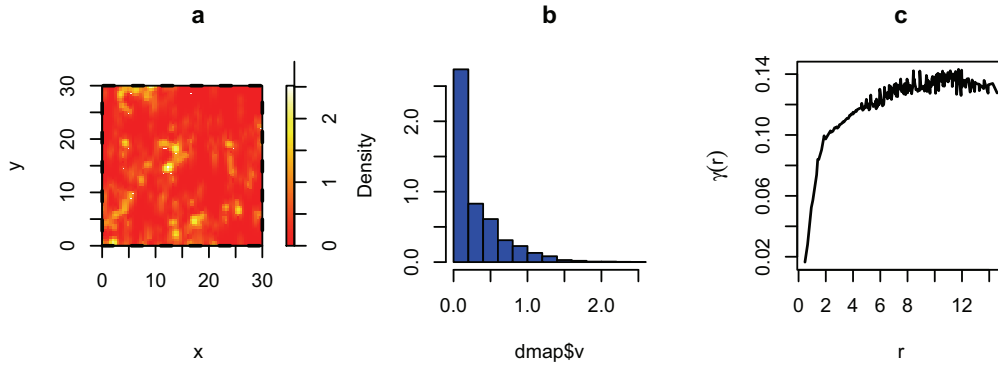


Figure 5.29. (a) Density map obtained from spatial point pattern relative to *Avicennia germinans* within stand Lagoa B. (b) and (c) are respectively the Histogram and the Variogram obtained from this density map in (a).

The variogram in **Figure 5.30** (*Laguncularia racemosa*) indicates that the density map also shows structures with scales greater than 2 meters. The density calculated for the point pattern inside this stand is $\lambda_p = 0.190$, while the mean value obtained for the density map is $\lambda_d = 0.191$. Again the transformation performed by the KDE preserved the global density of the stand.

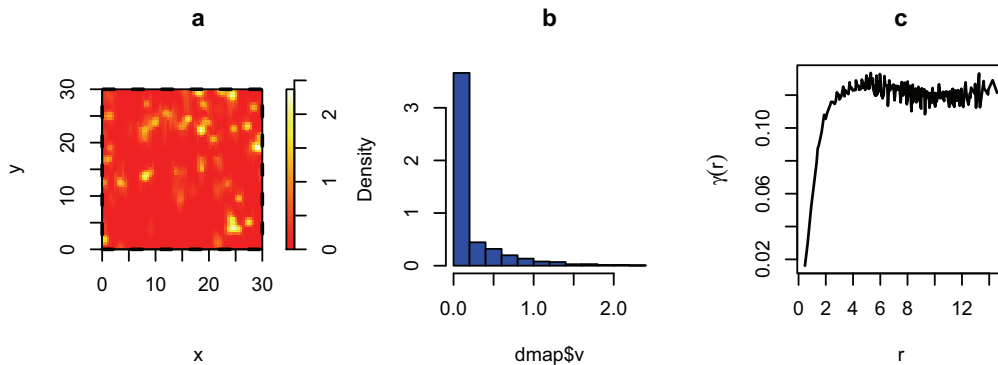


Figure 5.30. (a) Density map obtained from spatial point pattern relative to *Laguncularia racemosa* within stand Lagoa B. (b) and (c) are respectively the Histogram and the Variogram obtained from this density map in (a).

The variogram relative to the approximation **A4** (**Figure 5.31**) shows that the decomposition filtered out all structures with scale smaller than or equal to 12 meters. The mean

density calculated for the image **A4** remains the same ($\lambda_d = 0.236$). Visually I can see from the image **A4** (**Figure 5.31**) that there are some areas in the stand with a high density of trees of species *Avicennia germinans*.

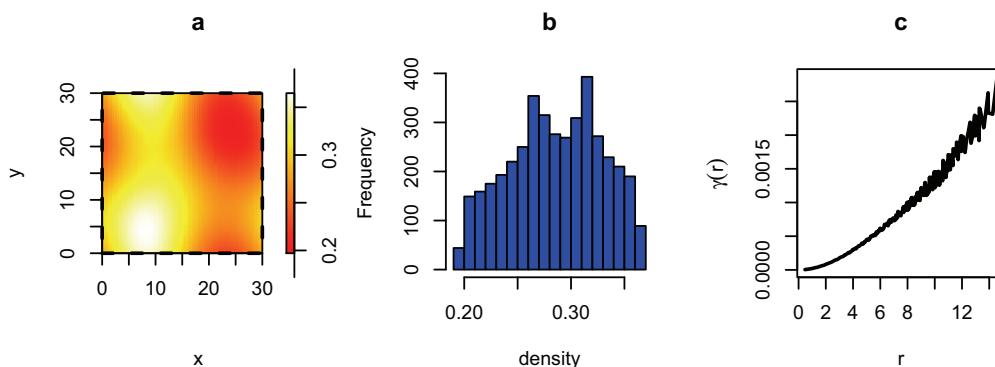


Figure 5.31. *Avicennia germinans* (a) Approximation **A4** relative to the density map at the **Figure 5.29**. (b) and (c) are respectively the Histogram and the Variogram obtained from this density map in (a).

This decomposition was also performed up to level 4. The variogram relative to the approximation **A4** shows that the decomposition filtered out all structures with scale smaller than or equal to 12 meters (**Figure 5.32**). The mean density calculated for the image **A4** remains the same ($\lambda_d = 0.191$). Visually I can see from image **A4** (**Figure 5.32**) that there are some areas of the stand with a high density of trees of species *Laguncularia racemosa*.

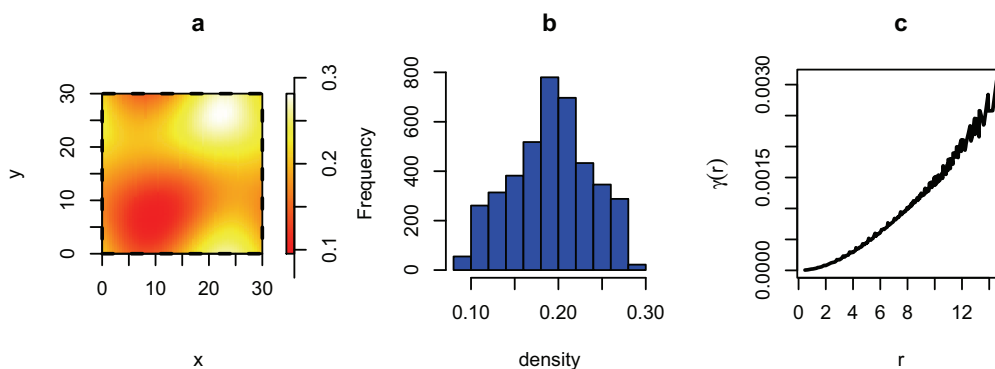


Figure 5.32. *Laguncularia racemosa* (a) Approximation **A4** relative to the density map at the **Figure 5.30**. (b) and (c) are respectively the Histogram and the Variogram obtained from this density map in (a).

The results presented in **Figure 5.33** also show a repulsive spatial pattern at larger scales exhibited by the trees of species *Laguncularia* and *Avicennia*. The pattern is the same as in Lagoa A. There are areas with a high density of *Laguncularia* trees located in regions with low density of *Avicennia* trees and vice-versa.

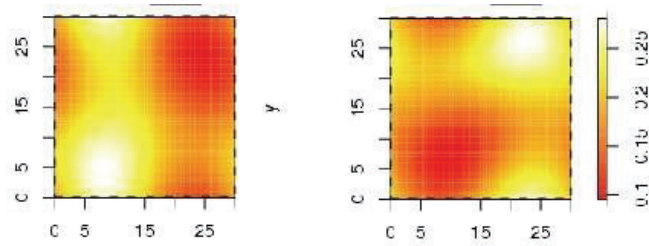


Figure 5.33. (a) Approximation **A4** relative to the density map obtained for the *Avicennia germinans* and (b) Approximation **A4** relative to the density map obtained for the *Laguncularia racemosa* within Lagoa B.

5.3.3 Simulating an Inhomogeneous Poisson Process

5.3.3.1 *Laguncularia racemosa* - Lagoa B

In this experiment, I simulated an inhomogeneous Poisson process to reproduce the point pattern presented by the *Laguncularia* trees in the site Lagoa B. The local density $\lambda(x, y)$ required for this simulation was the approximation **A4** already shown in **Figure 5.19**.

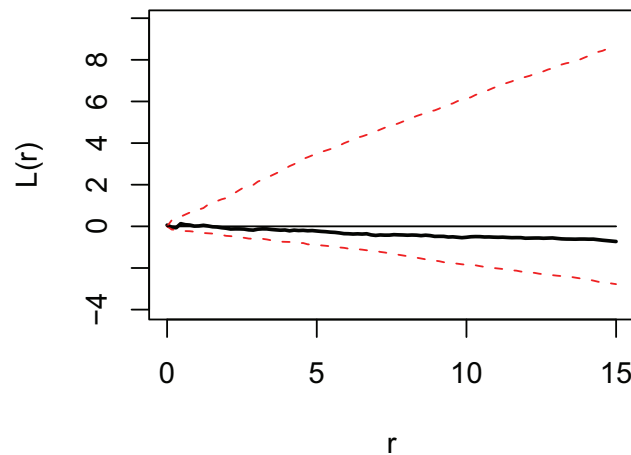


Figure 5.34. Inhomogeneous L-function (black) and 90% simulations interval (dashed red) calculated for the *Laguncularia* trees inside Lagoa B. The simulations interval was calculated via Monte Carlo method (Besag 1977) for the inhomogeneous Poisson hypothesis with 1000 simulations.

The results shown in **Figure 5.34** shows that the *Laguncularia* trees in the site Lagoa B can be simulated as an inhomogeneous Poisson process.

5.3.3.2 Dead trees - Lagoa B

Then I simulated an inhomogeneous Poisson process reproducing the point pattern presented by dead trees in the site Lagoa B. The local density $\lambda(x, y)$ required for this simulation was the approximation **A4** already shown in **Figure 5.21**.

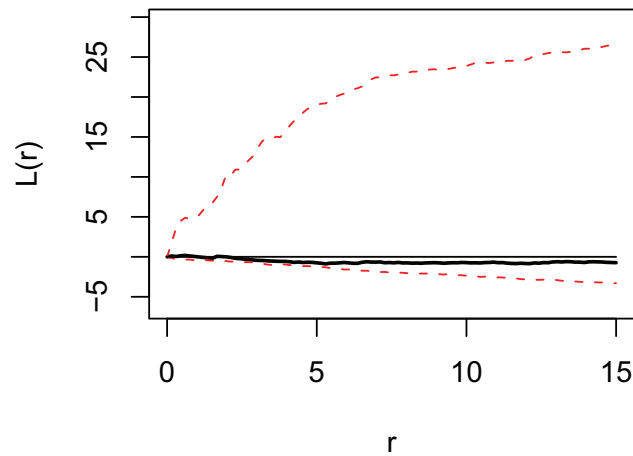


Figure 5.35. Inhomogeneous L-function (black) and 90% simulations interval (dashed red) calculated for the dead trees inside Lagoa B. The simulations interval was calculated via Monte Carlo method (Besag 1977) for the inhomogeneous Poisson process hypothesis with 1000 simulations.

The results shown in **Figure 5.35** shows that the dead trees in the site Lagoa B can be simulated as an inhomogeneous Poisson process.

5.4 Discussion

The main proposal of this Chapter was to present a new methodology (Kernel-MDA Method) to be applied to the analysis of spatial configuration of tree individuals in plant ecology. This methodology combines Kernel Density Estimation Method and Wavelet Transform, in order to supply some limitations of the classical spatial statistical methods (Quadrat Count Method, Nearest Neighbor Method and Ripley K-function, for example), such as no spatial-scale resolution.

The results presented in Chapter 3 and Chapter 4 show that the spatial configuration of the *Laguncularia racemosa* trees contained in study sites Lagoa A and Lagoa B, as well as the configuration of dead trees inside Lagoa B is clustered at higher scales (see **Figure 3.9**, **Figure 3.20** and **Figure 3.21** respectively). This is a strong indication of heterogeneity of exogenous (soil, climate, nutrient, etc.) and/or endogenous (life history, competition, facilitation, etc.) factors occurring inside these stands (Pelissier & Goreaud 2001).

Heterogeneity of point patterns is a main problem when using classical spatial statistical methods, such as Quadrat Count Method, Nearest Neighbor Method and Ripley K-Function) because these methods base on the assumption of homogeneity inside the stands.

In the first experiment, the MDA obtained via CWT and KDE Methods enabled the heterogeneous study site Lagoa A and Lagoa B to be divided into homogeneous subplots (Pelissier & Goreaud 2001). This methodology provides the direct application of classical spatial statistical methods within these subplots. The Ripley K-Function shows that the point processes present variation only at lower and intermediate scales (see **Figure 5.17**, **Figure 5.20** and **Figure 5.23** respectively). These variations can be addressed to plant-plant interactions, such as seed dispersion, nurse-plant effect, succession, zonation, inter and intra-specific competition, etc... (Pelissier & Goreaud 2001, Malkinson *et al.* 2003).

In the second application, the MDA Method reveals a repulsive process determining the spatial location of *Laguncularia racemosa* and *Avicennia germinans* trees inside Lagoa A and Lagoa B. This could be an indication of succession and/or zonation because such ecological processes are characterized by strong inter-specific competition which might lead to an exclusion of trees in presence of another species at a given location. The experiments described in **Chapter 3** and **Chapter 4** detect this spatial pattern, but they were not able to indicate where it occurred. However, they clearly indicate the existence and show also the location of the preferential zones occupied by each of the species.

The third and last experiment shed light on another interesting feature of the Kernel-MDA Method. The mean density of each approximation map obtained using was very nearly the same as the mean density of the original density map. This aspect is very important, if I am considering using these maps to simulate an Inhomogeneous Poisson Process (Baddeley *et al.* 2000). This characteristic guarantees that the number of points simulated inside the virtual stand will be approximately the same number presented inside the real study site, here used as reference data for the simulation. This is an interesting aspect which shows the great potential of this method together with spatial point pattern modeling methods that

requires the use of a density map to simulate the spatial configuration of individuals (Clausen et al. 2000, Jensen et al. 2000, Jensen et al. 2001).

All the results described above demonstrate quite well the power of the obtained via Wavelet Transform method to analyze heterogeneous stands. This method was able to show aspects of the point processes occurring in the sites Lagoa A and Lagoa B that are not revealed by classical spatial statistical methods (Fischer 1922, Clark & Evans 1954, Cressie 1993, Ripley 1977). In general, the methodology described in this chapter demonstrates its potential and direct applicability for the analysis of spatial point patterns in plant ecology.

At present, there are few examples of the application of the Wavelet Transform in plant ecology, but there are an increasing number of studies directly related to this area and I believe that my work has made an important contribution to this ongoing work. It is important to note, however, that methodology presented is not a substitute of the classical methods, but a complementary approach to be used together with them.

Chapter 6

Conclusion

In this study, I proposed some modifications, methodologies and alternatives to the classical spatial statistical methods applied to plant ecology. The intention was to improve the statistical power and the sensitivity of these methods, and thereby to enable the underlying ecological processes occurring within a forest stand to be inferred from the spatial configuration of individual trees.

At the start of **Chapter 2**, I presented a short summary of some classical spatial statistical methods widely used in plant ecology, such as Quadrat Count Analysis, First-Order and Second-Order methods. I then presented some practical examples of the application of these methods to a real dataset collected from two forest stands, called site Lagoa A and site Lagoa B, located in Northeastern Brazil. These sites exhibit structural differences; abiotic conditions at the two sites are also certainly different but information on this aspect is unavailable.

The main advantage of Quadrat Count Analysis and Nearest Neighbor Methods (First-Order Method) is their simplicity of application. However, these methods have at least one serious limitation. They reduce all spatial information about the individual trees in a forest stand to a single one-dimensional index. This characteristic leads to at least two problems. First, these methods are not able to provide information about the scales of the underlying ecological processes taking place in a stand. Second, the spatial positions of the trees in the stand are completely lost. These methods can only indicate if the point pattern associated with the individual trees in the stand exhibits complete spatial randomness (hereinafter CSR), or a regular or clumped distribution. But in plant ecology, depending on the objective of the analysis, the information about the scales of these ecological processes is often very important and has to be taken into consideration.

I then moved on to present the Ripley K-function, a Second-Order Method developed to overcome some of the limitations associated with the Quadrat Count Analysis and Nearest Neighbor Methods. The main feature of the Ripley K-function is that it preserves information about the distances between individuals. It provides not only information about the point processes (CSR, regular or clumped pattern) occurring within a stand, but also provides information about the scales at which these point processes are occurring. This information is very relevant for plant ecology, if I consider, for example, that facilitation (positive interaction among the tree individuals) and competition (negative interaction among the tree individuals) are ecological processes that are usually occurring at different scales at any given time within the stand.

Additionally, I provided explicit formulas for an edge correction factor method based on area (Area Method). This method was used in combination with the Ripley K-function, in order to improve its sensitivity for the analysis of the spatial configurations of point patterns. It is important to note that the application of the Area Method is not restricted to the Ripley K-function. The method can be applied in combination with any spatial statistical method that requires the use of an edge effect correction factor. Comparison of the Area method and the Ripley method, a widely edge effect correction used in plant ecology, clearly showed clearly the greater sensitivity of the Area method in detecting clustering and/or regularity in spatial point patterns. Additionally, the Area method needed less processing time to obtain better results than those obtained via the Ripley method. This is an important advantage of the method, which enables the spatial analysis of large datasets to be performed. Additionally, this characteristic of the method permits the generation of statistically more robust simulation envelopes .

In **Chapter 3** I present the explicit formulas provided for the Area method can be applied only to a rectangular study site and the maximum scale of observation of the analysis is half the shortest dimension of the forest stand. But in future, the intention is to provide a complete set of formulas that permits the analysis of irregular stands of any shape and at all scales of observation.

In **Chapter 3**, I applied the Ripley K-function and the Area method presented in **Chapter 2** to perform a more complete analysis of the spatial configuration of the tree individuals in the sites Lagoa A and Lagoa B. The particular challenge of this chapter was to try to make valid inferences about the underlying ecological processes occurring in these stands from the spatial configurations exhibited by the individual trees.

The results obtained from this analysis were noteworthy and, despite the lack of information about the abiotic conditions in the two forest stands and the probable spatial environmental heterogeneity at sites Lagoa A and Lagoa B, the Ripley K-function was still able to provide important information about the ecological processes which are likely to be occurring at these sites.

In this chapter, I was particularly interested in detecting the succession processes that are probably occurring between the species *Laguncularia racemosa* and *Avicennia germinans*. Mangrove forests are in a continuous process of growth and constantly establishing and renewing themselves. Therefore, it is plausible to suppose that succession processes are occurring among trees of the species *Avicennia* and *Laguncularia* at these sites. The Ripley K-function detected a tendency to repulsion at different scales between tree individuals of *Laguncularia racemosa* and *Avicennia germinans*. This could be a result of succession processes occurring at the sites Lagoa A and Lagoa B.

In **Chapter 4**, I described Object Pattern Analysis. This method was proposed in order to overcome some of the limitations of the methods in **Chapter 2** and **Chapter 3**. The main feature of Object Pattern Analysis is its capacity to perform the spatial analysis of tree individuals considering them as circles, instead of points. The idea was to overcome the problems that arise when I consider a three dimensional individual as a single point.

The results obtained by Object Pattern Analysis showed greater sensitivity for the detection of the ecological processes occurring at the study sites Lagoa A and Lagoa B. In particular, the method was better able to characterize the probable succession processes occurring between trees of species *Laguncularia racemosa* and *Avicennia germinans*.

In this chapter I considered just two simple models that can be used to simulate a spatial distribution of circular objects. This procedure starts by generating a simulation envelope using the Monte Carlo method (Besag 1977). This simulation envelope is used to detect the tendency of an object pattern to CSR, regularity or clustering. An alternative procedure, using a different null model, would be to simulate the position of the trees following a CSR distribution and randomize the observed radius in the study site for the simulated "trees". But at the moment, this is no more than an idea for a future study.

It is important to note that the Object Pattern Analysis also has its limitations. The application of the method is only possible, if the shape of the individuals to be analyzed is approximately circular. Additionally, Object Pattern Analysis shares with the Ripley K-function the limitation that neither method provides spatial resolution of the ecological processes occurring in the stand. In order to overcome this limitation, I presented a new methodology in the next chapter.

In **Chapter 5** I described the application of **MDA** obtained via **KDE** and **WT** methods to the analysis of the spatial configuration of trees in plant ecology. The main advantage of the **MDA** method is its capability to provide spatial-scale information (subject to certain restrictions related to the Heisenberg's uncertainly principle). The method was shown to be able to detect both the scale of ecological processes occurring in the study sites Lagoa A and Lagoa B and show where these ecological processes are occurring. This is an important characteristic, if I consider that mangrove forest stands commonly exhibit environmental heterogeneity.

The **MDA** method enabled a heterogeneous study site to be divided into subplots that could be considered as homogeneous. In this case, I suppose that spatial variability at lower scales and higher scales is associated with plant-plant interactions and environmental heterogeneity respectively. This procedure permits the subsequent application of classical statistical methods (that require the hypothesis of heterogeneity) to analyze each one of these subplots individually.

The **MDA** method identified and determined the spatial location of succession processes probably occurring among the trees of species *Laguncularia* and *Avicennia* in the sites Lagoa A and Lagoa B. This information is not obtainable using the classical spatial statistical methods presented in **Chapters 2, 3 and 4**. The result obtained via **MDA** method clearly showed the existence of preferential zones being occupied by each one of the species *Laguncularia* and *Avicennia* in the study site.

Additionally, the **MDA** method successfully generated the large scale density maps necessary for the simulation of the point patterns of tree individuals at the sites Lagoa A and Lagoa B, assuming the hypothesis of heterogeneity within the stand. The results revealed that the spatial configuration of the tree individuals in these forest stands can be simulated

using an Inhomogeneous Poisson process. This result could be a strong indicator of the heterogeneity of abiotic factors in these forest stands.

In summary, all simulations performed in these experiments revealed the power of the **MDA** method obtained via the **WT** method when applied to the study and analysis of heterogeneous study sites. This procedure was shown to be able to detect aspects of the spatial configuration that were not revealed by the classical spatial statistical methods (Ripley K-function, for example). These results confirmed the potential and the applicability of the **MRA** method for the analysis of spatial point patterns in plant ecology.

In general, all the experiments performed and described in this study were successful and I have no doubt that, the methods described provide important tools for use in combination with classical spatial statistical methods applied to plant ecology. All the proposed modifications and new methodologies substantially improved the statistical power and the sensitivity of these methods. Additionally, the Object Ring and **MDA** methods were able to overcome some of the limitations of these classical statistical methods. The Object Ring Analysis now permits us to analyze the spatial configuration of tree individuals considering them as circles, instead of points. This procedure avoids the tree-point transformation problem described in **Chapter 3**. Finally, the **MDA** method permits us to analyze the spatial configuration of the tree individuals within a forest stand. The method does not require the hypothesis of homogeneity of the spatial configuration of the point pattern of trees individuals in a forest stand.

In future, the idea is to develop Object pattern method to perform the analysis considering environmental heterogeneity within the study sites. Additionally, I intend to develop or adapt the spatial statistical methods presented in this work to perform also the point pattern analysis over the time (Spatial temporal analysis).

Chapter 7

Acknowledgements

First off all, I would like to thank Dr. Uta Berger for her advice, contribution, and support for this work. From her, I have acquired an initiative for research and learned to better focus my ideas. She has exhibited to offer her support at anytime regarding any situation.

I would like to thank Dr. Ulrich Saint-Paul, Dr. Thorsten Wiegand, Dr. Juliane Filser, Helenice dos Santos and Jürgen Bischoff for being member of my committee for the defense of this thesis.

I would like to thank to Dr. Venugopalan Ittekkot, Dr. Ulrich Saint-Paul and all of the ZMT family for letting me be part of this team.

Special thanks to Gaby Boheme, Dr. Ruben Lara, Carlos Jiménez, Jenny Leal Flores, Dr. Hanno Hildenbrandt, Ana Rosa Araujo, Paula Cilene, Helenice Santos, Moirah Menezes, Ursula Mendonza, Silvia Schwamborn, Arturo Dominici, Mark Taylor, Gonzalo Olivares, Soledad Luna, Cyril Piou and Martha Fontalvo for their friendship.

Gostaria agora de agradecer o meu querido pai Joao dos Santos Protazio, que me deu apoio incondicional em todos os momentos que passei por conta de meu doutorado aqui na Alemanha.

Quero agradecer tambem toda a minha familia no Brasil, em especial aos meus irmaos Alessandro Brazao Protazio e Pablo Brazão Protázio e minha mae Iolanda Protazio.

Gostaria de agradecer tambem a minha ex-esposa Mirella Protazio, que tambem contribuiu de alguma forma para o sucesso desta empreitada.

Beijos especiais no meu filho Marcelo Protazio, a minha fortaleza e principal motivacao que me levou a continuar meu trabalho, apesar das confusoes em que me meti :) !!! Te amo meu filho, voce e o orgulho de seu pai e pode contar comigo pro que der e vier.

Gostaria de dedicar esta tese in memorian a meu pequeno filho Caio Protazio, que nao esta aqui entre nos e que com certeza torceu pelo meu sucesso la de cima. Saudades suas meu coracao. Papai tem muitas saudades de voce. Mas deixa estar que um dia a gente se encontra :)

Abracos especiais a familia que me acolheu aqui em Bremen e que me fez esquecer um pouco o banzo de estar longe tanto tempo da minha terra natal. Brunao, Joyce, Karina, Jürgen & Stephe, Marcao, Fabiola, Antonio & Christine e Fabiana & Thomas.

Agradecimentos também a todo o pessoal da B.U.N.D.A. (Brasileiros Unidos Na Deutschland-Alemanha) por ter me aturado tanto tempo na comunidade com meus ataques nonsense :) Em especial para Marianne Kische, Ana & Frank, Eduardo Sonntag, Andrea Tonks, Eva, Alimac e Moa, Frau Monkey, Hirondino, Anjo, Patricia Bentlin e Patricia (da terra da Rainha).

Abracos aos meus colegas brasileiros de Goethe também. Foi com eles que minha saga aqui na Alemanha se iniciou. Leandro, Luciano, Giorgio, Herculano, Eduardo Insfran & Silvana, Giovanna, Gustavo Baldo & Liliane. Agradeço também o apoio de todos os meus amigos que fiz durante o meu período em terras germanicas.

Abracos aos meus colegas do Brasil pelos intermináveis papos no MSN, as vezes varando as madrugadas: Pablo Rouco, Fabiana Deon e Gisella Fada.

Não poderia esquecer também do meu cumpadi Wilfried Strehlau. O meu querido amigo o qual dividi o apartamento aqui em Bremen e que aturou minhas maluquices durante todos estes quase 3 anos.

Dedico também a tese a uma pessoa que já está me aturando um bom tempo aqui no Brasil. Minha linda Manu que tem me dado apoio e me trouxe tranquilidade nesta fase que foi a correção final da tese ... te amo minha querida.

Agradecimentos ao DAAD pelo lado alemão e ao CNPq pelo lado brasileiro pelo suporte financeiro e pela oportunidade de realizar meu doutorado aqui na Alemanha.

Em resumo patota ... Ich liebe euch !!!

E parafraseando cascudinho Leandro ... Valeu DAAD :)

Chapter 8

References

- Abry, P. 1997. *Ondelettes et turbulence*. Diderot, Paris, 292 pp.
- Ball, M. 1988. Ecophysiology of mangroves. *Trees* 2: 129-142.
- Barot, S., J. Gignoux, and J. Menaut. 1999. Demography of a savanna palm tree: predictions from comprehensive spatial pattern analyses. *Ecology* 80: 1987-2005.
- Begon, M., Harper, J. L. & Townsend, C. R. 1986. *Ecology: Individuals, populations, and communities*. Smauer Associates, Inc. Sunderland, Massachusetts.
- Berger, U. Glaser, M. Koch, B. Krause, G. Lara, R. Saint-Paul, U. Schories, D. Wolff, M. 1999a. MADAM - An Integrated Approach to Mangrove Dynamics and Management. *Journal of Coastal Conservation* 5: 125-134.
- Berger, U., Wagner G. and Wolff, W.-F. 1999b. Virtual biologists observe virtual grasshoppers: an assessment of different mobility parameters for the analysis of movement patterns. - *Ecological Modelling* 115 (2-3): 119-127.
- Berger, U. & Hildenbrandt, H. 2000. A new approach to spatially explicit modelling of forest dynamics: spacing, ageing and neighbourhood competition of mangrove trees. *Ecological Modelling*. 132: 287-302
- Berger, U.; Adams, M.; Grimm, V.; Hildenbrandt, H. 2006. Modelling secondary succession of neotropical mangroves: causes and consequences of growth reduction in pioneer species. *Perspectives in Plant Ecology, Evolution and Systematics* 7(4): 243-242.
- Bertness, M.D. and R. Callaway. 1994. Positive interactions in communities. *Trends in Ecology and Evolution* 9: 191-193.
- Besag, J.E. 1977. Comments on Ripley's paper, *Journal of the Royal Statistical Society B* 39(2): 193-195.
- Blate, G. M., D. R. Peart, and M. Leighton. 1998. Postdispersal predation on isolated seeds: a comparative study of 40 tree species in a southeast Asian rainforest. *Oikos* 82: 522-538.
- Chui, C. K. 1992. *An Introduction to Wavelets*; Academic Press, London.
- Callaway, R.M. and L.R. Walker. 1997. Competition and facilitation: a synthetic approach to interactions in plant communities. *Ecology* 78: 1958-1965.
- Clark, P.J. & Evans, F.C. 1954. Distance to nearest neighbor as a measure of spatial relationships in populations. *Ecology*. 35: 445-453.

- Clausen, W. H. O., Rasmussen, H. H. and Rasmussen, M. H. 2000. Inhomogeneous point processes. Doctoral Thesis, Aalborg University.
- Cole, R.G. and C. Syms. 1999. Using spatial pattern analysis to distinguish causes of mortality: an example from kelp in north-eastern New Zealand. *J. Ecol.* 87: 963-972.
- Condit, R., Ashton, P. S., Baker, P. et al. 2000. Spatial patterns in the distribution of tropical tree species. *Science* 288: 1414-1418.
- Connell, J. H. & Slatyer, R. O. 1977. Mechanisms of Succession in Natural Communities and their Role in Community Stability and Organization. *Am. Nat.* 111: 1119-1144.
- Couteron, P., & Kokou, K. 1997. Woody vegetation spatial patterns in a semi-arid savanna of Burkina Faso, West Africa. *Plant Ecology* 132, 211-227.
- Couteron, P. 1998. Relations spatiales entre individus et structure d'ensemble dans les peuplements ligneux soudanosaéliens au Nord-ouest du Burkina Faso. Thèse de Doctorat, Université Paul Sabatier, Toulouse.
- Cressie, N.A.C. 1993. *Statistics for Spatial Data*, John Wiley, New York.
- Cressie, N.A.C. 1991. *Statistics for Spatial Data*. Wiley Series in Probability and Mathematical Statistics. John Wiley & Sons. New York, NY, 1st edition.
- Daubechies, I. 1990. The wavelet transform time-frequency localization and signal analysis. *IEEE Trans. Inform. Theory*, 36: 961-1004.
- Daubechies, I. 1992. *Ten Lectures on Wavelets*. Society for Industrial and Applied Mathematics, 357 pp.
- Dale, M. R. T. and Powell, R. D. 2001. A new method for characterizing point patterns in plant ecology. *Journal of Vegetation Science*. 12: 597-608.
- David F.N. and Moore, P.G. 1954. Notes on contagious distributions in plant populations. *Annals of Botany*, 18: 47-53.
- Desouhant, E., Debouzie, D. & Menu, F. 1998. Oviposition pattern of phytophagous insects: on the importance of host population heterogeneity. *OEcologia* 114: 382-388.
- Diggle, P.J. 1983. *Statistical Analysis of Spatial Point Patterns*. Academic Press, London.
- Diggle, P. J. 1985. A kernel method for smoothing point process data. *Journal of the Royal Statistical Society: Ser. C (Applied Statistics)* 34: 138-147.
- Douglas, J.B. 1975. Clustering and aggregation. *Sankhya B*, 37: 398-417
- Duke, N.C., M.C. Ball and J.C. Ellison 1998. Factors influencing biodiversity and distributional gradients in mangroves. *Global Ecology and Biogeography Letters*, Mangrove Special Issue 7: 27-47.
- Duke, N.C. 2001. Gap creation and regenerative processes driving diversity and structure of mangrove ecosystems. *Wetlands Ecology and Management*, 9: 257-269.
- Fisher, R.A., T.H., and Mackenzie W. 1922. The Accuracy of the Plating Method of Estimating the Density of Bacterial Populations, with Particular Reference to the Use of Thornton's Agar Medium with Soil Samples. *Annals of Applied Biology* 9: 325-359.
- Fisher, R.A., T.H., and Mackenzie W. 1922. Bacterial Populations, with Particular Reference *Annals of Applied Biology*, 9, 325-359.

- Kumar, P., and Foufoula-Georgiou, E. 1994. Wavelet analysis in geophysics: An introduction, in *Wavelets in Geophysics*, edited by E. Foufoula-Georgiou and P. Kumar, pp. 1743, Academic, San Diego, Calif.
- Forget, P.-M. 1994. Recruitment pattern of *Vouacapoua americana* (Caesalpinaceae), a rodent-dispersed tree species in French Guiana. *Biotropica* 26: 406-419.
- Fromard, F., H. Puig, E. Mougin, G. Marty, J. L. Betoulle, and L. Cadamuro. 1998. Structure, above-ground biomass and dynamics of mangrove ecosystems: new data from French Guiana. *Oecologia* 115: 39-53.
- Goreaud, F. & Pélissier, R. 1999. On explicit formulas of edge effect correction for Ripley's K-function. *Journal of Vegetation Science*, 10(3): 433-438.
- Goreaud F., Courbaud B., Collinet F. 1997. Spatial structure analysis applied to modelling of forest dynamics : a few examples. *Présentation orale au Workshop IUFRO, Empirical and process based models for forest tree and stand growth simulation*, 20-26 September 1997, Oeiras, Portugal.
- Goreaud, F. & Pélissier, R. 2003. Avoiding misinterpretation of biotic interactions with the intertype K12-function: population independence vs. random labelling hypotheses. *Journal of Vegetation Science*, 14(5): 681-692.
- Getis, A. and Franklin, J. 1987. Second-order neighborhood analysis of mapped point patterns. *Ecology* 68: 474-477.
- Greig-Smith, P. 1964. *Quantitative plant ecology*. 2nd ed. Butterworths, London.
- Haase, P., F.I. Pugnaire, S.C. Clark, and L.D. Incoll. 1996. Spatial patterns in a two-tiered semi-arid shrubland in south-eastern Spain. *Journal of Vegetation Science*. 7: 527-534.
- Harun E.N. 2004. *Spatial Structure, Leaf Area Index and Light Reception of different Mangrove Forest Stands in Caeté Mangrove Estuary, Bragança, Pará, Northern Brazil*. Master Thesis, University of Bremen.
- He, F., Legendre, P., Bellehumeur, C. & LaFrankie, J.V. 1994. Diversity pattern and spatial scale: a study of a tropical rain forest of Malaysia. *Environ. Ecol. Stat.* 1: 265-286.
- Holling, C.S. 1992. Cross-scale morphology, geometry, and dynamics of ecosystems. *Ecol. Monogr.* 62: 447-502.
- Hogarth, P.J. 1999. *The Biology of Mangroves*. Oxford Univ. Press. 228 p.
- Jiménez Ramón, J. A., and A. E. Lugo. 1985. *Avicenia germinans* (L) L. , Black mangrove. In: [Silvicultural Manual], Chapter 4. U.S. Forest Service.
- Jeltsch, F., Moloney, K. A. and Milton, S. J. 1999. Detecting process from snap-shot pattern: lessons from tree spacing in the southern Kalahari. *Oikos* 85: 451-467.
- Jensen, E. B. V. and Nielsen, L. S. 2000. Inhomogeneous Markov point processes by transformation. *Bernoulli* 6, 761-782.
- Jensen, E. B. V. and Nielsen, L. S. 2001. A review on inhomogeneous spatial point processes. In *Selected Proc. Symp. Inference for Stoch. Process. (IMS Lecture Notes Monogr. Ser. 37)*, eds I. V. Basawa, C. C. Heyde and R. L. Taylor, Institute of Mathematical Statistics, Beachwood, OH, pp. 297-318.

- Kenkel, N.C. 1988. Pattern of self-thinning in jack pine: testing the random mortality hypothesis. *Ecology* 69: 1017-1024.
- King, T.J. & Woodell, S.R.J. 1973. The cause of regular pattern in desert perennials. *Journal of Ecology*. 61: 761-765.
- Kjerfve, B. and L.D. Lacerda. 1993. Mangroves of Brazil. In: Lacerda L.D. ed. Conservation and sustainable utilization of mangrove forests in Latin America and Africa Regions. Part I: Latin America. International Society for Mangrove Ecosystems and the International Tropical Timber Organization.
- Klaas, B. A., Moloney, K. A. and Danielson, B. J. 2000. The tempo and mode of gopher mound production in a tallgrass prairie remnant. *Ecography* 23: 246-256.
- Kolasa, J. and S.T.A. Pickett. 1991. *Ecological Heterogeneity*. Springer.
- Kolasa, J. & Rollo, D.C. 1991. The heterogeneity of heterogeneity: a glossary. In: Kolasa, J. & Pickett, S.T.A. (eds.) *Ecological heterogeneity*, pp. 1-23. Springer-Verlag, New York, NY.
- Little, E.L.Jr. 1983. *Common fuelwood crops: a handbook for their identification*. McClain Printing Co., Parsons, WV.
- Lloyd. M. 1967. Mean crowding. *Journal of Animal Ecology*, 36: 1-30.
- Lotwick, H. W. and B. W. Silverman. 1983. Methods for analysing spatial processes of several types of points. *Journal of the Royal Statistical Society, Series B*, 39: 172-212.
- Lovelock, C. E. & I. C. Feller. 2003. Photosynthetic performance and resource utilization of two mangrove species coexisting in hypersaline scrub forest. *Oecologia* 134: 455-462.
- Malkinson D., Kadmon R., & Cohen, D. 2003. Pattern analysis in successional communities - An approach for studying shifts in ecological interactions. *Journal of Vegetation Science*, 14: 213-222
- Mallat S. 1988. *Multiresolution Representation and Wavelets*, Grasp. Lap 153, University of Pennsylvania, Philadelphia.
- Matheron G. 1963. Principles of geostatistics. *Econ Geol* 58: 1246-1266.
- Mehlig, U. 2001. Aspects of tree primary production in an equatorial mangrove forest in Brazil. Unpublished Doctoral Thesis, University of Bremen.
- Menezes M, Berger U, Worbes M. 2003. Annual growth rings and longterm growth patterns of mangrove trees from the Bragança peninsula, North Brazil. *Wetlands Ecology and Management* 11: 233-242.
- Menezes, M.P.M. 2006. Investigations of mangrove forest dynamics in north Brazil, Amazonia. Unpublished Doctoral Thesis, University of Bremen.
- Meyer, Y. 1993. *Wavelets*, pp 130, SIAM, Philadelphia.
- Morista. M. 1959. Measuring the dispersion and analysis of distribution patterns. *Memoires of the Faculty of Science. Kyushu University. Series E. Biology*, 2: 215-235.
- Muller, C.H. 1953. The association of desert annuals with shrubs. *American Journal of Botany*. 40: 53-60.
- Pélissier R., Goreaud F. 2001. A practical approach to the study of spatial structure in simple cases of heterogeneous vegetation. *Journal of Vegetation Science* 12 : 99-108.

Forget, P.M. 1996. Removal of Seeds of *Carapa procera* (Meliaceae) by Rodents and Their Fate in Rainforest in French Guiana Pierre-Michel Forget *Journal of Tropical Ecology*, Vol. 12, No.6, pp. 751-761.

Pélissier R., Goreaud F. 2001. A practical approach to the study of spatial structure in simple cases of heterogeneous vegetation. *Journal of Vegetation Science*, 12 : 99-108.

Powell, T.M. & Jassby A. D. 1990. Detecting changes in ecological time series. *Ecology* 71: 2044-2052.

Prentice, I.C. & Werger, M.J.A. 1985. Clump spacing in a desert dwarf shrub community. *Vegetatio* 63: 133-139.

Quarto, A. 2001. The mangrove forest. Mangrove Action Project (MAP).

Rabinowitz, D. 1978. Early growth of mangrove seedlings in Panama, and an hypothesis concerning the relationship of dispersal and zonation. *Journal of Biogeography* 5: 113-133

Revilla, E. and Palomares, F. 2002. Spatial organization, group living and ecological correlates in low-density populations of Eurasian badgers, *Meles meles*. *J. Anim. Ecol.* 71: 497-512.

Ricklefs, R.E. and Latham, R.E. 1993. Continental comparisons of temperate-zone tree species diversity. Pages 294-314 in R. E. Ricklefs and D. Schluter (eds.), *Species Diversity in Ecological Communities: Historical and Geographical Perspectives*, University of Chicago Press.

Ripley, B.D. 1976. The second-order analysis of stationary point processes. *Journal of Applied Probability*. 13: 255-266.

Ripley, B. D. 1977. Modelling spatial patterns (with discussion). *Journal of Royal Statistical Society. B* 39: 172-212.

Roels, B., During H.J. 2001. Utrecht University, section Plant Ecology. Report Department of Plant Ecology, nr. D220301.

Silverman, B. (1978). Weak and strong uniform consistency of the kernel estimate of the density and its derivatives. *Annals of Statistics* 6: 177-184.

Silvertown, J. W. and J. L. Doust. 1993. *Introduction to plant population biology*. Blackwell Scientific Publications.

Simberloff, D. 1979. Nearest-neighbor assessment of spatial configurations of circles rather than points. *Ecology* 60: 679-685.

Sterner, F. J., Ribic, C. A. and Schatz, G. E. 1986. Testing for life history changes in spatial patterns of tropical tree species. *Journal of Ecology*. 74: 621-633.

Stoyan, D. and Penttinen, A. 2000. Recent application of point process methods in forest statistics. *Statistical Science*. 15: 61-78.

Tielbörger, K. & Kadmon, R. 2000: Indirect effects in a desert plant community: is competition among annuals more intense under shrub canopies? *Plant Ecology* 150: 53-63.

Tomlinson, Philip B. 1986. *The Botany of Mangroves*. Cambridge University Press, Cambridge.

Tomppo, E. 1986. Models and methods for analysing spatial patterns of trees. *Communications Instituti Forestalis Fenniae* 138. 65 pp.

Torrence, C. and Compo, G.P. 1998: A practical guide to wavelet analysis. *Bull. Amer. Meteor. Soc.*, 79: 61-78

Yamada, I. and P. A. Rogerson. 2003. An Empirical Comparison of Edge Effect Correction Methods Applied to K-function Analysis. *Geographical Analysis*. 35(2): 97-109.

Wiegand T., and K. A. Moloney 2004. Rings, circles and null-models for point pattern analysis in ecology. *Oikos* 104: 209-229.

Wiegand, T., Kissling, W.D., Cipriotti, P.A., and Aguiar, M.R. 2006. Extending point pattern analysis to objects of finite size and irregular shape. *Journal of Ecology* 94: 825-837.

Wiens, J. A., Stenseth, N. C., Van Horne, B. et al. 1993. Ecological mechanisms and landscape ecology. *Oikos* 66: 369-380.

Wiens, J.A. 1989. Spatial scaling in ecology. *Funct. Ecol.* 3: 385-397.

Young, C.G., Dale, M.R.T. and Henry, G.H.R. 1999. Spatial pattern of vegetation in arctic sedge meadows. *Ecoscience* 6: 583-592

Chapter 9

Appendix

```
cc -----
cc Joao Marcelo Brazao Protazio
cc Biologiedoktorand an die Bremen Universität
cc Zentrum für Marine Tropenökologie
cc Büro 207
cc Fahrenheitstrasse 6
cc 28359 Bremen
cc Deutschland
cc Tel 00 49 0421 2380058
cc Fax 00 49 0421 2380050
cc marcelo.protazio@uni-bremen.de
cc mprotazio@gmail.com
cc -----
function ka(x,y,r,xmin,ymin,xmax,ymax,nr,np,k)
real x,y,r,k
real xmin,ymin,xmax,ymax,pi
integer np,nr dimension
x(np),y(np),r(nr),k(nr)
parameter (pi = 3.1415927)
cc -----
cc Ripley L-function calculation
cc -----
call kfun(x,y,r,xmin,ymin,xmax,ymax,nr,np,k)
k = sqrt(k/pi)-r
end
cc -----
cc Function 01
cc -----
cc Distance between two points
cc -----
cc p1 = (x1,y1)
cc p2 = (x2,y2)
```

```

cc -----
function dist(x1,y1,x2,y2)
real x1,y1,x2,y2
dist = sqrt((x1-x2)**2+(y1-y2)**2)
end
cc -----
cc Function 02
cc -----
cc Indicator function
cc -----
cc p1 = (x1,y1)
cc p2 = (x2,y2)
cc id = 1 if d(p1,p2) <= r
cc id = 0 otherwise
cc -----
function ind(x1,y1,x2,y2,r)
real x1,y1,x2,y2,r
d = dist(x1,y1,x2,y2)
if (d.le.r) then
ind = 1
else
ind = 0
endif
end
cc -----
cc Function 03
cc -----
cc Area edge correction
cc -----
cc p = (x,y)
cc xmin,ymin,xmax,ymax
cc w = area edge correction
cc -----
function edge(x,y,xmin,ymin,xmax,ymax,r) integer c,i real
x,y,xmin,ymin,xmax,ymax,r
real alpha,alpha1,alpha2,e,e1,e2,d,d1,d2,dd,pi,t1,t2
dimension dd(2)
parameter (pi = 3.1415927)
c = 0
if ((x-xmin).lt.r) then
c = c + 1

```

```

dd(c) = x - xmin
endif
if ((y-ymin).lt.r) then
c = c + 1
dd(c) = y - ymin
endif
if ((xmax-x).lt.r) then
c = c + 1
dd(c) = xmax - x
endif
if ((ymax-y).lt.r) then
c = c + 1
dd(c) = ymax - y
endif
if (c.eq.0) then
edge = 1
elseif (c.eq.1) then
d = dd(1)
e = sqrt((r**2)-(d**2))
alpha = acos(d/r)
edge = pi*(r**2)*(1/(e*d+(pi-alpha)*(r**2)))
else d1 = dd(1)
d2 = dd(2)
e1 = sqrt((r**2)-(d1**2))
alpha1 = acos(d1/r)
e2 = sqrt((r**2)-(d2**2))
alpha2 = acos(d2/r)
if ((r**2).gt.((d1**2)+(d2**2))) then
t1 = e1*d1+e2*d2
t2 = 0.75*pi-0.5*alpha1-0.5*alpha2
edge = pi*(r**2)*(1/(d1*d2+0.5*t1+t2*(r**2)))
else
edge = pi*(r**2)*(1/(e1*d1+e2*d2+(pi-alpha1-alpha2)*(r**2))) endif
endif
end
cc -----
cc Function 04
cc -----
cc Ripley K-function
cc -----
cc p(x,y)

```

```
cc xmin,ymin,xmax,ymax
cc nr - r discretization
cc np - number of points
cc -----
subroutine kfun(x,y,r,xmin,ymin,xmax,ymax,nr,np,k)
real x,y,r,w,xmin,ymin,xmax,ymax,area,pi,k
integer nr,np,i,j,q,c
dimension x(np),y(np)
dimension r(nr),k(nr)
parameter (pi = 3.1415927)
area = (xmax-xmin)*(ymax-ymin)
do 10 q = 1,nr
k(q) = 0
do 20 i = 1,np
w = edge(x(i),y(i),xmin,ymin,xmax,ymax,r(q))
c = 0
do 30 j = 1,np
c = c + ind(x(i),y(i),x(j),y(j),r(q))
30 continue
c = c - 1
k(q) = w * c + k(q)
20 continue
k(q) = area*k(q)/(np*np)
10 continue
end
```